ANALYSIS OF THE MECHANISMS FOR URONATE ISOMERASE FROM *E. COLI*, COBYRINIC ACID *A,C*-DIAMIDE SYNTHETASE FROM *S. TYPHIMURIUM*, AND COBYRIC ACID SYNTHETASE FROM *S. TYPHIMURIUM*

A Dissertation

by

LAKENYA WILLIAMS

Submitted to the Office of Graduate Studies of
Texas A&M University
in partial fulfillment of the requirements for the degree of

DOCTOR OF PHILOSOPHY

August 2007

Major Subject: Chemistry

ANALYSIS OF THE MECHANISMS FOR URONATE ISOMERASE FROM *E. COLI*, COBYRINIC ACID *A,C*-DIAMIDE SYNTHETASE FROM *S. TYPHIMURIUM*, AND COBYRIC ACID SYNTHETASE FROM *S. TYPHIMURIUM*

A Dissertation

by

LAKENYA WILLIAMS

Submitted to the Office of Graduate Studies of
Texas A&M University
in partial fulfillment of the requirements for the degree of

DOCTOR OF PHILOSOPHY

Approved by:

Chair of Committee, Frank Raushel
Committee Members, Donald Pettigrew
Paul Lindahl
David Barondeau
Head of Department, David Russell

August 2007

Major Subject: Chemistry

ABSTRACT

Analysis of the Mechanisms for Uronate Isomerase from *E. coli*, Cobyrinic Acid *a,c*-Diamide Synthetase from *S. typhimurium*, and Cobyric Acid Synthetase from *S. typhimurium*. (August 2007)

LaKenya Williams, B.S., Prairie View A&M University;

M.S., Texas A&M University

Chair of Advisory Committee: Dr. Frank M. Raushel

Uronate isomerase catalyzes the isomerization of D-glucuronate and D-fructuronate. This enzyme has been classified as a member of the amidohydrolase superfamily. The reaction catalyzed by uronate isomerase is analogous to the isomerization of aldose/ketose sugars. These interconversions can occur via two mechanisms, a hydride or proton transfer. The solvent exchange experiments and the elimination of fluoride from 3-deoxy-3-fluoro-D-glucuronate catalyzed by the enzyme support a proton transfer. Assignment of the transferred proton as the *proR* proton further supports a proton transfer mechanism via a *cis*-enediol intermediate for uronate isomerase from *E. coli*.

Cobyrinic acid *a,c*-diamide synthetase and cobyric acid synthetase from *S. typhimurium* catalyze ATP dependent amidations of carboxylate groups on the periphery of cobyrinic acid utilizing glutamine or ammonia as a nitrogen donor. The role of ATP in the reaction has been probed by positional isotope exchange (PIX). The results confirm

the presence of phosphorylated intermediate species in the reactions catalyzed by cobyrinic acid *a,c*-diamide synthetase and cobyric acid synthetase from *S. typhimurium.*

Cobyric acid synthetase catalyzes the amidation of carboxylate groups *b, d, e,* and *g* of adenosyl-cobyrinic acid *a,c*-diamide in the biosynthetic pathway for coenzyme B_{12}. Analysis of the reaction time courses demonstrate the appearance of three unique intermediate species which are released from the active site after each amidation reaction. The identification of the intermediate species was accomplished by ^{1}H, ^{15}N HSQC NMR spectroscopy. The NMR spectrum of a sample quenched at the beginning of the reaction shows a single intermediate species corresponding to carboxamide *e*. Subsequent spectra establish the amidation order as *e*, *d*, *b*, and *g*. The structural basis for the dissociative and sequential reaction mechanism coupled with the rigid regiochemistry is unknown. However, mutations to aspartate 146 perturb the order of amidation. A NMR spectrum quenched early in the reaction with the D146N mutant shows two intermediate species corresponding to carboxamides *e* and *d*. Spectra of samples later in the reaction confirm the presence of multiple *e, d*, and *g* amide species. The reaction is completed with the amidation of carboxylate *b*.

DEDICATION

To my family:

Thank you all for your love, support, and encouraging words over the years.

TABLE OF CONTENTS

Page

LIST OF FIGURES

FIGURE Page

LIST OF TABLES

CHAPTER I

INTRODUCTION

The amidohydrolase superfamily was identified in 1997 by Holm and Sander (*1*). Discovery of this superfamily was based on the similar X-ray crystal structures of urease (URE), adenosine deaminase (ADA), and phosphotriesterase (PTE). It was shown that these enzymes featured an $(\alpha/\beta)_8$ barrel with metal binding sites at the C-terminal end of multiple β-strands. Since then many enzymes have been classified as amidohydrolase superfamily members, most of which catalyze hydrolytic reactions with ester or amide functional groups attached to carbon or phosphorus centers. The substrates include amino acids, sugar acids, nucleic acids, and organophosphates. Dihydroorotase (DHO), isoaspartyl dipeptidase (IAD), N-acetyl glucosamine-6-phosphate deacetylase (AGD), D-amino acid deacetylase (DAA), and uronate isomerase (URI) are some of the structurally characterized members of the amidohydrolase superfamily. The reactions catalyzed by these amidohydrolase superfamily members are shown in **Scheme 1**.

The $(\alpha/\beta)_8$ structural fold was first identified in the crystal structure of triose phosphate isomerase from chicken muscle (*2*). Roughly 10% of reported enzyme structures contain an $(\alpha/\beta)_8$ barrel (*3*). The fold consists of eight parallel beta-strands arranged in a barrel formation surrounded by alpha-helices, which connect the parallel strands of the beta-sheets and run anti-parallel to the beta-sheets. The $(\alpha/\beta)_8$ motif of triose phosphate isomerase from chicken muscle is depicted in **Figure 1**.

This dissertation follows the style and format of *Biochemistry*.

Scheme 1. Reactions catalyzed by some members of the amidohydrolase superfamily.

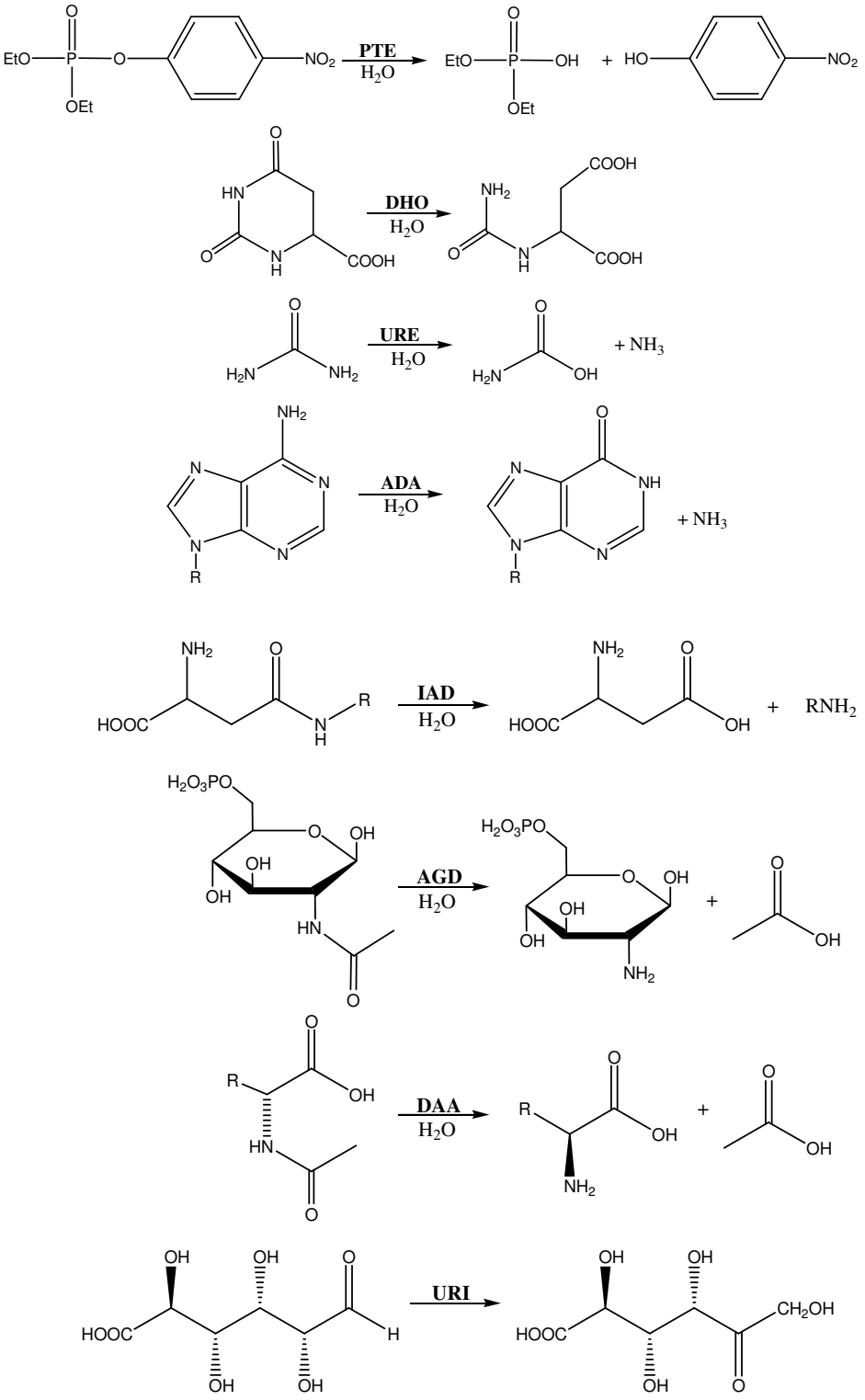

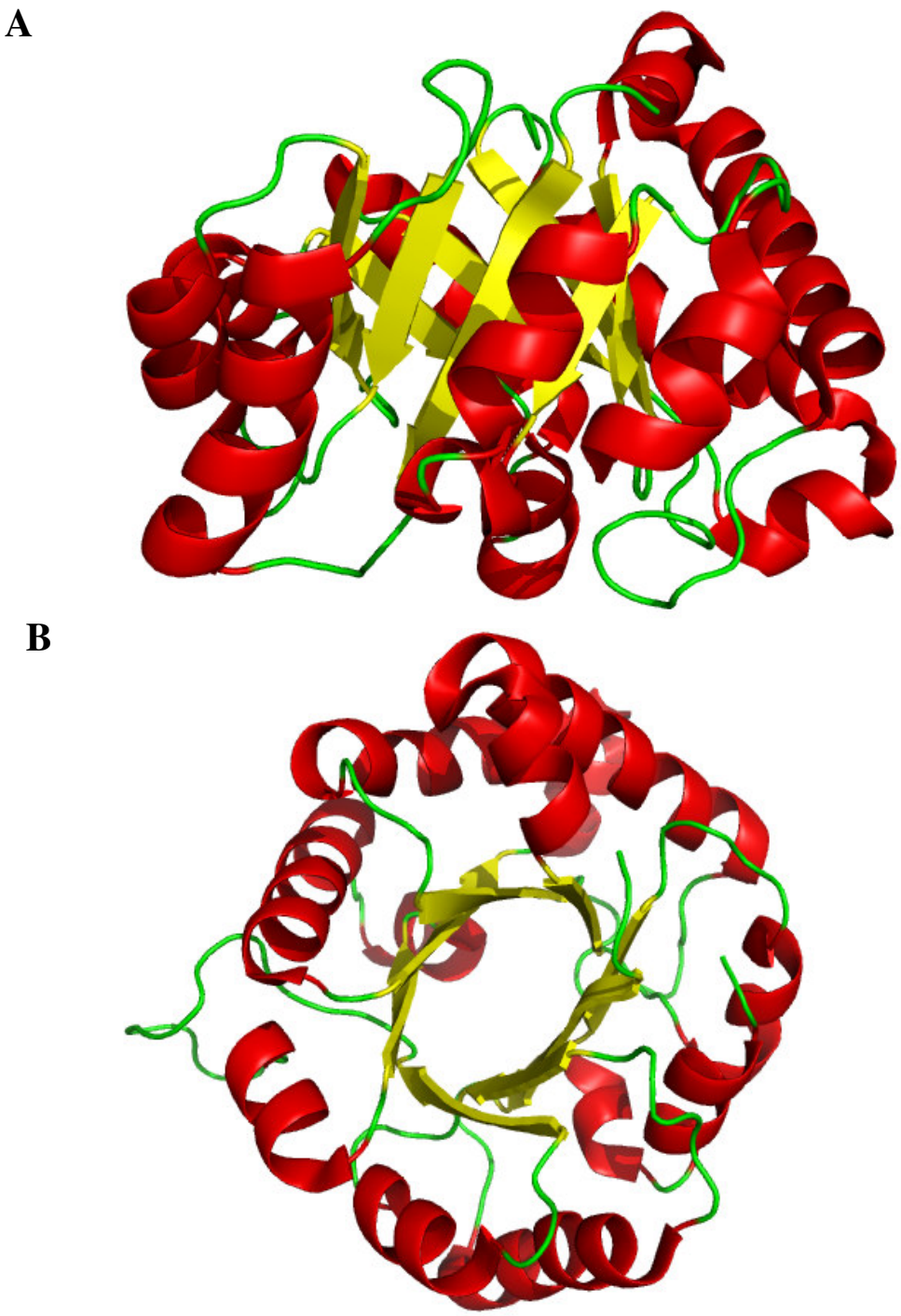

Figure 1. The $(\alpha/\beta)_8$ barrel of TIM from chicken muscle. A. Side view of the $(\alpha/\beta)_8$ barrel. B. Top view of the $(\alpha/\beta)_8$ barrel. PDB file 2ypi.

The frequency of the $(\alpha/\beta)_8$ barrel fold in structurally characterized enzymes demonstrates its versatility. According to the SCOP database, there are 32 superfamilies that utilize this motif (as of October 20, 2006). The reactions catalyzed include isomerizations, hydrolysis, reductions, dehydrations, oxidations etc. Triose phosphate isomerase boasts a k_{cat}/K_m value of 10^9 M^{-1} s^{-1}, and is called the "perfect enzyme" in some textbooks (*4*). Therefore, it is no surprise that the characteristics of TIM would offer a template for efficient enzymatic activity. This doesn't suggest that TIM was the building block for $(\alpha/\beta)_8$ barrel enzymes, but the presence of this structural fold in so many enzymes does suggest that $(\alpha/\beta)_8$ barrel enzymes evolved from a common structural ancestor. Reaction diversity is not only evident among enzymes containing $(\alpha/\beta)_8$ barrels, but is evident within the superfamilies also.

All the structurally characterized members of the amidohydrolase superfamily contain the $(\alpha/\beta)_8$ barrel fold, and are capable of binding one or two metal ions. The metal binding site(s) are found at the C-terminal end of β-strands 1, 5, 6 and 8. Based on the metal binding sites, the superfamily enzymes can be grouped into subcategories (*5*). Subtype I includes PTE, DHO, URE, and IAD. Subtype II is defined by PHP from *E. coli* which is a PTE homolog. Adenosine deaminase, AGD, and DAA comprise subtypes III, IV, and V respectively. Members categorized in subtypes VI and VII are renal dipeptidase (RDP) and URI, respectively. The various metal centers are shown in **Table 1** as reported by Seibert and Raushel (*5*).

Table 1. Metal binding sites of various amidohydrolase superfamily members.

			β-strand							
Subtype	Metals	Metal Site	1	2	3	4	5	6	7	8
I	Zn, Ni	α, β	HxH			K	H	H		D
II	Zn	α, β	HxH			E	H	H		D
III	Zn, Fe	α	HxH				H	h[b]		D
IV	Fe	β	hxh[a]		E		H	H		d[b]
V	Zn	β	hxh[a]	C			H	H		d[b]
VI	Zn	α, β	HxD		E		H	H		d[b]
VII			HxH				H			D

[a] Residues are not metal ligands.
[b] Residues are not ligands but are hydrogen bonded to the active site water molecule.

The great diversity within the amidohydrolase superfamily is clearly pointed out by the various metal centers. Subtypes I, II, and VI require two metal ions for catalysis whereas subtypes III, IV, and V require only one. The fact that the site occupied by the metal differs among the enzymes that bind one metal ion is interesting. Even more intriguing is the lack of bound metal ions in the crystal structure of URI. Metal centers for PTE (*6*), ADA (*7*) , DAA (*8*), and URI (*9*) are illustrated in **Figure 2**. The various metal requirements in this superfamily suggest that these enzymes, possibly evolving from a common structural ancestor, have diverged to be catalytically active with one or possibly no metal ions. Evidence of divergence also lies in the diversity of chemical reactivity amid superfamily members.

All of the characterized chemical reactions catalyzed by enzymes in the amidohydrolase superfamily are hydrolytic reactions with the exception of uronate isomerase. Uronate isomerase catalyzes the isomerization of D-glucuronate to D-

fructuronate or D-galacturonate to D-tagaturonate in the first step of the hexauronate catabolism pathway in *E. coli* (*10*). D-Glucuronate and D-galacturonate are uronic acids that are believed to be present in the intestinal tract at high concentrations. D-glucuronate in humans is used for drug and toxin conjugation and is excreted in the urine and bile (*11*). Bile is then secreted into the small intestine through the biliary tract. These uronic acids, and other sugar acids, are believed to be substrates which support the growth of *E. coli* in the gut (*10*). The acids, D-glucuronate and D-galacturonate, are degraded in parallel pathways to form a common intermediate, 2-keto-3-deoxy-D-gluconate. This intermediate is then phosphorylated and utilized in the Entner-Doudoroff pathway as shown in **Scheme 2**. The 72 strains of *E. coli* isolated from natural populations all possess the Entner-Doudoroff pathway and have the ability to grow on gluconate and glucuronate (*10*). Thus the reaction catalyzed by uronate isomerase is important for the survival of *E. coli* in intestinal environments. Therefore, the characterization of uronate isomerase as an amidohydrolase superfamily member is very interesting and offers a striking illustration of divergence in chemical reactivity amid proteins which presumably share a common structural ancestor.

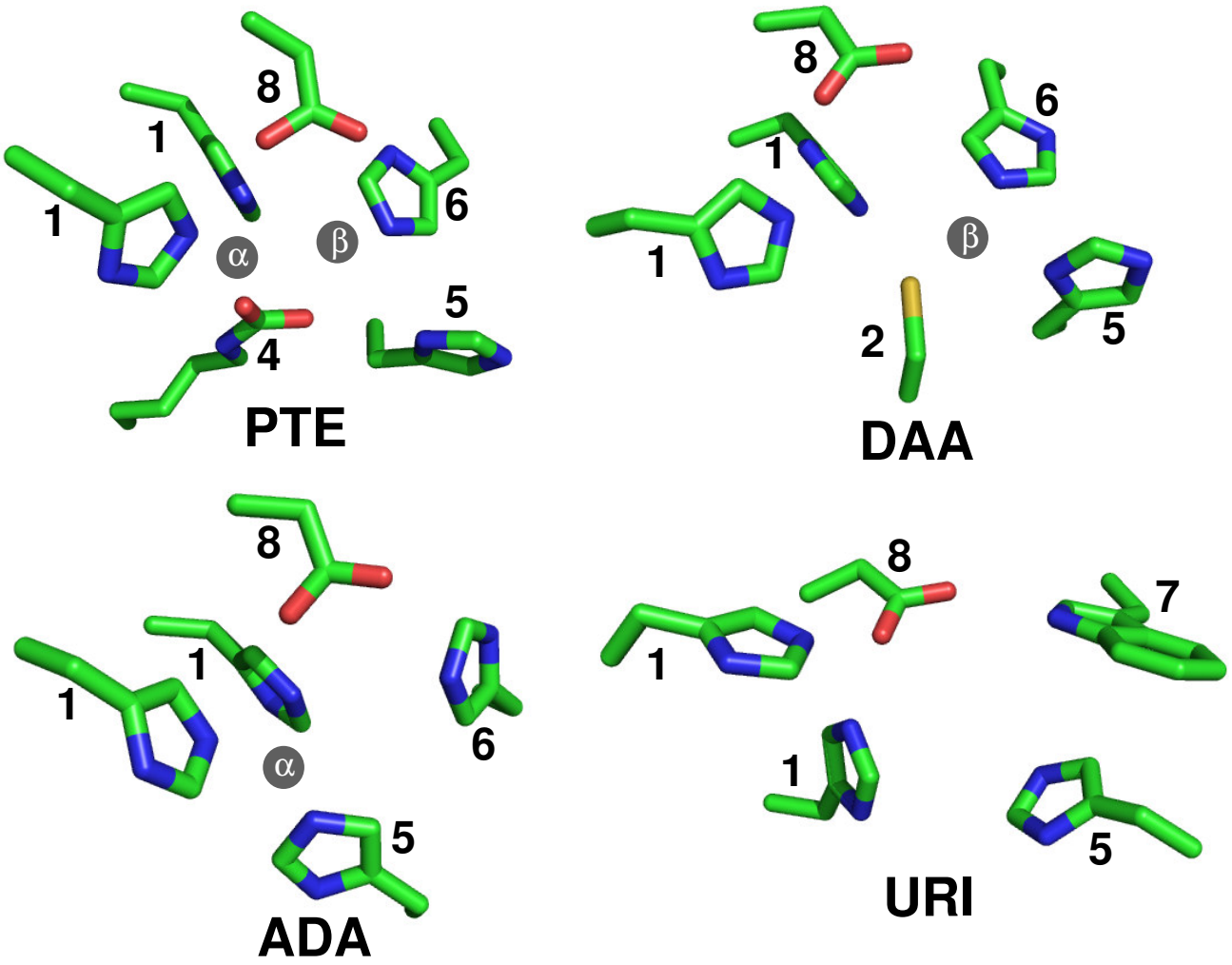

Figure 2. Metal centers of PTE, ADA, DAA and URI. Numbers indicate the β-strand of origin. PDB codes for these structures are 1hzy, 1a4m, 1m7j, and 1j5s respectively.

Scheme 2. Hexauronate catabolism pathway in *E. coli* (*10*).

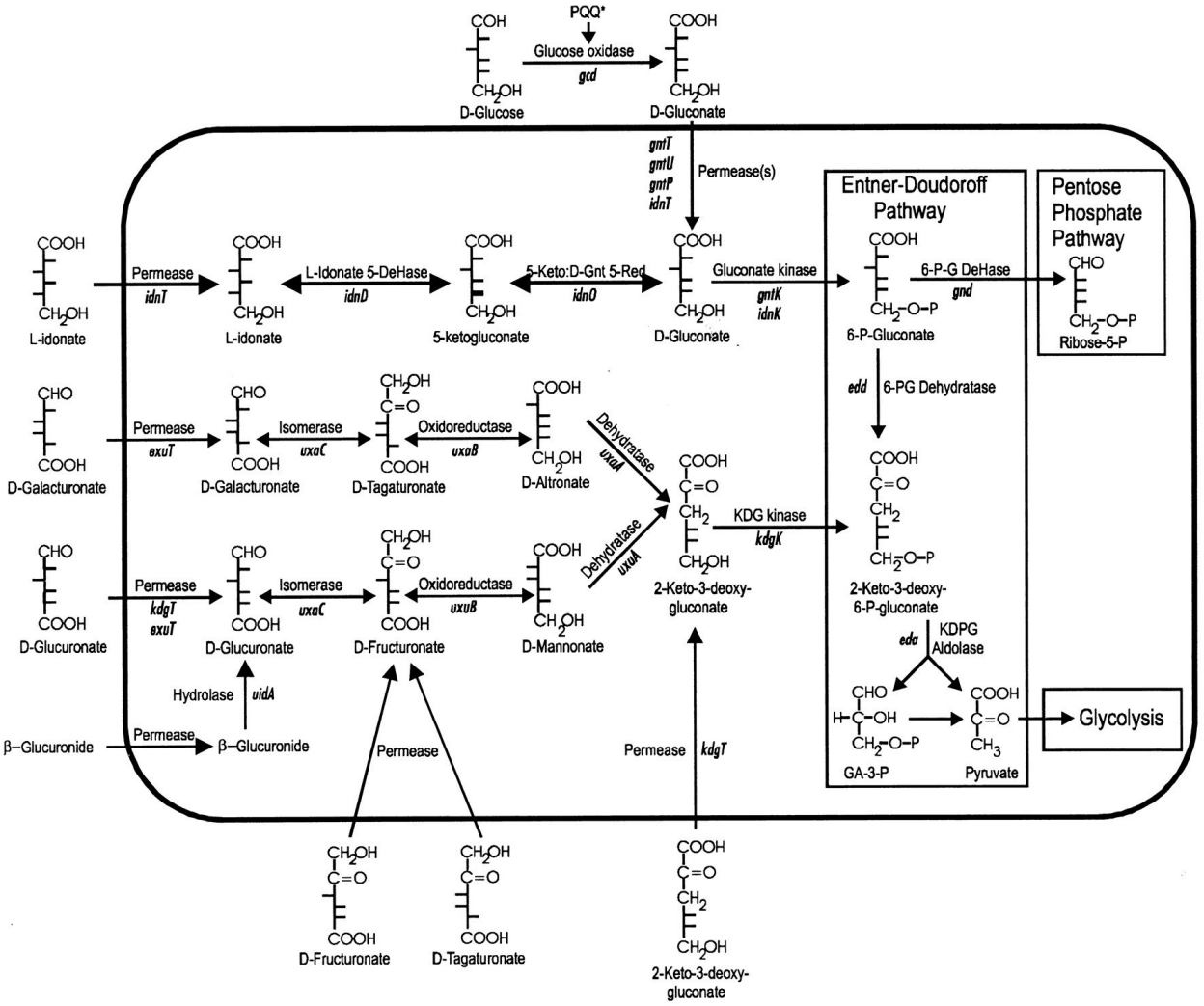

Vitamin B_{12} is commonly known as cyanocobalamin and is an essential B vitamin. Derivatives of B_{12} are used as cofactors in several enzyme catalyzed reactions found in eubacteria, archaebacteria, and eukaryotes. Higher plants don't need cobalamins and animals must acquire B_{12} from their diet (*12*). Deficiency of this vitamin causes pernicious anemia and is suspected to be a risk factor in neural tube defects (*13*). The biosynthetic pathway requires more than 20 enzymes to produce the complex macromolecule. The aerobic B_{12} biosynthetic pathway in *Pseudomonas denitrificans* has been well documented and contains two enzymes, cobyrinic acid *a,c*-diamide synthetase and cobyric acid synthetase (CobB and CobQ), that catalyze the six amidations of cobyrinic acid to produce cobyric acid (*12*). CobB catalyzes the amidation of carboxylate groups *c* and *a* of hydrogenobyrinic acid to produce hydrogenobyrinic acid *a,c*-diamide, see **Scheme 3**, while CobQ catalyzes the amidation of carboxylate groups *b, d, e,* and *g* on adenosyl-cobyrinic acid *a,c*-diamide to produce cobyric acid.

Scheme 3. Reaction catalyzed by CobB from *P. denitrificans*.

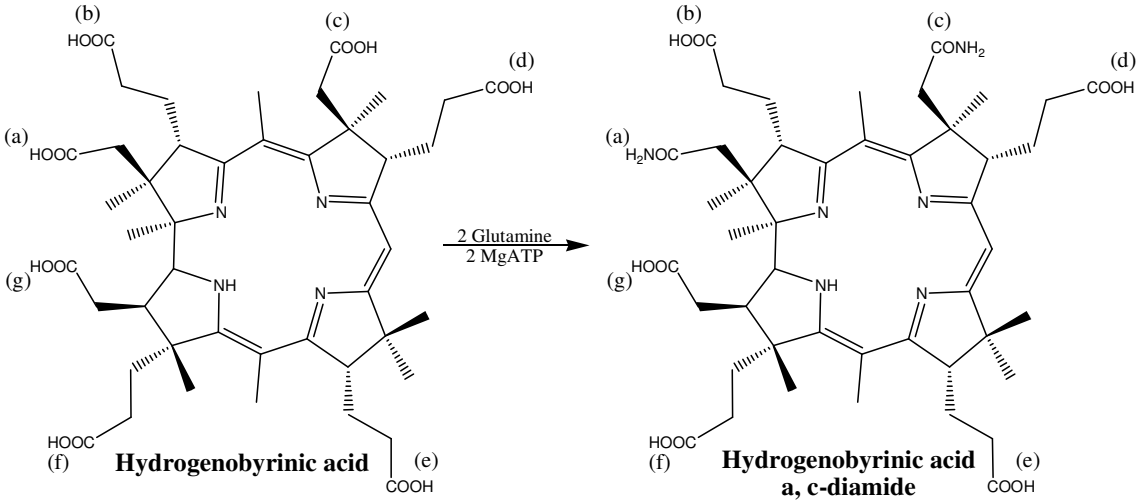

The CobQ reaction in the aerobic pathway is preceded by 4 enzymes which insert Co^{3+}, reduce the cobalt, and reacts the adenosine 5'carbon of adenosine with Co^{1+} to produce the cobalt-carbon bond of adenosyl-cobyrinic acid *a,c*-diamide, the substrate for CobQ. The reaction catalyzed by CobQ is shown in **Scheme 4.**

Scheme 4. The reaction catalyzed by CobQ from *P. denitrificans*.

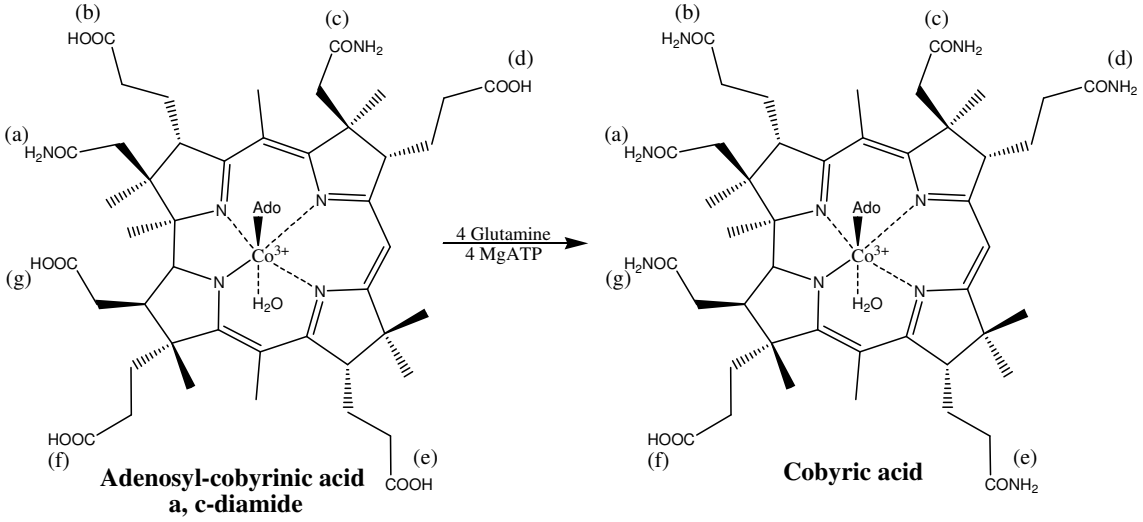

CobB and CobQ belong to the Triad family of amidotransferases (*14*). These enzymes contain glutamine amidotransferase domains like those found in carbamoyl phosphate synthetase (CPS) and GMP synthetase (*15, 16*). In these enzymes an active site histidine, which is hydrogen bonded to a glutamate, activates a cysteine residue for nucleophilic attack on the carboxamide moiety of glutamine forming a thioester intermediate and ammonia (see **Figure 3**). The ammonia is then translocated to an adjacent domain where it reacts with an activated intermediate. The cysteine and histidine residues of the catalytic triad are conserved in CobB and CobQ however the glutamate residue is missing. An alignment of CPS, GMP synthetase, CobB and CobQ is shown in **Figure 4**.

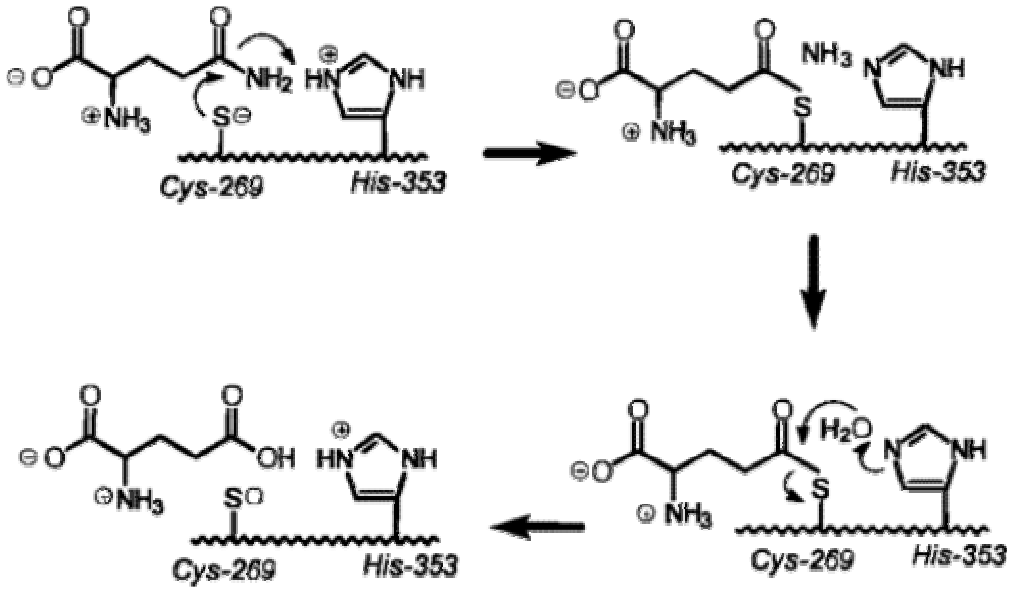

Figure 3. Model of chemical mechanism for hydrolysis of glutamine in CPS (*17*).

Cobyrinic acid a,c-diamide synthetases

COBB_PSEDE 284 AADAVYL-PGGYPEL-20-RGARIFGECGGYMVLGEGLVA-39-
CBIA_SALTY 292 DCQMIWL-GGGYPEL-20-RGVAIYAECGGLMYLGSTLED-42-

Cobyric acid synthetases

COBQ_PSEDE 291 DAGLVVI-PGSKSTI-20-RGGRVIGICGGYQMLGRRVTD-40-
CBIP_SALTY 290 DVDLVIL-PGSKNTL-20-QGVPVMGICGGYQMLGDTIVD-47-

GMP Synthetases

GUAA_ECOLI 50 NPSGIILSGGPESTT-13-AGVPVFGVCYGMQTMAMQLGG-36-
GUAA_YEAST 53 TPKGVILSGGPYSVY-13-LNVPILGICYGMQELAWINGK-28-

Carbamoyl phosphate synthetases

CARA_ECOLI 232 NPDGIFLSNGPGDPA-13-TDIPVFGICLGHQLLALASGA-22-
CARA_YEAST 223 EFDGIFLSNGPGNPE-18-DCIPIFGICLGHQLLALASGA-22-

Cobyrinic acid a,c-diamide synthetases		**NCBI id**
GPMTAHEFHYATIV-27-PVAGSFMHLIDVAGA	433	116833
EIVRGHEFHYSDFI-27-NTFASYLHVHFFAQR	447	543955
Cobyric acid synthetases		
VVLEGYEIHLGKTQ-23-RVMGTYLHGLFTSDA	437	231832
LPVRGYEIHMGETV-27-LAFGTYLHGLFDSDA	447	543955
GMP Synthetases		
PLLDVWMSHGDKVT-25-RFYGVQFHPEVTHTR	188	1GPN
NDSTVWMSHGDKLH-25-PIYGIQFHPEVTHST	183	1708073
Carbamoyl phosphate synthetases		
VVMITAQNHGFAVD-28-PAFSFQGHPEASPGP	360	1JDG
QCHITSQNHGYAVD-29-PIFSTQFHPEAKGGP	357	115625

Figure 4. Sequence alignment of the glutaminase domains of cobyrinic acid *a,c*-diamide synthetase, cobyric acid synthetase, GMP synthetase, and CPS. The amino acid residues of the catalytic triad are shown as white letters on red background. Yellow shading indicates conserved hydrophobic amino acid residues. Small residues and prolines which are conserved are highlighted in green.

Residues which could mimic the glutamate have not yet been identified but it was concluded with CPS that Glu355 is not essential for catalysis (*17*). In all of the amidotransferases studied so far, the activated intermediate that ammonia reacts with is located at a different domain, and sometimes a different polypeptide chain, far from the glutaminase active site (*15, 16, 18-21*). It has been demonstrated that many structurally characterized amidotransferase enzymes feature molecular tunnels which are used to translocate the ammonia to the activated intermediate (*21*). This is best illustrated in the crystal strucuture of CPS, **Figure 5**. The molecular tunnel spans nearly 100 Å connecting 3 distinct active sites (*15*). The glutaminase domains of amidotransferase enzymes share sequence and structural similarity. However, the synthetase domains are completely unrelated (*15, 16, 22*). The synthetase domain binds ATP and the corresponding substrate and in most cases, the substrate is activated via formation of a phosphorylated intermediate by ATP. The first half reaction of CPS offers a great example of this activation, see **Scheme 5** (*23*)**.**

Scheme 5. First half reaction of CPS showing substrate activation using ATP.

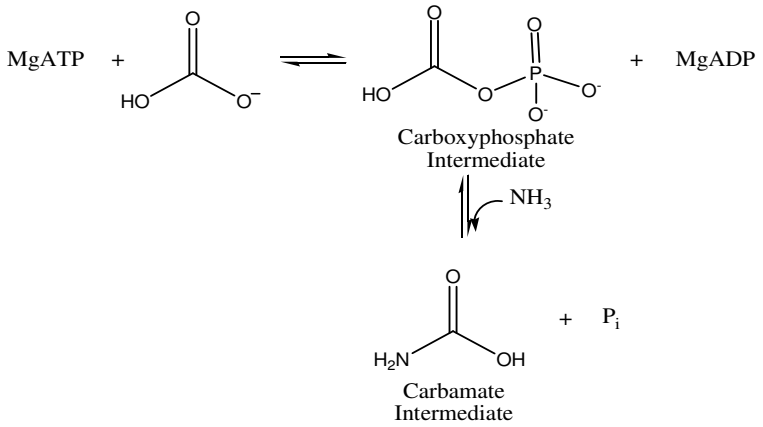

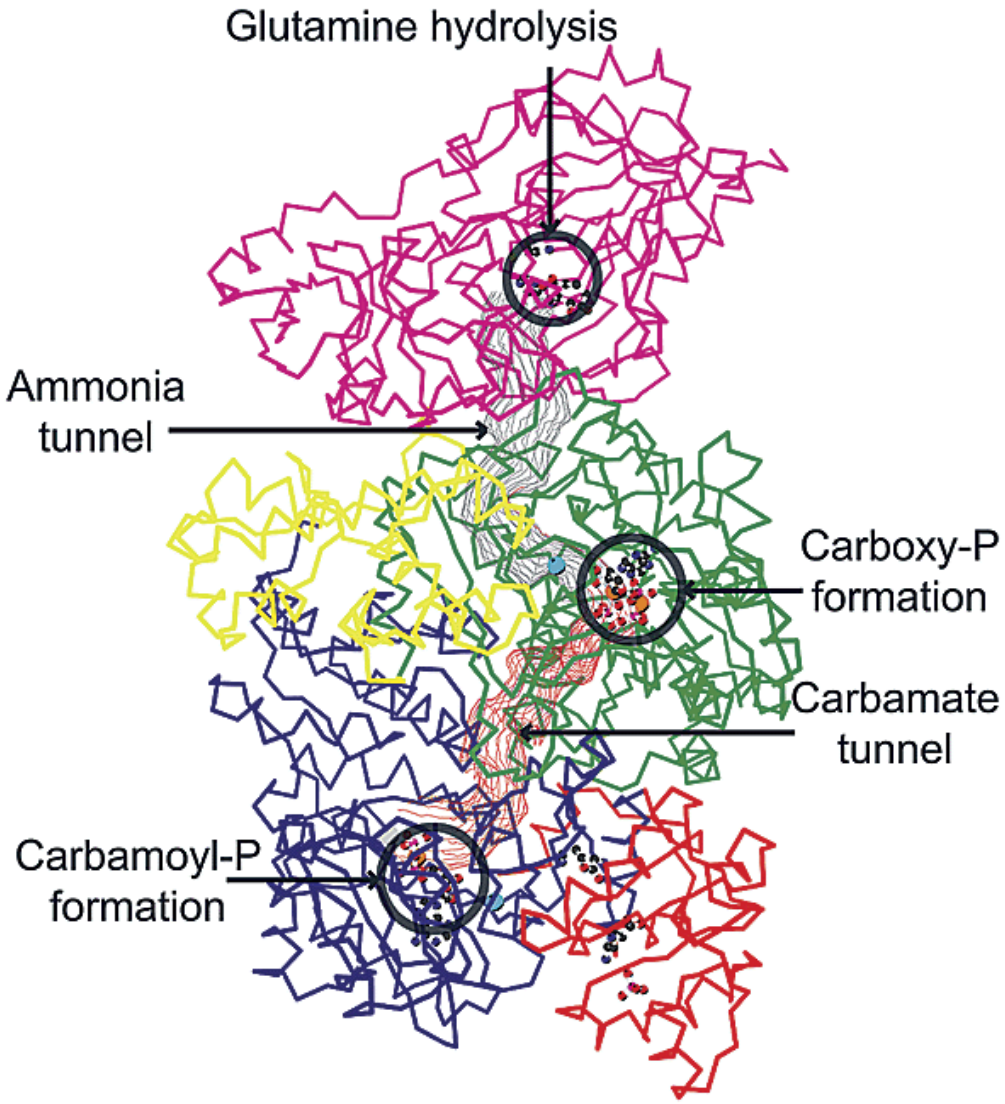

Figure 5. Structure of CPS from *E. coli* with the three active sites. The active sites are circled in black. The molecular tunnel is shown in gray and red. The amidotransferase domain is pink and labeled as the glutamine hydrolysis site (*15*).

The CobB and CobQ homologs in the anaerobic *Salmonella typhimurium* pathway were identified by sequence comparison (*14*). The genes cbiA and cbiP correspond to cobyrinic acid *a,c*-diamide synthetase and cobyric acid synthetase, respectively, which have been identified as the two enzymes responsible for these amidations in *S. typhimurium.* The substrate for CbiA differs slightly from the substrate utilized by CobB since the cobalt is inserted in the substrate prior to the CbiA reaction in the *S. typhimurium* pathway. The substrate for CbiA and the reaction catalyzed is shown in **Scheme 6.**

Scheme 6. Reaction catalyzed by *S. typhimurium* CbiA.

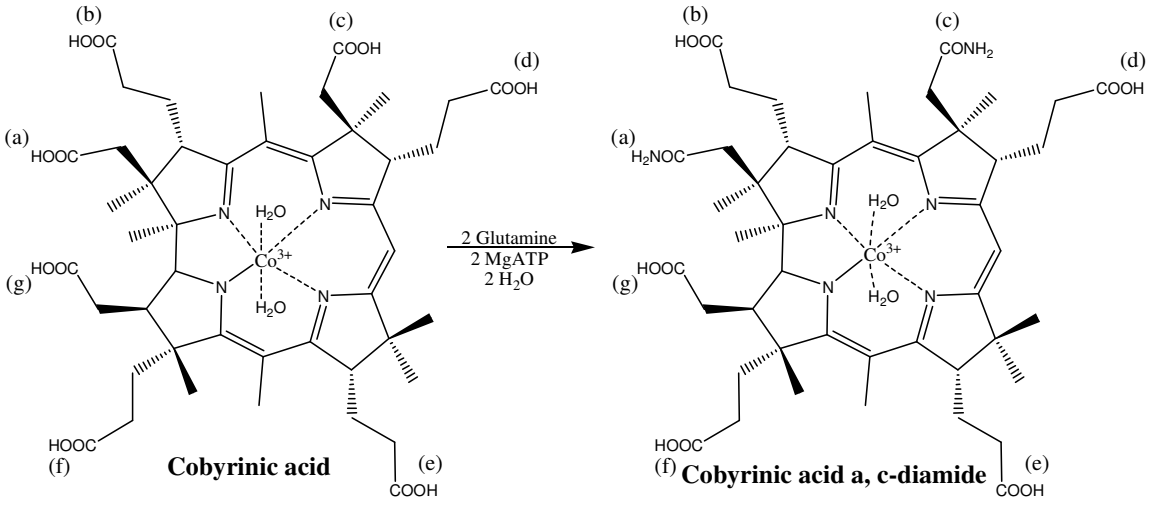

CbiA and CbiP are very intriguing since they catalyze successive reactions at different sites of the same substrate. CbiA catalyzes the amidation of carboxylate groups *c* and *a*, while CbiP catalyzes the amidation of carboxylate groups, *b, d, e*, and *g*. Other enzymes

catalyzing successive reactions at different sites of a substrate include uroporphyrinogen decarboxylase and 5-epiaristolochene 1,3-dihydroxylase.

5-Epiaristolochene 1,3-dihydroxylase (EDH) is a cytochrome P450 enzyme which catalyzes successive hydroxylations of 5-epiaristolochene (EA) at C1 and C3 to yield capsidiol, see **Scheme 7**. The reaction catalyzed by EDH has been shown to be regiospecific, stereospecific, and ordered (*24*). The possible intermediates of the EDH reaction, 1β(OH)EA and 3α(OH)EA, were synthesized and kinetic constants determined using either compound as a substrate (*24*). Though it is evident that EDH catalyzes the conversion of both monohydroxylated intermediates to capsidiol, the relative efficiency for 1β(OH)EA conversion is 10-fold greater. Reactions at high substrate concentrations demonstrate accumulation of 1β(OH)EA which suggests that the substrate, EA, must first be converted to 1β(OH)EA before capsidiol formation.

Scheme 7. Reaction catalyzed by 5-epiaristolochene 1,3-dihydroxylase (EDH).

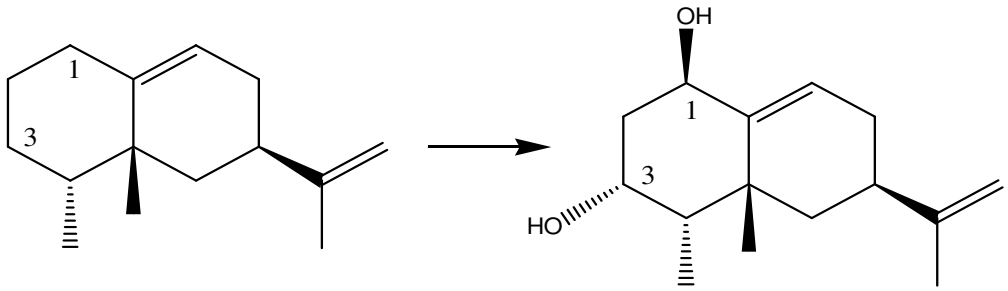

5-Epiaristolochene (EA) **Capsidiol**

A more interesting example is that of uroporphyrinogen decarboxylase which catalyzes successive decarboxylations in the heme biosynthetic pathway. The decarboxylation of 4 acetate side chains on uroporphyrinogen III to form coproporphyrinogen III is shown in **Scheme 8** (*25*). It has been concluded that the protein is a monomer, however, an ordered, processive, or dissociative mechanism has not been identified for this reaction. These reactions are interesting, but explanations for preferential binding orientation of a substrate with more than one reactive site are lacking, and assignment of the reaction order can be challenging.

Scheme 8. Successive decarboxylations catalyzed by uroporphorynigen decarboxylase.

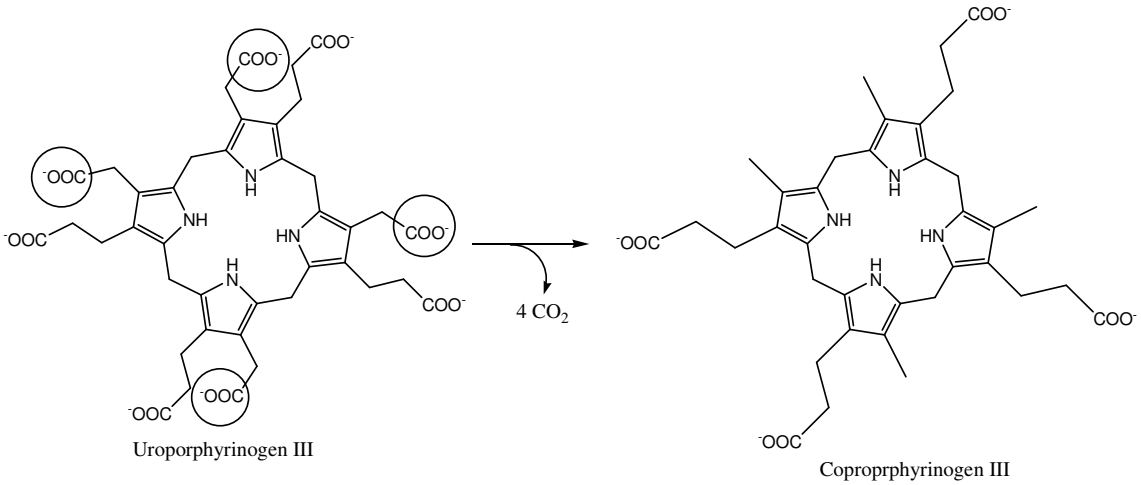

Uroporphyrinogen III

Coproprphyrinogen III

In this dissertation, the mechanism of uronate isomerase from *E. coli*, cobyrinic acid *a,c*-diamide synthetase from *S. typhimurium*, and cobyric acid synthetase from *S. typhimurium* will be investigated. Uronate isomerase has been classified as a member of the amidohydrolase superfamily from the structural characterization of the *T. maritima*

enzyme. Since this enzyme represents the first reported member of this superfamily that does not catalyze a hydrolysis reaction and does not require divalent cations for catalysis, uronate isomerase is an example of protein function divergence within a superfamily. The reaction catalyzed by uronate isomerase, an isomerization of D-glucuronate to D-fructuronate, is analogous to aldose-ketose isomerizations. Although the activity of uronate isomerase can be monitored with a coupled assay, this offers no insight into the mechanism of catalysis. Therefore, NMR spectroscopy has been employed to decipher the details of the mechanism, stereospecificity, and intermediate species. The activation of the substrates, cobyrinic acid and adenosyl-cobyrinic acid *a,c*-diamide, in the reactions catalyzed by CbiA and CbiP, respectively, have been studied by the positional isotope exchange technique. It is believed that the substrates are activated by phosphorylation, however, phosphorylation of an enzyme active site residue is feasible. The amidation of carboxylate groups *c* and *a* catalyzed by CbiA has been determined to be ordered and dissociative (*26*). CbiP is the amidotransferase that is responsible for the amidation of carboxylate groups *b, d, e*, and *g*. Since the enzymes catalyze similar successive reactions, it is assumed that the mechanism of CbiP is also ordered and dissociative. The order or the residues responsible for the order have not yet been identified. Analytical HPLC and 2D NMR spectroscopy have been used to elucidate these very intriguing details about the CbiP mechanism.

CHAPTER II

THE MECHANISM OF URONATE ISOMERASE: A NONHYDROLYTIC MEMBER OF THE AMIDOHYDROLASE SUPERFAMILY

Uronate isomerase catalyzes the isomerization of D-glucuronate to D-fructuronate as shown in **Scheme 9**. This reaction is analogous to other aldose-ketose isomerizations. Enzymes catalyzing these isomerizations are known to proceed via two mechanisms, a proton or hydride transfer. The proton transfer mechanism utilizes an active site base to abstract the proton from C2 while an active site acid donates a proton to the carbonyl oxygen at C1 forming an enediol intermediate. Intermediate formation is followed by transfer of the proton abstracted from C2 to C1 and abstraction of the hydrogen from the C2 hydroxyl thus forming the ketose product.

Scheme 9. Reaction catalyzed by uronate isomerase

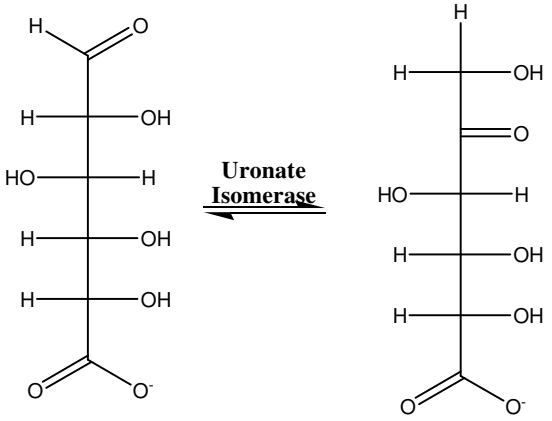

D-Glucuronate **D-Fructuronate**

.

The hydride transfer mechanism is achieved by deprotonation of the C2 hydroxyl by an active site base accompanied with a [1,2] hydride transfer and subsequent protonation of the C1 carbonyl by an active site acid yielding the product. These mechanisms are illustrated in **Scheme 10**. The distinctive feature of the proton transfer mechanism is the exchangeability of the C2 hydrogen with solvent in the presence of enzyme. Proton transfer mechanisms have been studied extensively with non-metalloenzymes phosphoglucose isomerase and triosephosphate isomerase (*27, 28*). The interconversion of (R)-glyceraldehyde-3-phosphate to dihydroxyacetone phosphate catalyzed by triosephosphate isomerase was shown to exchange a proton of the substrate and/or product with deuterium from solvent at a rate ~10-fold higher than the rate of product formation (*28*). D-Xylose isomerase is a metalloenzyme that requires Mg^{2+} as a cofactor and catalyzes the isomerization of D-xylose to D-xylulose via a [1,2] hydride transfer mechanism (*29*). Proton exchange with xylose isomerase occurred once every 1 billion turnovers which is 9 orders of magnitude slower than product formation (*30*).

Enzyme catalyzed aldose-ketose isomerizations are stereospecific. The abstracted hydrogen from C2 of the aldose substrate can be transferred on the *re*- or *si*-face of the carbonyl carbon at C1. Addition of the hydrogen to the *si*-face of the C1 carbonyl would designate the proton *pro-S* at C1 of the product. Alternatively, the proton would be assigned as the *pro-R* proton on C1 of the product if added to the *re*-face of the C1 carbonyl. This stereospecific transfer has been demonstrated with triosephosphate isomerase, phosphoglucose isomerase, and D-xylose isomerase.

Scheme 10. Mechanisms of enzyme catalyzed aldose-ketose isomerizations.

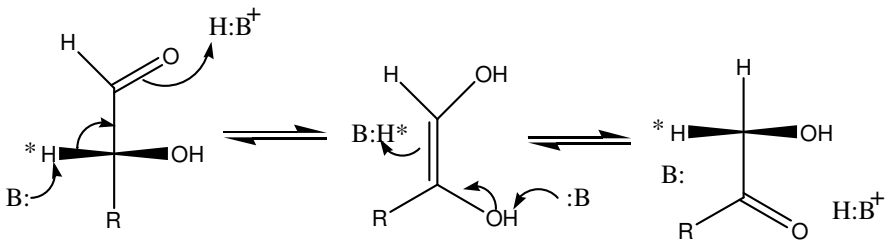

Proton Transfer Mechanism

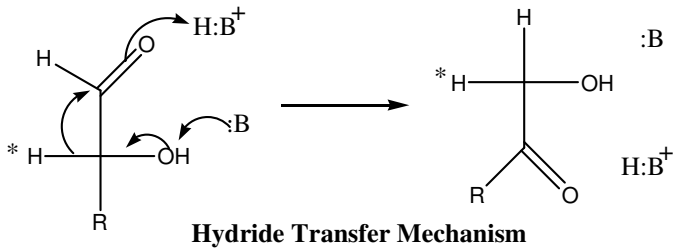

Hydride Transfer Mechanism

An active site glutamate from triosephosphate isomerase abstracts the C2 proton of (R)-glyceraldehyde-3-phosphate and transfers the proton to the *pro-R* position at C1 of dihydroxyacetone phosphate (*28*). Phosphoglucose isomerase exhibits similar stereospecific transfer of the reactive species *pro-R* proton via a cis-enediol intermediate (*31, 32*). Crystal structure data has assigned the hydrogen transferred in the reaction catalyzed by D-xylose isomerase as the *pro-R* proton on C1 of D-xylulose and confirmed metal interaction with the open chain aldehyde of the reactive anomer (*33*).

Uronic acids, like many six-carbon sugars, can exist as anomeric five and six member rings, open chain aldehydes, and trace amounts of hydrate species. Anomers are diastereomeric pairs that result from cyclization of monosaccharides and similar cyclizing uronic acids. Many enzymes catalyzing isomerizations of these acids/sugars are anomer specific. Therefore, the rate of the enzymatic reaction may be limited by 1)

the concentration of the reactive anomer, 2) the anomer interconversion rate, and/or 3) the ability of the enzyme to catalyze anomer interconversion. For example, the reversible isomerization of D-glucose-6-phosphate (G6P) to D-fructose-6-phosphate (F6P) is catalyzed by phosphoglucose isomerase (PGI) and has been demonstrated to be specific for α-G6P and β-F6P as shown in **Scheme 11** (*34, 35*).

Scheme 11. Reactions catalyzed by phosphoglucose isomerase.

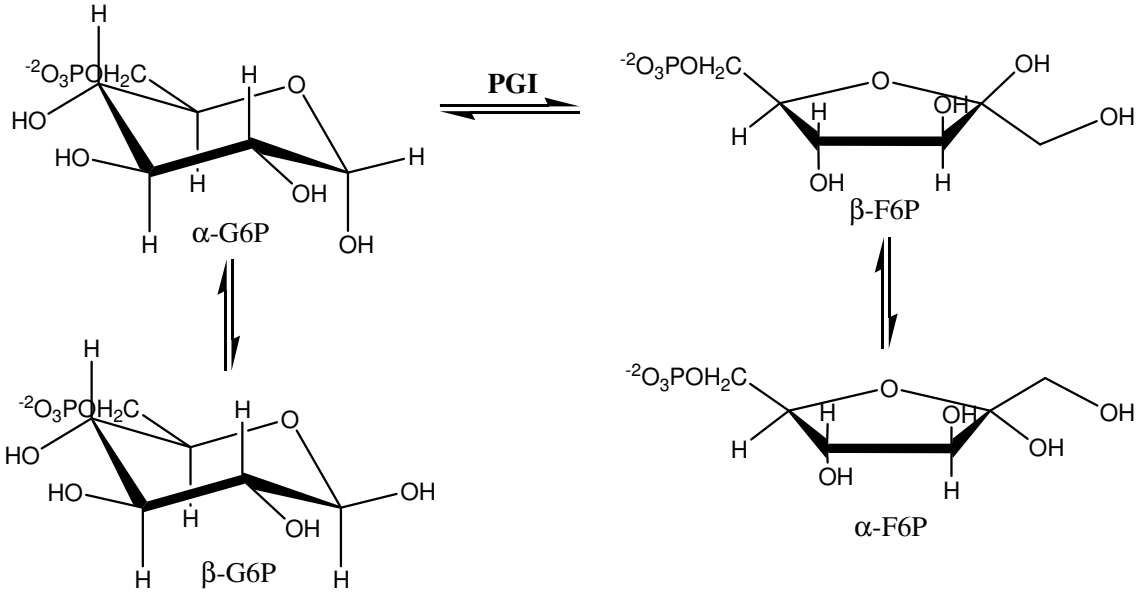

Thus the rate of the PGI reaction could be limited by the anomerization rate of β-G6P to α-G6P or α-F6P to β-F6P. The rate constants for the anomerization of G6P at 25ºC in aqueous solution have been reported as $k_{\alpha\beta} = 0.060\ s^{-1}$ and $k_{\beta\alpha} = 0.036\ s^{-1}$ (*34*). However, these rate constants increase to $1.38\ s^{-1}$ and $0.61\ s^{-1}$, respectively, when phosphoglucose isomerase is added to the solution (*35*). Therefore, the formation of product is not limited by the concentration of the α-anomer or the slow non-enzymatic anomerization

rate. D-glucuronate and D-fructuronate exist in solution as anomeric pyranose and furanose rings, respectively. Hence, an understanding about the equilibrium concentration of anomers in solution, anomer interconversion rates, and anomeric specificity of the enzyme are important when trying to elucidate details about the uronate isomerase mechanism. In addition to the possible rate limiting effects described above, various chemical events could be rate limiting factors also.

Kinetic isotope effects, changes of rate that occur upon isotopic substitution, have been widely used to elucidate reaction mechanisms. When deuterium is substituted for hydrogen, the changes in rate are attributed to the difference in zero-point energy of a C-H bond from a C-D bond. The zero-point energy is inversely proportional to the square root of the mass which means heavier isotope atoms lie at a lower energy in the ground state than lighter isotopes. These differences in energies result in different activation energy values thus giving rise to the kinetic isotope effect. Isotope effect experiments can provide information about kinetic and chemical mechanisms, as well as transition state structure, and rate limiting steps (*36*). Rate limiting steps involving isotope atoms or adjacent isotope atoms, will yield primary or secondary isotope effects. Primary isotope effects are a result of bond breaking to the isotope atom and secondary isotope effects result from bond cleavage of atoms adjacent to isotope atoms in the rate limiting step of the reaction. Values for k_H/k_D ranging from 2-15 are indicative of a C-H/C-D bond breaking in the rate limiting step of the reaction and values smaller could be secondary isotope effects (*37*). Kinetic isotope effects above unity are normal whereas

values below unity are called inverse effects. Experiments with isotope labeled D-glucuronate can determine whether the bond breaking is rate limiting or not.

In this chapter, the mechanism of uronate isomerase has been established by investigating the ability of the abstracted proton to exchange with solvent. The stereochemistry of the transferred proton has been determined and fluoro- substituted analogs have been demonstrated to be substrates. Kinetic isotope effects can be monitored by coupled assay, however, the isomerization mechanism, stereospecificity, anomerization, and anomeric specificity have been studied using NMR spectroscopy and molecular modeling.

Materials and Methods

Materials. D-Glucuronic acid was purchased from Acros Organics. HPLC columns and Ni^{2+} affinity resin were purchased from Amersham Biosciences. D-Mannonate and the D-mannonate dehydratase expression plasmid from *Novosphingobium aromaticivorans*, which was constructed by Dr. Wen Shan Yew, were generous gifts from the laboratory of Dr. John Gerlt at University of Illinois. 3-Deoxy-3-fluoro-D-glucuronate and [2-^{2}H]-D-glucuronate were synthesized by Dr. Yingchun Li in Dr. Raushel's laboratory.

NMR Measurements. ^{1}H NMR spectra were acquired on a Varian Unity or Inova-500 operating at a frequency of 500 MHz. Spectra were obtained using a 8000-Hz sweep width with a 2.5 s acquisition time and a 3 s relaxation delay between pulses. Saturation transfer (ST) NMR spectra were collected using the presaturation program in the Varian

software package. Saturation times were varied from 0.5 to 10 seconds at a saturation power of 10, a 0.005 second hardware delay was used in addition to a 60 second relaxation delay. The equilibrated solution used for ST-NMR contained 150 mM sodium D-glucuronate unbuffered at 24º C. ^{13}C exchanging systems (EXSY) NMR spectra were collected on a Varian Unity 500 operating at a frequency of 125 MHz. The 2D NOESY pulse sequence was used with an acquisition time of 0.164 seconds, relaxation delay of 2 seconds, and a maximum mixing time of 0.2 seconds. Standard parameters were used unless specifically noted. The total concentration of [1-^{13}C]-D-glucuronate was 52 mM and the enzyme concentration was 207 μM.

Proton Exchange Catalyzed by Uronate Isomerase. The ability of uronate isomerase to incorporate solvent isotopes into the substrate was studied by incubating the reaction in D_2O. The 1 mL assay contained 5 mM D-glucuronate, 50 mM P_i buffer, pD 8.0, and 10 μM uronate isomerase. ^1H NMR spectra were collected every hour for 24 hours and the exchange was monitored at the α-H1 and β-H1 resonance of D-glucuronate.

*Preparation of 2-keto-3-deoxy-*D*-Gluconate.* D-Mannonate, 25 mM, 50 mM P_i buffer, pH 7.8, 5 mM $MgCl_2$, and 695 nM D-mannonic acid dehydrase were incubated at room temperature overnight and then dried using a rotary evaporator. The solution was redissolved in 50 mM P_i buffer, pD 8.0 for NMR analysis.

Preparation of 2-keto-3-deoxy-[6-^2H]-D-Gluconate. D-Glucuronate was incubated with 10 μM uronate isomerase, 50 mM P_i, pD 8.0, in 99% D_2O. After 12 hours the proton at C2 is 92% substituted with deuterium. D-Mannonate dehydrogenase that

had been desalted into 50 mM P_i, pD 7.0, was added to the solution with 10 mM NADH and 1 μM uronate isomerase to ensure complete enzymatic production of [1-^{2}H]-D-mannonate. After 4 hours, the solution was checked by NMR to observe the product. The mixture was vortexed with 2 drops of CCl_4, filtered with a 0.2 Corning syringe filter to remove the enzymes then treated with activated charcoal to remove any NAD/NADH. The [1-^{2}H]-D-mannonate was incubated with 700 nM D-mannonic acid dehydratase, 50 mM P_i, pH 7.8, and 5 mM $MgCl_2$. After 8 hours, the solution was dried using a dry ice rotary evaporator and then redissolved in P_i, pD 8.0 for NMR analysis.

Purification of D-Mannonic Acid Dehydratase. The expression plasmid for D-mannonic acid dehydratase from *Novosphingobium aromaticivorans* was transformed into BL21 (DE3) competent cells and diluted in 1 mL of LB to be incubated at 37 ºC for 1 hour. After one hour, 100 μL of the small culture was plated on an ampicillin resistant plate and incubated overnight at 37 ºC. Single colonies were added to 5 mL of LB supplemented with 100μg/mL ampicillin and allowed to grow overnight at 25 ºC. These starter cultures were used to innoculate 3x 1L of LB supplemented with 100 μg/mL ampicillin and the cells were grown at 25 ºC for 48 hours. Ampicillin was added to the flask approximately every 10 hours. The cells were harvested and resuspended in 100 mL of buffer solution A, containing 5 mM imidazole, 500 mM NaCl, 5 mM $MgCl_2$, and 20 mM Tris-HCl, pH 7.9. The cells were lysed by sonication (15 minutes total, 5 seconds on, 2 seconds off) and centrifuged for 1 hour at 13,000g. The cell lysate was applied to a Chelating Sepharose Fast Flow column in buffer solution A. The Ni^+ affinity column had been previously charged with 50 mM $NiSO_4$, and then washed with buffer

solution A. After the cell lysate was applied to the column, it was washed with 200 mL of buffer solution A, 300 mL of 95% buffer solution B-5% buffer solution C. Buffer solution B contained 60 mM imidazole, 500 mM NaCl, 5 mM $MgCl_2$, and 20 mM Tris-HCl, pH 7.9. Buffer solution C contained 1M imidazole, 500 mM NaCl, 5 mM $MgCl_2$, and 20 mM Tris-HCl, pH 7.9. The protein was then eluted with 360 mL of 50% buffer A-50% buffer D. Buffer D contained 100 mM EDTA, 500 mM NaCl, and 20 mM Tris-HCl, pH 7.9. Thirty-six fractions were collected. The pooled enzyme was dialyzed against 20 mM P_i buffer, pH 7.8 with 5 mM $MgCl_2$ for a total of 8 hours with buffer changes every two hours.

Purification of Uronate Isomerase. The cells used were a generous gift from Tinh Nguyen and were resuspended in 50 mM HEPES buffer, pH 8.0 (plus 1 mM DTT final concentration) in a volume that was three times the weight of the cells. The cells were then sonicated at 60% duty for 20 minutes in an ice bath in a cold room. A solution of protamine sulfate (determined by the cell pellet weight) was added slowly to the cell solution with stirring for 15 minutes while still in the ice bath. The cell solution was then centrifuged at 13000g for 20 minutes and the volume of the supernatant was measured. An amount of ammonium sulfate was weighed out to obtain a 60% ammonium sulfate solution. The ammonium sulfate was ground up and added to the supernatant in ten to fifteen parts until dissolved (about 45 minutes). The solution was centrifuged at 13000g for 20 minutes, and the cell pellet was resuspended in a minimal amount of 50 mM HEPES buffer, pH 8.0. A maximum volume of 13 mL of the filtered protein was loaded onto the equilibrated HPLC-Superdex 200 column and collected

using 50 mM HEPES buffer, pH 8.0, with 1 mM DTT at a flow rate of 2.5 mL/minute. To determine the purity of the UAI, SDS-PAGE gels were taken and activity assays were performed. For further purification, a maximum volume of 50 mL of the filtered Superdex 200 pool was loaded onto the equilibrated HPLC-Resource Q column and collected using 20 mM HEPES, pH 8.0 as buffer A and 20 mM HEPES, pH 8.0 with 1 M NaCl as buffer B at 4 mL/minute and a 30% gradient. When further purification was desired, the filtered protein was collected and applied to the Superdex 200 and eluted at a flow rate of 1.5 mL/minute.

Purification of D-Mannonic Acid Dehydrogenase. Cell paste was a generous gift from Tinh Nguyen in the Raushel laboratory. The cells were sonicated at a 60% duty for 20 minutes in an ice bath in the cold room. A solution of protamine sulfate (determined by the cell pellet weight) was added slowly to the cell solution with stirring for 15 minutes while still in the ice bath. The cell solution was then centrifuged at 13,000g for 20 minutes and the volume of the supernatant was measured. Ammonium sulfate was weighed out in order to get a 70% ammonium sulfate solution. The ammonium sulfate was ground and added to the supernatant in ten parts until dissolved (about 60 minutes). The solution was centrifuged at 13,000g for 20 minutes, and the cell pellet was resuspended in a minimal amount of 50 mM HEPES buffer, pH 8.0. A maximum volume of 13 mL of the filtered protein was loaded onto the equilibrated HPLC-Superdex 200 column and collected using 50 mM HEPES buffer, pH 8.0 with 1 mM DTT at a flow rate of 2.5 mL/minute. To determine the purity of the MDH, SDS-page gels were taken and activity assays performed. For further purification, a maximum

volume of 50 mL of the filtered Superdex 200 pool was loaded onto the equilibrated HPLC-Resource Q column and collected using 20 mM HEPES, pH 8.0 as buffer A and 20 mM HEPES, pH 8.0 with 1 M NaCl as buffer B at 4 mL/minute and a 50% gradient.

Purification of D-*Glucuronate and [2-^{2}H]*-D-*Glucuronate by HPLC.* Twenty-six micromoles of [2-^{2}H]-D-glucuronate was applied to a 5 mL High Performance Q Sepahrose anion exchange column purchased from Amersham Biosciences. The compound was eluted at 1 mL min^{-1} with 75 mM TEA-HCO_3 pH 7.6 as buffer B using a linear gradient. The target concentration was 30% buffer B and 45 column volumes long. Eighty micromoles of D-glucuronate was applied to the same column and eluted in the same manner. The fractions were assayed for uronate isomerase activity via coupled assay.

Synthesis of [1-^{13}C]-D-*Glucuronate.* Methyl [1-^{13}C]-D-glucose was prepared following the procedure outlined by Podlasek (*38*). Methyl [1-^{13}C]-D-glucose (0.5 g., 2.8 mmol) and sodium bromide (0.32 g., 3.1 mmol) were dissolved in water (40 mL) and sodium hypochlorite (6 mL, 10-13% aqueous solution, 12 mmol) was added and the pH adjusted to 10 by the addition of HCl (1 M). The reaction was initiated by adding TEMPO (2,2,6,6-tetramethyl-1-piperidinyloxy, 10 mg) while stirring. To keep the pH of the reaction mixture ~10, NaOH (1 M) was added dropwise during the reaction. After 60 minutes, the pH of the solution stopped changing significantly and the reaction was quenched with methanol (5 mL). After removal of the water under reduced pressure, the solid residue was washed with methanol 3 times. The methanol solutions were combined, condensed to dryness and the residue dissolved in water (20 mL) and passed

through a Dowex-H+ cation exchange column. Methyl [1-^{13}C]-D-glucuronic acid was dissolved in concentrated HCl (37%). The resulting solution was stirred at 4 ^{o}C for 4.5 days and then the reaction mixture was condensed to dryness. The residue was dissolved in water (50 mL) and purified on a DEAE- Sephadex anion exchange column (HCO_3^- form). The compound was eluted with a 2.4 L gradient of sodium bicarbonate (10 mM to 80 mM). Fractions containing [1-^{13}C]-D-glucuronic acid were collected and condensed to dryness. The residue was treated with Dowex-H^+ cation exchange resin to remove the bicarbonate. The solution was then condensed to dryness to yield [1-^{13}C]-D-glucuronic acid with 53% yield.

Isotope Effect Assays. D-Glucuronate and [2-^{2}H]-D-glucuronate were varied from 0.2 – 3.5 mM in assays containing 0.25 mM NADH, 0.03 mg ml^{-1} MDH, and 1 nM uronate isomerase. The reaction was initiated by addition of uronate isomerase and the decrease in absorbance at 340 nm monitored as a function of time. The values of k_{cat}, K_a, and k_{cat}/K_a for the conversion of D-glucuronate or [2-^{2}H]-D-glucuronate to D-fructuronate or [1-^{2}H$_1$]-D-fructuronate were determined by fitting the velocity data to equation 1.

$$v / E_t = (k_{cat}[A]) / (K_a + [A]) \qquad (1)$$

*Enzymatic Transformation of 3-deoxy-3-fluoro-*D*-glucuronate.* 3-Deoxy-3-fluoro-D-glucuronate was used to probe the presence of a C2 carbanion intermediate species which would result in fluoride elimination. ^{19}F NMR spectra were collected every 30 minutes for a sample containing 10 mM 3-deoxy-3-fluoro-D-glucuronate, 50

mM P_i pD 8.0, and 0.1 μM UAI. The concentration of fluoride increased from 0.6 mM to 5.6 mM after 18 hours and upon further incubation or addition of more UAI, no starting material could be detected.

Results

Proton Exchange Catalyzed by Uronate Isomerase. The mechanism of uronate isomerase was probed by incubating the enzyme in 98% D_2O and examining the changes in the ^1H NMR spectra over a period of 24 hours. Spectral differences were observed at the C1 and C2 proton resonances of α- and β-D-glucuronate. The C1 proton of α-D-glucuronate is coupled to the C2 proton with a ^3J value of 4.0 Hz, thus giving rise to a doublet at 5.09 ppm in the starting material. After 8 hours, the species which are coupled to the C2 proton have decreased, and after 24 hours the C1 proton resonance appears as a singlet shifted slightly upfield. These spectral changes are shown in **Figure 6 A-C**. Similar changes occur at the C1 proton resonance of β-D-glucuronate with the exception that the chemical shift did not change, shown in **Figure 7 A-C**. Resonances for the C2 proton of both α- and β-D-glucuronate are reduced to levels consistent with the proton content of the assay. These spectra illustrate decreased vicinal proton coupling as a result of deuterium substitution at C2 of D-glucuronate. The ^2H-C2 species were quantified using integration values for coupled and uncoupled species at C1, plotted as a function of time, and fit to a single exponential rate equation which yielded a rate constant of 0.13 hr^{-1}. After the total substrate and enzyme concentration are taken in to account, this represents a deuterium substitution every 11,000 turnovers.

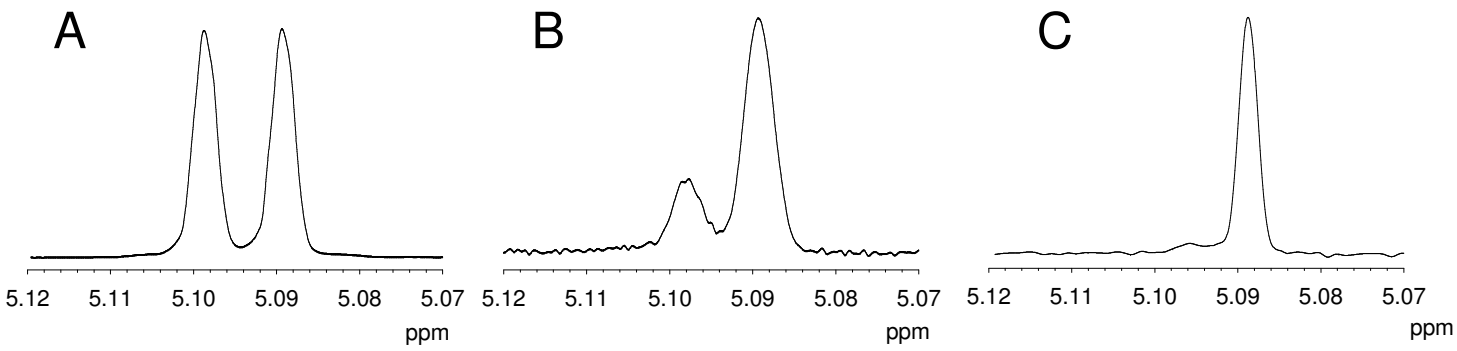

Figure 6. Spectral changes observed at H1 of α-D-glucuronate. A) Spectrum after 0 hours, B) 8 hours, and C) 24 hours incubation in 98% D_2O with 10 μM uronate isomerase at pH 8.0. The starting concentration of D-glucuronate was 5 mM.

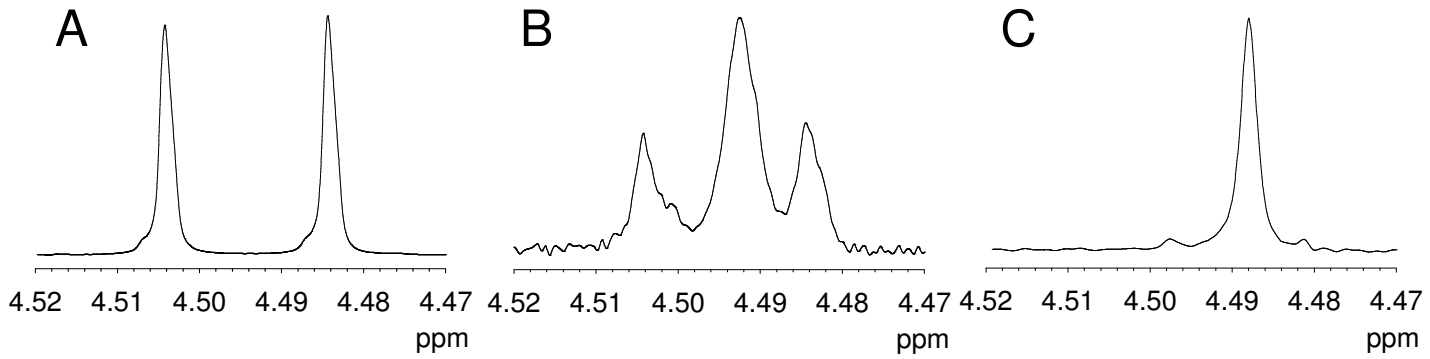

Figure 7. Spectral changes observed at H1 of β-D-glucuronate. A) Spectrum after 0 hours, B) 8 hours, and C) 24 hours incubation in 98% D_2O with 10 μM uronate isomerase at pH 8.0. The starting concentration of D-glucuronate was 5 mM.

Fluoride Elimination. If a cis-enediol intermediate is formed in the uronate isomerase reaction, the presence of an electron withdrawing group on C3 of D-glucuronate should result in rearrangement of the intermediate to eliminate the electron withdrawing group. The fluorinated substrate analogue, 3-deoxy-3-fluoro-D-glucuronate was used to probe this phenomenon. A representation of the proposed mechanism is shown in **Scheme 12**.

Scheme 12. Proposed mechanism for fluoride elimination catalyzed by uronate isomerase.

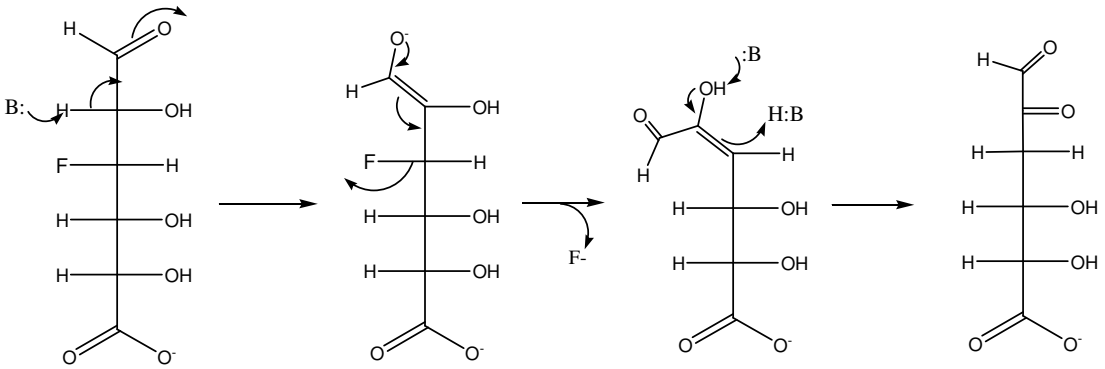

3-deoxy-3-fluoro-D-glucuronate

The fluoride concentration was calculated by integrating the ^{19}F NMR spectra collected over a period of 48 hours. The fluoride concentration increases to 8.9 mM after 48 hours of incubation with enzyme from 0.6 mM in the starting material. An approximate rate was calculated by plotting the concentration of fluoride as a function of time after 12 hours of incubation. The fit yielded a rate of 0.85 s^{-1}. In the absence of enzyme there was no increase in the fluoride concentration over a period of 48 hours at pH 8.0. The starting and ending spectra of the samples incubated with uronate isomerase are shown in **Figure 8**.

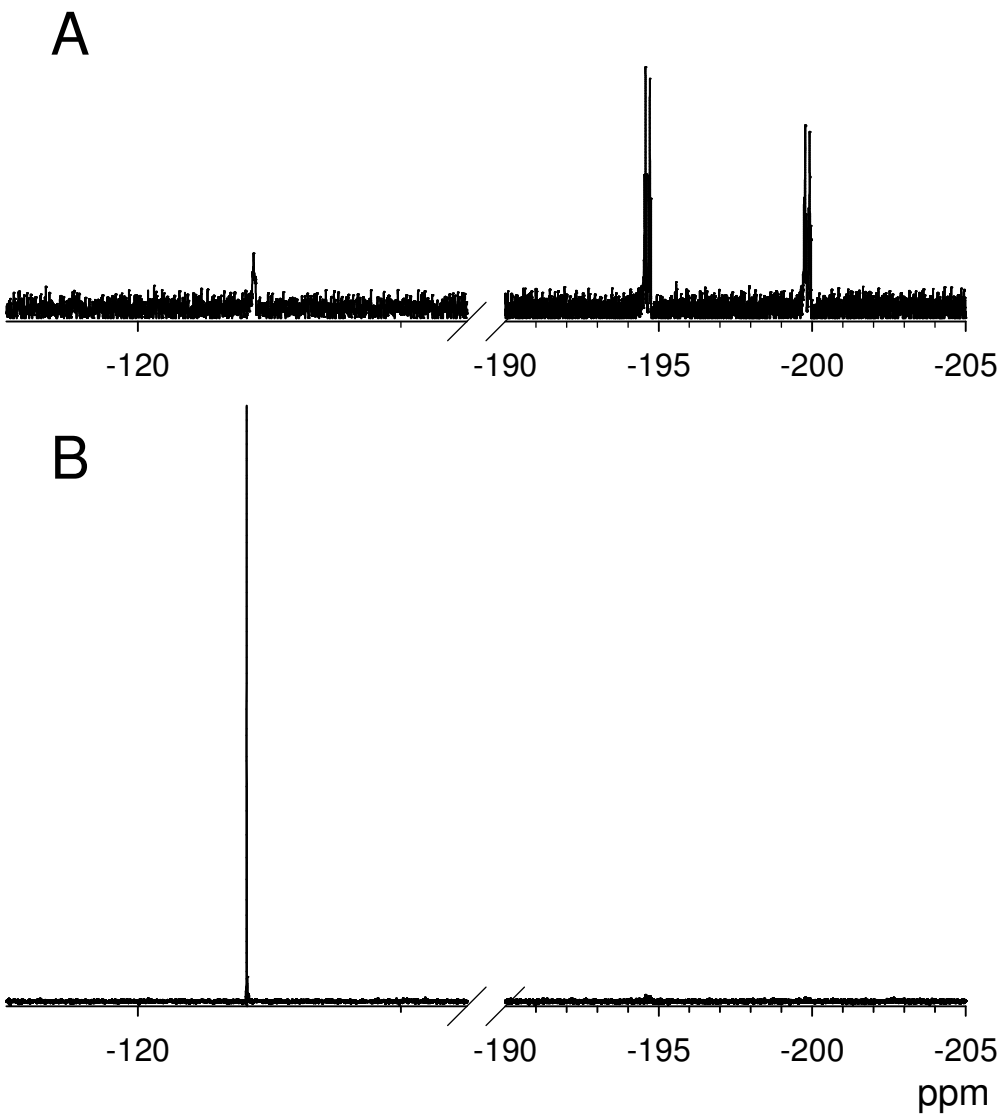

Figure 8. ^{19}F NMR spectra. (A) ^{19}F NMR spectra of 10 mM 3-deoxy-3-fluoro-D-glucuronate at pH 8.0 in the absence of uronate isomerase. The free F^- concentration was estimated to be 0.6 mM based on the integration of the NMR signal for the fluoride at -120.9 ppm and the two anomers of 3-deoxy-3-fluoro-D-gluconate at -194.6 and -199.8 ppm. (B) ^{19}F NMR spectrum of the reaction mixture after the addition of 0.1 μM uronate isomerase to a 10 mM sample of 3-deoxy-3-fluoro-D-glucuronate after 48 hours.

Stereospecificity of the Uronate Isomerase Reaction. The product of the uronate isomerase reaction, D-fructuronate, forms cyclic furanose anomers in solution. The methylene protons are indistinguishable by NMR due to small chemical shift differences and lack of vicinal proton coupling, so the stereochemistry of the methylene protons can not be established by analysis of the D-fructuronate ^{1}H NMR spectra. Subsequent enzymes in the uronic acid metabolism pathway have been used to assign the stereochemistry since the methylene carbon of interest is not altered in the reactions which follow. D-Mannonate dehydrogenase catalyzes the reduction at C2 of D-fructuronate to produce D-mannonate. It must be noted that the reduction of the keto-functional group changes the numerical assignment in D-mannonate, C1 of D-fructuronate becomes C6 in D-mannonate. D-Mannonate dehydratase then catalyzes the irreversible dehydration at C2 and C3 of D-mannonate to form cyclic 2-keto-3-deoxy-D-gluconate. These reactions are outlined in **Scheme 13**.

Scheme 13. Enzymes in the uronic acid metabolism pathway used to synthesize 2-keto-3-deoxy-D-gluconate.

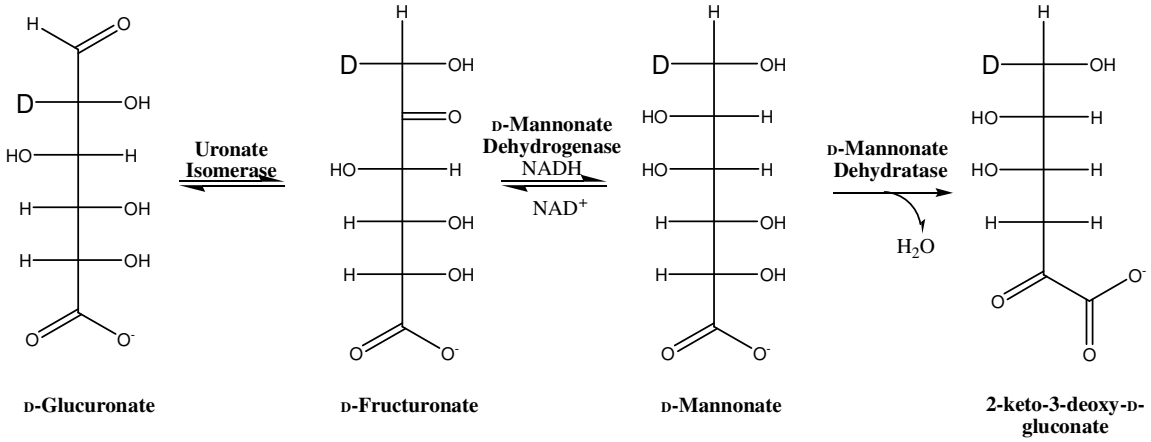

Therefore, the proton transferred in the uronate isomerase reaction is located on prochiral C6 of pyranose 2-keto-3-deoxy-D-gluconate, and the stereochemistry has been assigned by utilizing molecular modeling and ^{1}H NMR spectroscopy.

Molecular modeling has proved very useful for interpreting molecular structure and configuration of organic compounds. Approximation of vicinal coupling constant values using valence bond theory was outlined by Martin Karplus (*39, 40*). Theoretical formulas proposed by Karplus take in to account bond angles, bond lengths, and dihedral angles to calculate general trends of vicinal coupling constants and have been used to facilitate analysis of complex NMR spectra. Distinction between *pro-R* and *pro-S* protons on C6 of 2-keto-3-deoxy-D-gluconate may be achieved by considering the *cis* or *trans* coupling with the vicinal proton on C5. The Karplus relationship has shown that vicinal protons with dihedral angles near 0º or 180º, as in the *trans* configuration, yield large coupling constants, and vicinal protons with dihedral angles near 90º, the *cis* configuration, yield smaller coupling constants. Models of pyranose α-2-keto-3-deoxy-D-gluconate were constructed using Chem3D Ultra. The model adopts a chair conformation with the axial *pro-S* proton on C6 trans to its vicinal neighbor and the equatorial *pro-R* proton *cis*, this is shown in **Scheme 14.** The measured dihedral angles were 170º and 53º respectively.

Scheme 14. Structure of α-2-keto-3-deoxy-D-gluconate.

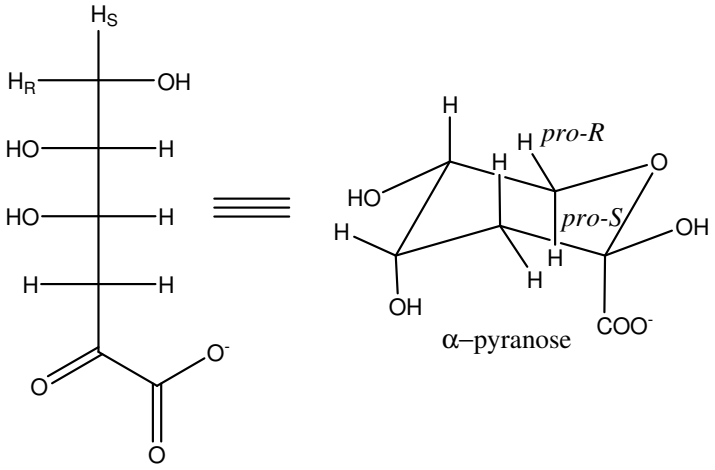

The dihedral angles were used in equations 2 or 3 to calculate approximate coupling constants between protons on C5 and C6 of pyranose α-2-keto-3-deoxy-D-gluconate (*39*). These equations yielded coupling constants of 8.9 Hz for ^{3}J*pro-S*-H and 2.7 Hz for ^{3}J*pro-R*-H of pyranose α-2-keto-3-deoxy-D-gluconate. These estimates were used to analyze the ^{1}H NMR spectrum of 2-keto-3-deoxy-D-gluconate.

$$^{3}J = 8.5\cos^{2}\Phi - 0.28 \quad (0° < \Phi < 90°) \qquad (2)$$

$$^{3}J = 9.5\cos^{2}\Phi - 0.28 \quad (90° < \Phi < 180°) \qquad (3)$$

Four species of 2-keto-3-deoxy-D-gluconate exist in aqueous solution at pH 8 as determined by ^{1}H NMR. The species and percentages are as follows: β-pyranose 49%, α-furanose 23%, β-furanose 17%, and α-pyranose 11%. Chemical shifts and coupling

constants for pyranose 2-keto-3-deoxy-D-gluconate species are listed in **Table 2**. Assignment of the prochiral methylene protons on C6 was based upon observed coupling constants for the *cis* or *trans* configuration. Double decoupled 1D NMR experiments allowed accurate assignment of values for the *pro-R* proton which was partially eclipsed by α- and β-furanose species. Experimental values were compared to values calculated from the model and are in agreement.

Table 2. Chemical shift and coupling constants for 2-keto-3-deoxy-D-gluconate and 2-keto-3-deoxy-[2-^{2}H]-D-gluconate. Chemical shift values of 2-keto-3-deoxy-[2-^{2}H]-D-gluconate which differ are represented in parentheses.

Proton	β-pyranose δ-values	Coupling Constants (Hz)	α-pyranose δ-values	Coupling Constants (Hz)
Ha	1.742	^{2}Ja-b = 13 ^{3}Ja-c = 5	2.043	^{2}Ja-b = 14 ^{3}Ja-c = 4
Hb	1.867	^{3}Jb-c = 12	1.813	^{3}Jb-c = 7
Hc	3.941	^{3}Jc-d = 3	3.903	^{3}Jc-d = 3
Hd	3.723 (3.726)	^{3}Jd-proS = 2.5	3.677 (3.669)	^{3}Jd-proS = 7
Hpro-S	3.656 (3.642)	^{2}JproS-proR = 13 (N/A)	3.762 (3.740)	^{2}JproS-proR = 12 (N/A)
Hpro-R	3.864 (N/A)	^{3}Jd-proR = 1.5 (N/A)	3.529 (N/A)	^{3}Jd-proR = 2.5-3 (N/A)

An equilibrium mixture of [2-^{2}H]-D-glucuronate/ [1-^{2}H$_{1}$]-D-fructuronate was used to enzymatically synthesize 2-keto-3-deoxy-[6-^{2}H]-D-gluconate for the stereochemistry assignment of the proton transferred in the uronate isomerase reaction. The ^{1}H NMR spectrum of 2-keto-3-deoxy-[6-^{2}H]-D-gluconate was compared to the spectrum of 2-keto-3-deoxy-D-gluconate and the differences observed in the pyranose species are represented by parentheses in **Table 2**. The *pro-S* proton resonances shift upfield and ~93% of the geminal coupling is lost. The residual proton content is consistent with the

proton content of the glucuronate/fructuronate equilibrium mixture used to synthesize the compound. The *pro-R* resonances were reduced to less than 6% which is also consistent with the proton content of the equilibrated glucuronate/fructuronate mixture. The spectral differences for α-2-keto-3-deoxy-D-gluconate are outlined in **Figure 9**, and the spectral differences for β-2-keto-3-deoxy-D-gluconate are shown in **Figure 10**.

Anomerization of D-*glucuronate.* The equilibrium composition of pyranose or furanose compounds in solution can be determined by standard ^{1}H or ^{13}C NMR spectroscopy. However the anomerization rate at equilibrium may not be detectable by standard NMR techniques. ^{1}H and ^{13}C ST NMR has been used to evaluate the reaction kinetics of furanose and pyranose systems (*41, 42*). The saturation transfer technique involves saturating one resonance of the exchanging components in a solution which is in slow chemical exchange. Upon saturation by steady-state irradiation of one resonance, the transfer of saturation can be observed at the corresponding resonance of the other species in solution.

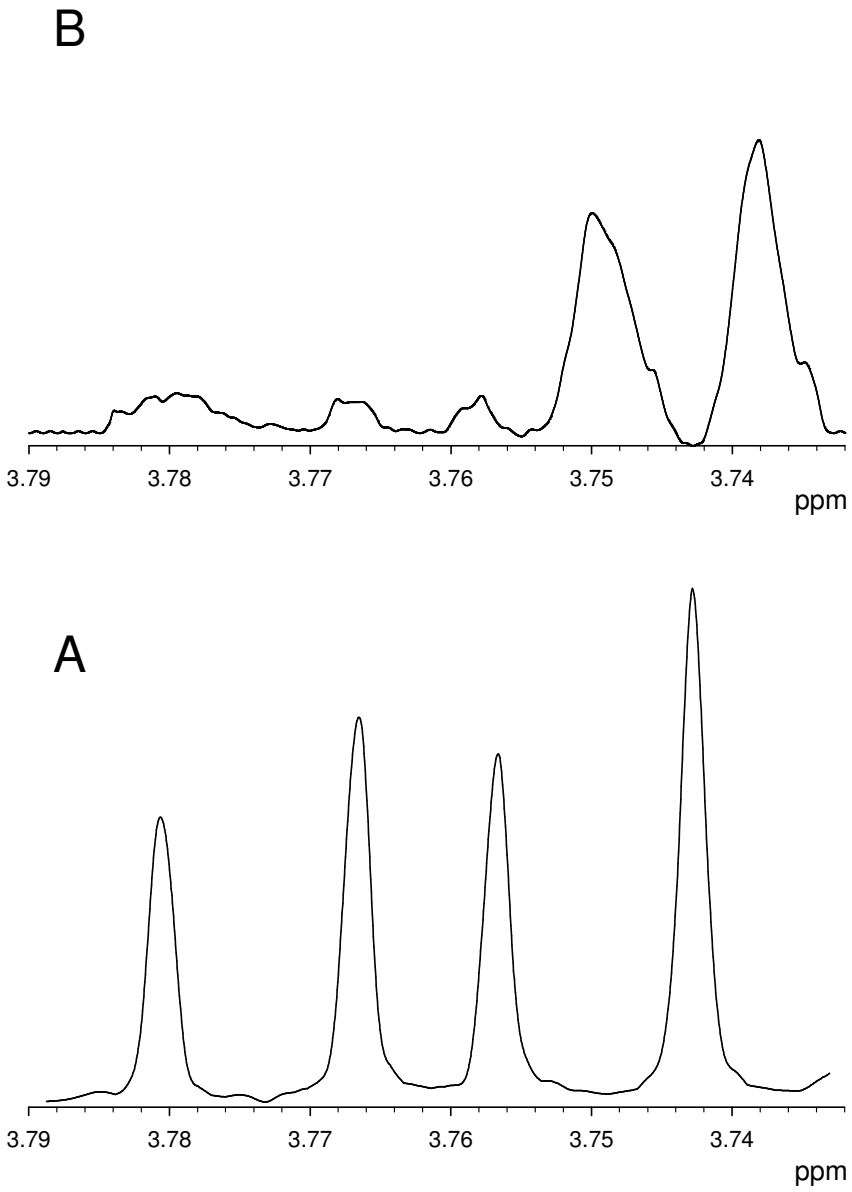

Figure 9. NMR spectra of α-KDG. (**A**) ^{1}H NMR spectrum of the *pro-S* hydrogen at C6 of the α-pyranose anomer of 2-keto-3-deoxy-D-gluconate. (**B**) ^{1}H NMR spectrum of the *pro-S* hydrogen at C6 of the α-pyranose anomer 2-keto-3-deoxy-[6-^{2}H]-D-gluconate.

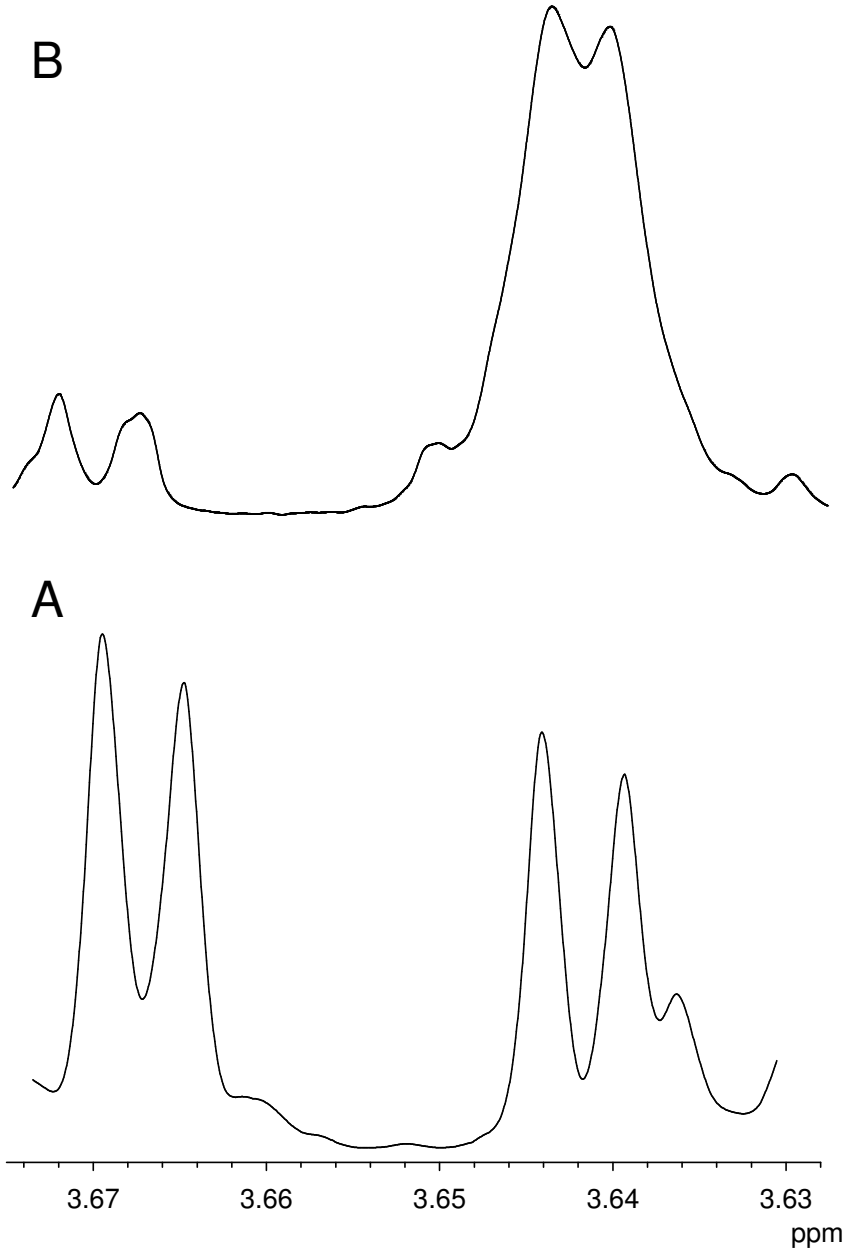

Figure 10. NMR spectra of β-KDG. (**A**) ^{1}H NMR spectrum of the *pro-S* hydrogen at C6 of the β-pyranose anomer of 2-keto-3-deoxy-D-gluconate. (**B**) ^{1}H NMR spectrum of the *pro-S* hydrogen at C6 of the β-pyranose anomer 2-keto-3-deoxy-[6-^{2}H]-D-gluconate.

Measuring the peak intensities as a function of saturation time, τ, will provide a slope used to calculate the rate constant for ring-opening, $k_{\alpha a}$ and $k_{\beta a}$. Rate constants for ring-closure, $k_{a\alpha}$ and $k_{a\beta}$, can be calculated from equilibrium constants, K_α, K_β, and ring-opening constants, $k_{\alpha a}$ and $k_{\beta a}$. Using equations 4 and 5 will allow for calculation of anomerization rates $k_{\alpha\beta}$ and $k_{\beta\alpha}$ (*41*).

$$k_{\alpha\beta} = k_{\alpha a}k_{a\beta} / k_{a\alpha} + k_{a\beta} \qquad (4)$$

$$k_{\beta\alpha} = k_{\beta a}k_{a\alpha} / k_{a\alpha} + k_{a\beta} \qquad (5)$$

The substrate D-glucuronate exists as two anomeric pyranose rings, α and β-glucuronate, and the aldehyde (**Scheme 15**). The equilibrium ratios at 25 ºC in D_2O have been measured by ^1H NMR and found to be 1:1.3:0.002 corresponding to the α, β, and aldehyde species respectively.

Scheme 15. Anomerization of glucuronate species in solution.

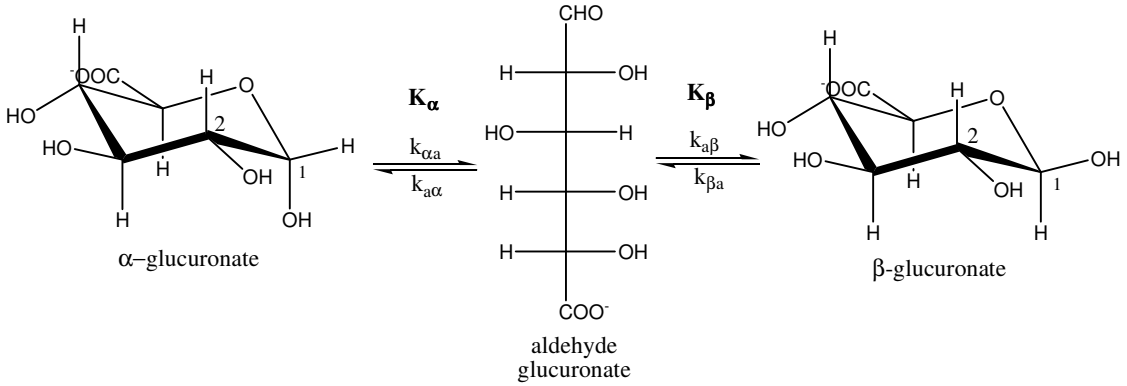

^{1}H saturation transfer NMR was used to investigate the interconversion rates of the three species present. In the glucuronic acid system, complete saturation of the aldehyde proton should result in a peak intensity change of the α- and β-H_1 proton resonance as a function of saturation time. The saturation times, τ, were varied from 0.5-10 seconds and two spectra were taken at $\tau = 0$ s and $\tau > 20$s to obtain initial peak intensities, $M_z^x(0)$, and peak intensities at maximal saturation, $M_z^x(\infty)$, where x is α or β. $M_z^x(0)$ and $M_z^x(\infty)$ peak intensities for α-H_1 were 83.2, and 68.8, the β-H_1 intensities are 164.9, and 132.9. The experimental peak intensities were plotted as the ln $[M_z^x(\tau) - M_z^x(\infty)]$ v/s τ for each anomer and the slope set equal to $-1/\tau_{1x}$. The plots for the decay of each anomeric species are shown in F**igures 11 and 12**. This value along with the peak intensities, $M_z^x(0)$ and $M_z^x(\infty)$, are used to calculate T_{1x} , the relaxation time of the corresponding anomer in the presence of saturation, using equation 6 (*41*). Equation 7 gives the value for the ring opening rate constant.

$$M_z^x(0)/ M_z^x(\infty) = \tau_{1x}/ T_{1x} \qquad (6)$$

$$k_{xa} = 1/ \tau_{1x} - 1/ T_{1x} \qquad (7)$$

The ring opening rate constants $k_{\alpha a} = 0.020\ s^{-1}$, $k_{\beta a} = 0.013\ s^{-1}$ and equilibrium equations were used to calculate the ring closing rate constants $k_{a\alpha} = 10\ s^{-1}$ and $k_{a\beta} = 8.45\ s^{-1}$ and all values were used in equation 4 and 5 to yield anomerization rate constants of $k_{\alpha\beta} = 0.009\ s^{-1}$ and $k_{\beta\alpha} = 0.007\ s^{-1}$.

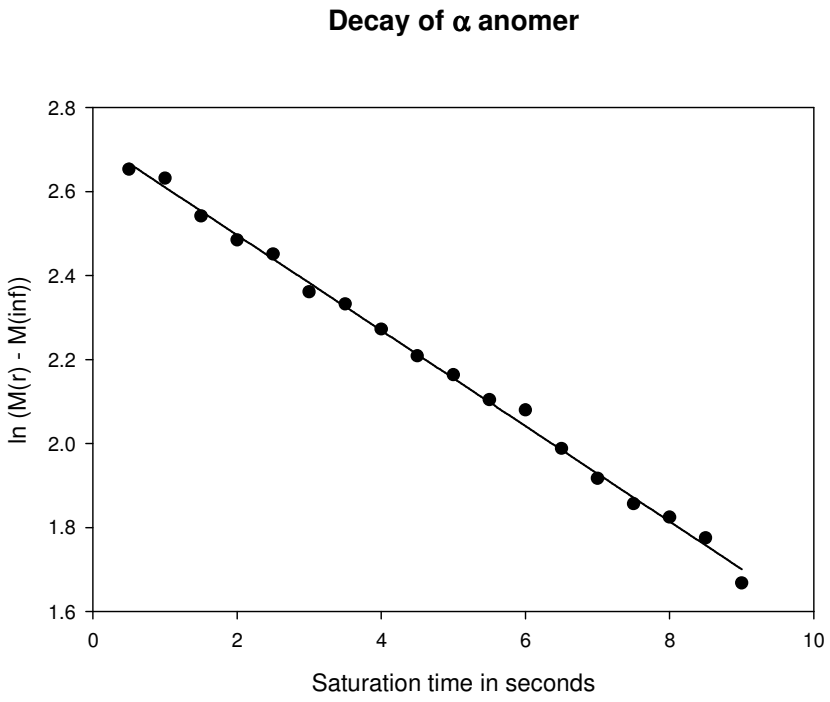

Figure 11. Decay of H1 resonance of α-D-glucuronate as a function of saturation time.

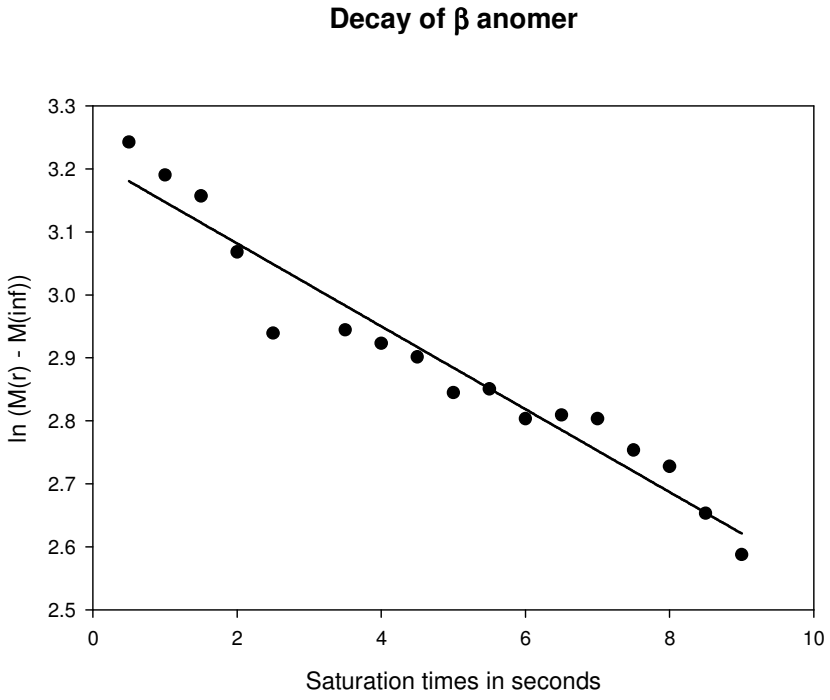

Figure 12. Decay of H1 resonance of β-D-glucuronate as a function of saturation time.

Anomeric Specificity of Uronate Isomerase. The anomeric specificity of uronate isomerase may be studied by 2D EXSY (exchanging systems) NMR. This technique allows simultaneous determination of site-to-site rate constants of each process of a multisite chemical exchange under equilibrium conditions. The anomeric specificity of phosphoglucose isomerase for α-D-glucose-6-phosphate was confirmed utilizing 2D phase sensitive ^{13}C EXSY NMR, and revealed enzyme specificity for β-D-fructose-6-phosphate in the reverse reaction (*35*). The anomerization activity in the presence of the enzyme was also calculated and found to be 2 orders of magnitude larger for D-glucose-6-phosphate and 5 orders of magnitude larger for D-fructose-6-phosphate. There are limitations for using this technique. The typical range for kinetic measurements using 2D NMR are between 10^{-2} and 10^{2} s^{-1}. There are some cases where results will be unreliable or not observed at all. 1) The chemical exchange occurs during a set mixing time, so the concentration of enzyme must be high enough to create sufficient exchange during that time. Otherwise, no cross peaks will be observed. 2) If any of the rates are $k \leq 1/T_1$ the spins may become fully relaxed and result in poor spectra due to insufficient magnetization transfer during the mixing time. 3) The concentration of substrate must be high enough to obtain good signal to noise in as few as 64 scans. 4) Rates that are too fast will broaden and coalesce the relevant signals which will obscure the data (*43*).
No cross peaks were ever observed for experiments carried out with uronate isomerase. This has been attributed to the low enzyme concentration in solution. All attempts to concentrate uronate isomerase to concentrations comparable to those used in the phosphoglucose isomerase system resulted in precipitation of the enzyme.

Therefore, the final concentration of enzyme in solution may have been insufficient to obtain spectra with observable cross peaks as a result of the chemical exchange. No significant signal broadening was observed so it is unlikely that the exchange was occurring too fast. Since no cross peaks were observed at maximum mixing time, the anomeric specificity of uronate isomerase was not assigned.

Isotope Effect Assays. The K_m and V_{max} values were obtained for each compound separately and then the corresponding Michaelis-Menten graphs plotted together for comparison. The graphs for V_{max} and k_{cat} are shown in **Figure 13**. The K_m values for D-glucuronate and [2-^{2}H]-D-glucuronate are 0.58 ± 0.02 mM and 0.61 ± 0.03 mM respectively. Maximal velocity (V_{max}) values received from the same plot were 4.1 x 10^{-5} (3.5 x 10^{-7}) μmol s^{-1} and 3.3 x 10^{-5} (7 x 10^{-7}) μmol s^{-1} for D-glucuronate and [2-^{2}H]-D-glucuronate respectively with corresponding errors in parentheses. After correcting for the enzyme concentration, a k_{cat} value of 164 s^{-1} was obtained for D-glucuronate and a k_{cat} of 132 s^{-1} for [2-^{2}H]-D-glucuronate.

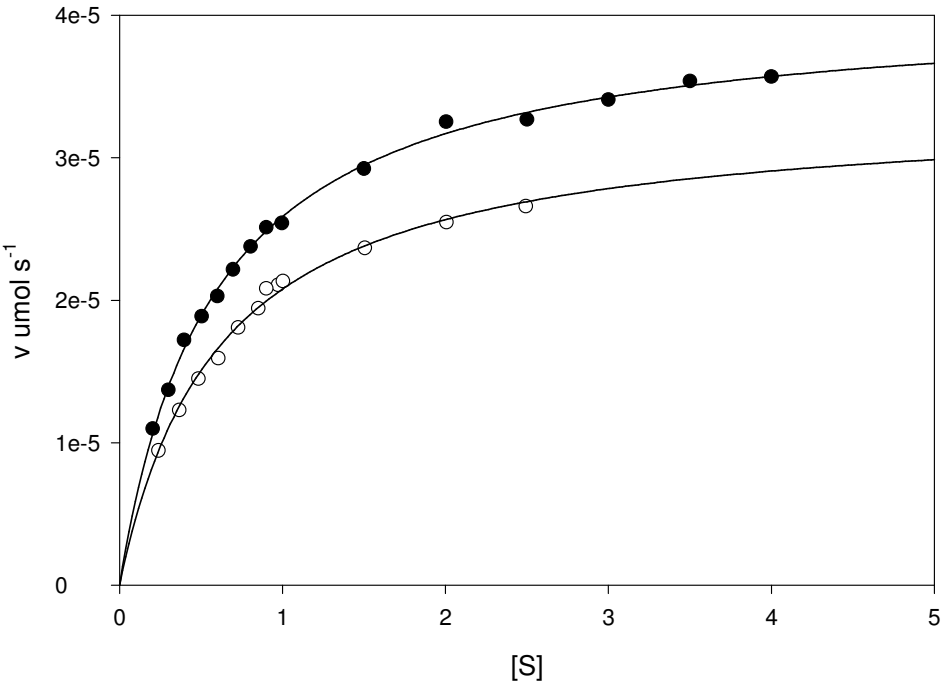

Figure 13. Isotope effect on k_{cat}. Initial velocity plots for D-glucuronate (●) and [2-^{2}H]-D-glucuronate (○).

Therefore the kinetic isotope effect on k_{cat}, $^{H}k_{cat}/^{D}k_{cat}$, is 1.24. The Lineweaver-Burk analysis of the data is presented in **Figure 14** and is used to calculate the kinetic isotope effect on V/K. The kinetic isotope effect on V/K, $^{H}V/K/^{D}V/K$, is 1.3. For assurance of accurate values, the experiments were run again with the same batch of purified substrates, same coupling system enzymes/substrates, and the same stock of uronate isomerase. Data obtained the second time yielded the following values for D-glucuronate and [2-^{2}H]-D-glucuronate: K_m values were 0.74 ± 0.06 mM and 0.43 ± 0.03 mM, V_{max} values of 5.4 x 10^{-5} (± 1.4 x 10^{-6}) μmol s^{-1} and 4.0 x 10-5 (± 9.6 x 10^{-7}) μmol s^{-1}, with k_{cat} values of 216 s^{-1} and 160 s^{-1} (all values reported respectively). Therefore the kinetic isotope effect on k_{cat} for the second isotope effect experiment is 1.35 and the kinetic isotope effect on V/K is 1.01. These two sets of data are in reasonable agreement with one another, an average of the two values yields a KIE on k_{cat} of 1.3 ± 0.05 and a KIE on V/K of 1.2 ± 0.1.

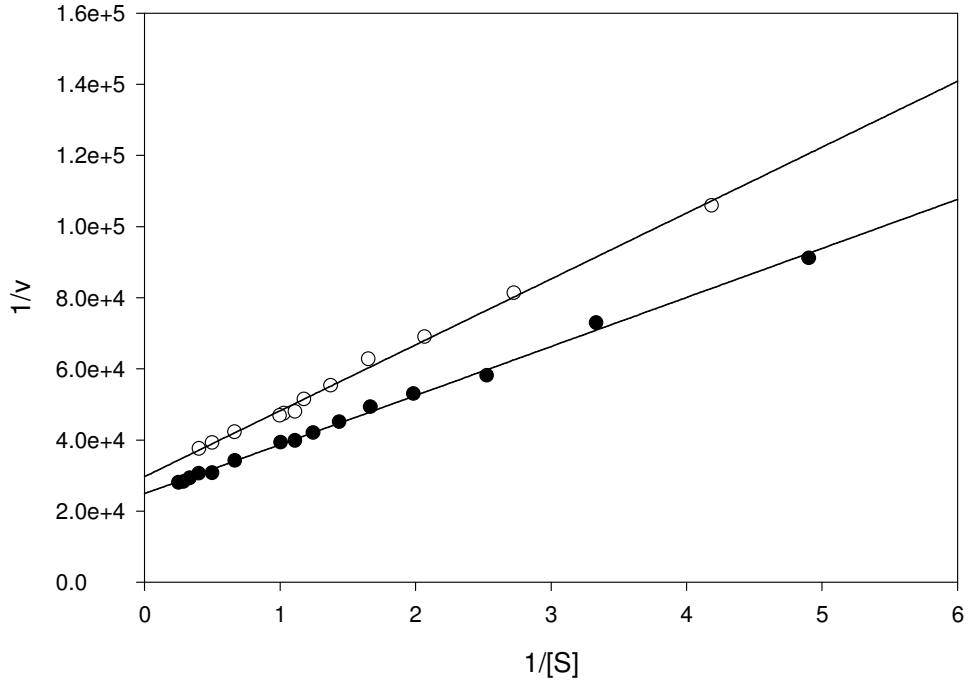

Figure 14. Isotope effect on V/K. Lineweaver-Burk plots for D-glucuronate (●) and [2-^{2}H]-D-glucuronate (○) from data presented in Figure 10.

Discussion

The two possible catalytic mechanisms of UAI, a proton or hydride transfer, result in a hydrogen transfer from C2 to C1 (**Scheme 10**). A proton transfer mechanism utilizes an active site base to abstract the proton from C2 while an active site acid donates a proton to the carbonyl oxygen at C1 forming an enediol intermediate. Intermediate formation is followed by transfer of the proton abstracted from C2 to C1 and abstraction of the hydrogen from the C2 hydroxyl thus forming the ketose product. The hydride transfer mechanism is afforded by deprotonation of the C2 hydroxyl by an active site base accompanied with a 1,2 hydride transfer and subsequent protonation of the C1 carbonyl by an active site acid. The distinctive feature of the proton transfer mechanism is the exchangeability of the C2 hydrogen with solvent in the presence of enzyme. With the hydride transfer mechanism, no exchange is possible. Uronate isomerase catalyzes the exchange of the C2 hydrogen of the substrate D-glucuronate when incubated in 98% D_2O at a rate of 0.018 s^{-1}. This exchange rate is significant although it is slow in comparison to other enzymes which catalyze similar reactions via proton transfer mechanisms. Triosephosphate isomerase exchanges the C2 hydrogen of glyceraldehyde-3-phosphate with solvent at a rate 10 times the rate of substrate/product interconversion. The relative magnitude of exchange was approximately twice the relative magnitude of substrate/product interconversion in the reaction catalyzed by phosphoglucose isomerase (*44*). These vast rate differences could be attributed to increased/decreased solvent accessibility to the active site conjugate acid which catalyzes the intramolecular proton transfer, or the relative concentration of the *cis*-

enediol intermediate in the steady state. Nevertheless, these data are consistent with a proton transfer mechanism and not a hydride transfer. D-xylose isomerase, known to utilize a hydride transfer mechanism, catalyzes substrate/solvent exchange at a rate which is 9 orders of magnitude slower than interconversion of substrate or product.

The stereospecific transfer of the proton from C2 of D-glucuronate to C1 of D-fructuronate is supported by ^{1}H NMR which shows that one hydrogen is exchanged with solvent in the presence of UAI. Addition of more enzyme to the equilibrated solution does not result in deuterium substitution at other carbons. The stereospecific transfer is further supported by ^{1}H NMR spectra of protonated and deuterium substituted substrate or product stored in D_2O without enzyme. The protonated substrate or product did not show exchange of either proton with solvent after one month of incubation. Similarly, there was no evidence of exchange when the deuterium substituted substrate or product were incubated in the same manner. These data are consistent with stereospecific enzyme catalyzed exchange and negates the possibility of nonenzymatic exchange of substrate or product protons.

The assignment of the stereospecifically transferred proton was achieved by molecular modeling and NMR analysis of the protonated and deuterium substituted D-mannonate dehydratase product 2-keto-3-deoxy-D-gluconate. The transferred proton was found in the *pro-R* position of the product thus establishing the stereospecific transfer of the D-glucuronate C2 proton to the *pro-R* position at C1 of D-fructuronate in the uronate isomerase catalyzed isomerization. These data imply that the transferred proton is added to the *re* face of the C1 carbonyl which is consistent with the formation of a *cis*-enediol

intermediate. The cis-enediol intermediate has been identified in the reactions catalyzed by triosephosphate isomerase, phosphoglucose isomerase, and glyoxylase I (7, 8, 25). The stereochemistry of the transferred protons in the triosephosphate isomerase and phosphoglucose isomerase reactions were both assigned as the *pro-R* proton as well. The relationship of stereochemistry has been evaluated among many isomerase enzymes. It has been proposed by Fersht, that the assignment of the transferred proton is directly related to the stereochemistry of the chiral center which it was abstracted from (*37*). Protons abstracted from *R* stereocenters will be transferred to the *pro-R* position at C1 of the ketose product when the *cis*-enediol intermediate is formed. Likewise, protons abstracted from *S* stereocenters are transferred to the *pro-S* position at C1 of the corresponding ketose product. The data obtained for uronate isomerase are in agreement with this theory.

The proton transfer mechanism via a *cis*-enediol intermediate is supported by the elimination of fluoride from 3-deoxy-3-fluoro-D-glucuronate catalyzed by uronate isomerase. When the proton at C2 of the substrate is abstracted by a basic group in the active site, the negative charge can be delocalized into the carbonyl at C1. The presence of the electronegative fluoride at C3 would allow the negative charge to alternatively shift toward C3 and expel the fluoride as represented in Scheme 5. The rate of fluoride elimination is 1% of the isomerization and is consistent with fluoride elimination studies of similar enzyme systems. Glyoxylase I has been proposed to catalyze a proton transfer through a *cis*-enediol intermediate and has been probed for enzyme catalyzed fluoride elimination. Fluoromethylglyoxal (0.5 mM) was incubated with 6 units of glyoxylase I

and fluoride elimination was complete in approximately 2 hours (*45*). However, dissimilar results were obtained for D-xylose isomerase which catalyzes a 1,2 hydride transfer. No changes in the ^{19}F NMR spectra were observed after a 40 day incubation of D-xylose isomerase with 3-deoxy-3-fluoro-D-glucose or 3-deoxy-3-fluoro-D-allose (*30*). These data and the lack of a substrate/solvent exchange reaction have been used to support the hydride transfer mechanism for D-xylose isomerase.

Therefore, the proton transfer mechanism of uronate isomerase has been supported by substrate/solvent exchange and fluoride elimination which are only catalyzed in the presence of enzyme. The *cis*-enediol intermediate is proposed in most aldose/ketose isomerization reactions utilizing a proton transfer mechanism. The presence of the intermediate was confirmed with the fluoride elimination experiments and further supported by the stereochemistry assignment of the transferred proton. All these data and inhibitor studies with *cis*-enediol mimics, carried out by Tinh Nguyen in the Raushel laboratory, were used to establish the mechanism of uronate isomerase as a proton transfer (*46*).

The anomerization of the substrate, D-glucuronate, was investigated by saturation transfer NMR. Saturation transfer studies (^{13}C and ^{1}H) have been used to investigate the interconversions of many furanose sugars/uronic acids. Pyranose systems have been shown to interconvert very slowly which limits the methods by which the interconversion can be monitored at equilibrium. The anomerization rates of D-glucose have been reported to be 0.006 min^{-1} and D-galactose mutarotation was reported as 0.03 min^{-1} by optical rotation studies (*47, 48*). The presence of a charge at C6 increases the

rate of anomerization as demonstrated with D-glucose-6-phosphate which has rate constants of $k_{\alpha\beta} = 0.060\ s^{-1}$ and $k_{\beta\alpha} = 0.036\ s^{-1}$ (*34*). Therefore it was assumed that the anomerization rates of D-glucuronate would be comparable to those of D-glucose-6-phosphate due to the presence of the charged carboxyl group at C6. The saturation transfer technique has been shown to be able to accurately determine ring opening rate constants in the range of 10^{-2} - $10^{1}\ s^{-1}$ and ring closing rate constants can then be calculated from equilibrium constants (*41*). The ring opening rate constants of D-glucuronate to the open chain aldehyde were obtained from saturation transfer NMR spectra and found to be $k_{\alpha a} = 0.020\ s^{-1}$ and $k_{\beta a} = 0.013\ s^{-1}$. These values are within the limits of detection for the saturation transfer NMR technique. The corresponding anomerization rate constants are an order of magnitude faster than the rate constants for D-glucose, $k_{\alpha\beta} = 0.009\ s^{-1}$ and $k_{\beta\alpha} = 0.007\ s^{-1}$, which suggests the presence of the carboxyl group accelerates the anomerization rate.

These rates are slower than the rate of enzyme catalyzed product formation by 5 orders of magnitude. This suggests that uronate isomerase has the ability to enhance the rate of anomerization. Similar results have been obtained for phosphoglucose isomerase as previously discussed. The mechanism or active site residues responsible for the rate enhancement have not yet been revealed but the studies with phosphoglucose isomerase did establish the specificity of the enzyme for the α anomer of G6P. No significant evidence was present in any of the experiments that suggested phosphoglucose isomerase was able to catalyze product formation with the β anomer of G6P.

The anomeric specificity of uronate isomerase was investigated using the same method as PGI, however, the enzyme concentration needed to obtain reliable results could not be reached without precipitation of the protein.

Kinetic isotope effects have been used to identify rate limiting steps in many enzyme catalyzed reactions. Primary isotope effects, ranging from 2-15 in value, indicate cleavage of a C-H/C-D bond in the rate limiting step of the reaction. Secondary isotope effects will be smaller and indicate that the bond which is broken is adjacent to the isotope atom. The lack of an isotope effect would suggest that the bond breaking is not the rate limiting step. Isotope effect experiments using [2-^{2}H]-D-glucuronate and D-glucuronate yielded values of 1.3 for the kinetic isotope effect on k_{cat} and the effect on V/K was 1.2. These values suggest that C-H bond cleavage at C2 of D-glucuronate is not rate limiting in the reaction catalyzed by uronate isomerase.

CHAPTER III

PROBING THE ROLE OF ATP IN THE COBYRINIC ACID *A,C*-DIAMIDE SYNTHETASE AND COBYRIC ACID SYNTHETASE REACTIONS

Cobyrinic acid *a,c*-diamide synthetase from *S. typhimurium* (CbiA) catalyzes the ATP dependent amidation of carboxylate groups *a* and *c* of cobyrinic acid utilizing glutamine or ammonia as a nitrogen donor as shown in **Scheme 16**. ATP is believed to activate the carboxylate groups by forming a phosphorylated or adenylated cobyrinic acid intermediate, which is attacked by ammonia or glutamine to afford the diamide product. Substrate activation by ATP is prevalent among many synthetase reactions. GMP synthetase, pantothenate synthetase, and aminoacyl-t-RNA synthetases produce activated substrates which have been adenylated (*49-53*). Glutamine synthetase and carbamoyl phosphate synthetase feature phosphorylated intermediate species which are then attacked by ammonia to afford the product or subsequent intermediate (*23, 54*). A phosphorylated enzyme was identified in the reaction catalyzed by pyruvate-phosphate dikinase (*55*). Though not commonly found in synthetase reactions, phosphorylated enzyme species must also be considered when investigating the mechanism of synthetase reactions. The PIX technique can be used to probe the role of ATP in the CbiA reaction as well as the cobyric acid synthetase (CbiP) reaction.

Scheme 16. Reaction catalyzed by Cobyrinic acid *a,c*-diamide synthetase (CbiA).

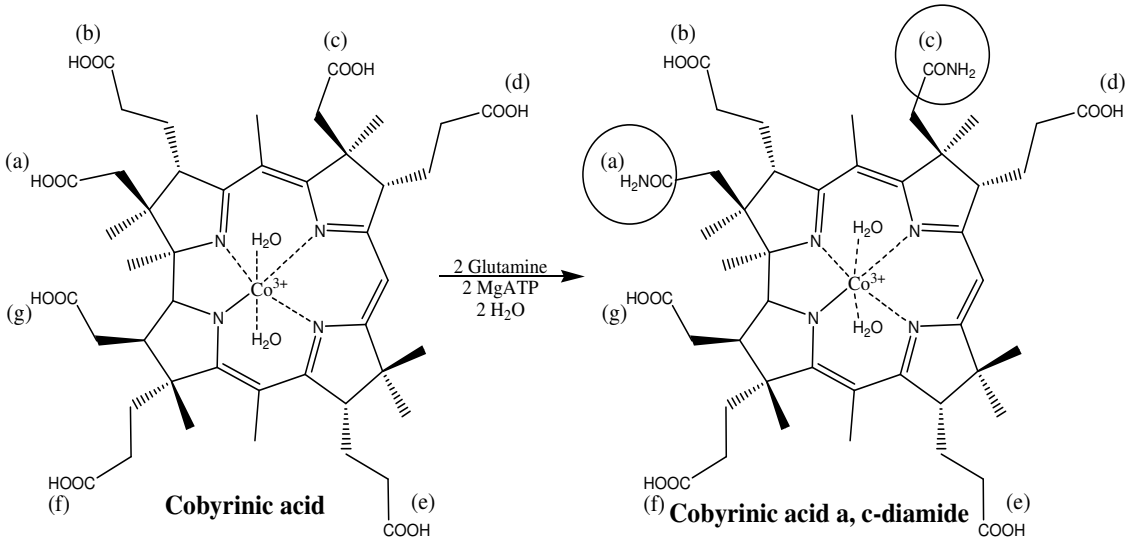

Cobyric acid synthetase from *S. typhimurium* (CbiP) catalyzes the amidation of carboxylate groups *b, d, e*, and *g* of adenosyl-cobyrinic acid *a,c*-diamide, shown in **Scheme 17**. This reaction is also ATP dependent and utilizes glutamine or ammonia as a nitrogen donor. There are no published kinetic studies that suggest an enzyme mechanism for CbiP, however, it is suggested that a phosphorylated adenosyl-cobyrinic acid *a,c*-diamide intermediate is formed in a similar manner as suggested for CbiA. It is proposed that the activated intermediate species in both the CbiA and CbiP reactions are then attacked by ammonia to form the corresponding products. The identity of the intermediate species will be probed using the positional isotope exchange technique.

Scheme 17. Reaction catalyzed by cobyric acid synthetase (CbiP).

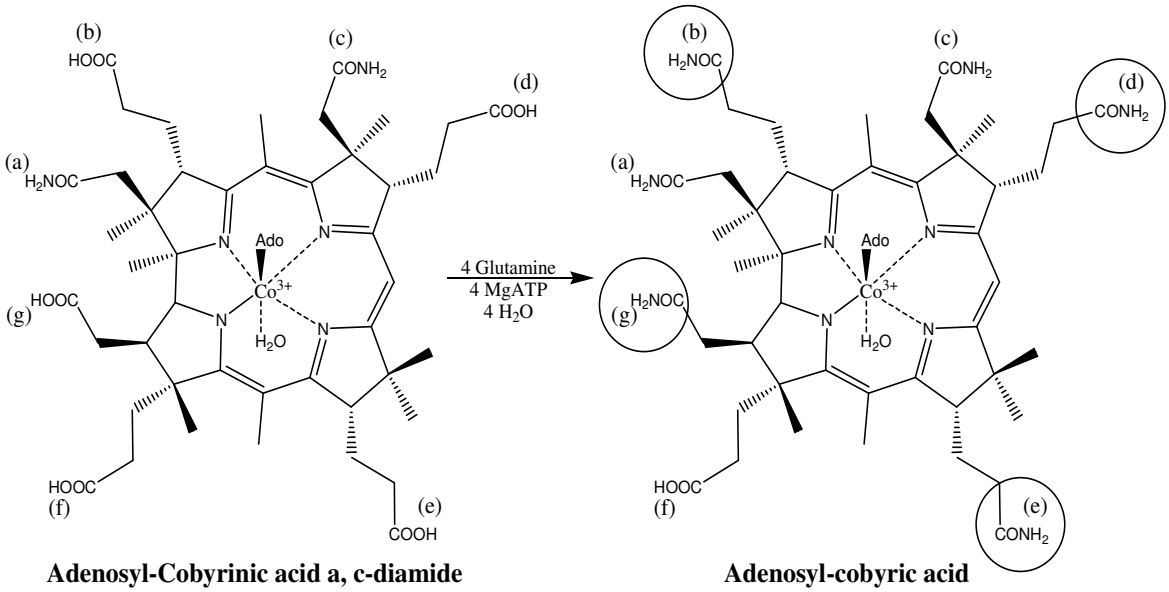

Adenosyl-Cobyrinic acid a, c-diamide **Adenosyl-cobyric acid**

Positional isotope exchange (PIX) is a technique that has been used to probe the role of ATP in the activation of substrates in many synthetase enzymes. The PIX technique was first developed by Midlefort and Rose in 1976 to investigate the kinetic competence of γ-glutamyl phosphate as a reactive intermediate in the glutamine synthetase reaction (*54*). The PIX technique can be used to analyze reversible enzyme-catalyzed reactions where functionally non-equivalent groups become torsionally equivalent during the formation of products/intermediates. Isotope labeled substrates which can be observed by fast atom bombardment mass spectroscopy (*56*) or ^{31}P and ^{15}N NMR spectroscopy (*57, 58*) are usually employed for this technique. Esters of phosphoric and carboxylic acids are among the most common functional groups used in PIX experiments (*59*). It was established by Cohn and Hu that substitution of ^{18}O for ^{16}O

in phosphate esters induces a 0.02 ppm upfield chemical shift in the phosphorus resonance (*60*). Therefore, all reactions with nucleotide triphosphates undergoing nucleophilic attack at phosphoryl groups can be analyzed by the PIX technique.

The PIX technique can be used for two interdependent probes of enzyme-catalyzed reactions. In the first probe, the formation of a particular intermediate can be verified as previously demonstrated with glutamine synthetase (*54*). The second probe allows quantitative determination of partition ratios of enzyme-ligand complexes. Experiments which probe intermediate formation are generally achieved by incubating the reaction mixture without one of the substrates. For example, the two intermediate species in the reactions catalyzed by carbamoyl phosphate synthetase (CPS) were identified by PIX (*57*).

Carbamoyl phosphate synthetase produces carbamoyl phosphate via two independent reactions with different intermediate species. CPS has also been shown to catalyze the formation of ATP from carbamoyl phosphate and ADP. These reactions are demonstrated in **Scheme 18**. The presence of the carboxyphosphate intermediate was first established by Wimmer et. al using PIX (*23*). Bicarbonate and [γ-$^{18}O_4$]-ATP were incubated with CPS in the absence of ammonia or glutamine to study only the first half reaction. After some time, the ^{18}O in the $\beta\gamma$-bridge position can be found in the β non-bridging positions of the reisolated ATP. This experiment supported the existence of a carboxyphosphate intermediate instead of phosphoryl transfer to a residue within the enzyme active site. PIX activity was not observed when bicarbonate was excluded from

the reaction mixture. The PIX rate was found to be 1.7 times the rate of ATP cleavage which established carboxyphosphate as a kinetically competent intermediate.

Scheme 18. Reactions catalyzed by carbamoyl phosphate synthetase (CPS).

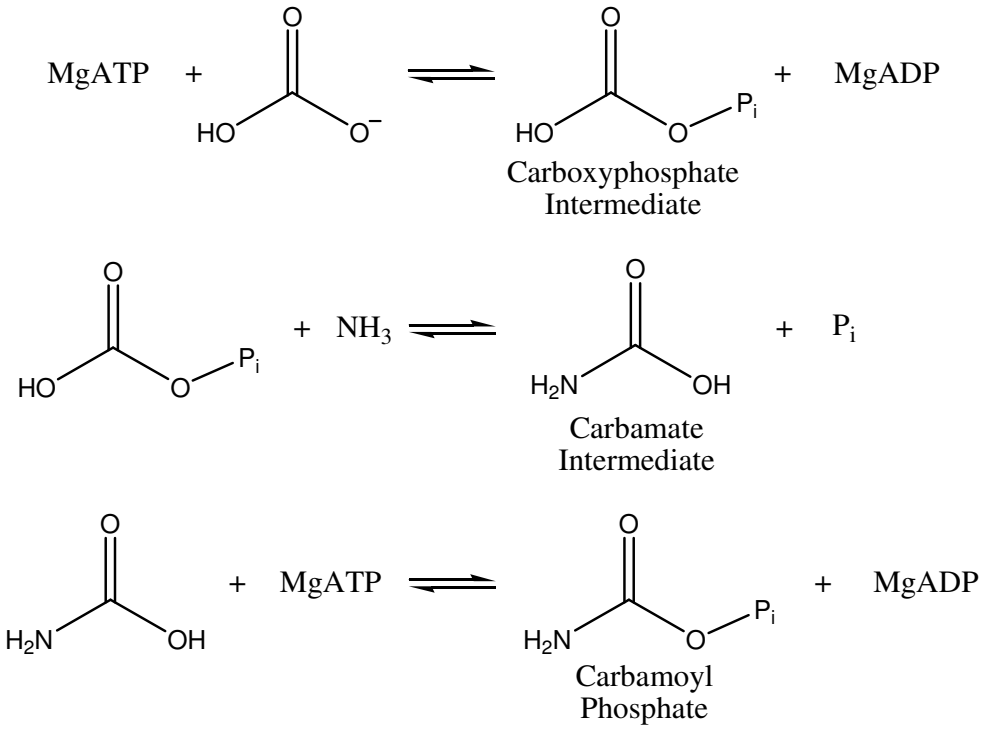

The formation of carbamate as an intermediate species was demonstrated by Raushel and Villafranca (*57*). The reverse reaction catalyzed by CPS forms ATP from carbamoyl phosphate and ADP. By using ^{18}O enriched carbamoyl phosphate as a substrate, PIX can be observed when ADP reversibly attacks carbamoyl phosphate to form ATP and carbamate. The oxygen atoms attached to the carbamate carbon become torsionally equivalent and the ^{18}O can be found in the non-bridging position upon reformation of carbamoyl phosphate, see **Scheme 19**. This demonstrated that carbamate is indeed the

intermediate species which reacts with ATP to form carbamoyl phosphate. Since the partial reverse reaction is 4 times faster than the steady-state rate of ATP synthesis, carbamate was shown to be a kinetically competent intermediate (*57*).

Scheme 19. PIX experiment used to identify carbamate as an intermediate in the reaction catalyzed by CPS (*57*).

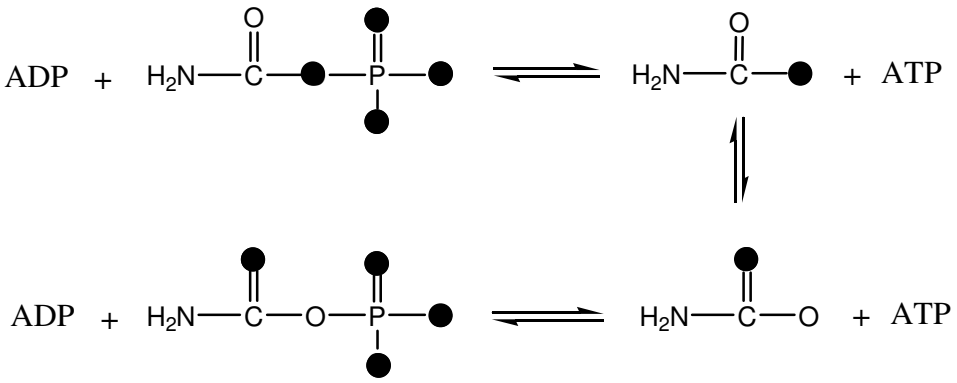

An intermediate species is described as kinetically competent if the intermediate reacts as fast or faster than the overall reaction of the substrates or the substrates that it replaces (*61*). The PIX reaction rate will determine whether an intermediate is kinetically competent. The minimum value for the PIX reaction, V_{ex}, is an approximate value based on the maximal velocities of the reaction. The experimental positional isotope exchange rate, v_{ex}, is calculated based on isotope exchange as a function of time. The equations used to solve for these values were outlined by Rose and are given in equations 8 and 9 (*62*). V_1 and V_2 are maximal velocities of the steady-state reaction in the forward and reverse directions, respectively. The PIX rate is calculated from experimental values for the concentration of isotope labeled substrate, A, and the fraction of positional isotope scrambling equilibrium, F, achieved at time, t, using

equation 9 (*62*). Utilizing these equations it can be determined whether an intermediate is formed rapidly enough to be kinetically competent. However, maximal velocity values need to be known.

$$V_{ex} \geq (V_1V_2)/(V_1 + V_2) \quad (8)$$

$$v_{ex} = -([A]/t)\ln(1 - F) \quad (9)$$

In the reactions catalyzed by CbiA and CbiP, the presence of a phosphorylated enzyme or intermediate species has been probed by incubating the enzyme with [γ-$^{18}O_4$]-ATP and the corresponding substrate, cobyrinic acid or adenosyl-cobyrinic acid *a,c*-diamide. Ammonia or glutamine will be excluded from these experiments to prevent irreversible product formation.

Materials and Methods

Oxygen-18 labeled water was obtained from Cambridge Isotope Laboratories. Oxygen-18 labeled potassium phosphate was prepared following the procedure of Risley and van Etten (*63*). The synthesis of [γ-$^{18}O_4$]-ATP was accomplished by using the method of Werhli et. al. (*64*) from ADP-morpholidate and $H_3P^{18}O_4$. The two stock solutions of [γ-$^{18}O_4$]-ATP showed ~ 90 and 93% ^{18}O incorporation by ^{31}P NMR spectroscopy, respectively. Cobyrinic acid was a gift from the laboratory of Dr. Ian Scott. Adenosyl-cobyrinic acid *a,c*-diamide was synthesized enzymatically and purified by Dr. Vicente Fresquet in the laboratory of Dr. Frank Raushel. Cobyrinic acid *a,c*-

diamide synthetase (CbiA) and cobyric acid synthetase (CbiP) were cloned and purified by Dr. Vicente Fresquet in the Raushel laboratory. All other materials were purchased from Sigma.

^{31}P Nuclear Magnetic Resonance Measurements. ^{31}P NMR spectra were acquired using a Varian Inova-400 multinuclear NMR spectrometer operating at a frequency of 162 MHz. Acquisition parameters were 5000-Hz sweep width, 6.0 s acquisition time, and a 2.0 s delay between pulses.

PIX Reactions for CbiA. By using γ-$^{18}O_4$ labeled ATP as a substrate, PIX activity can be observed by following the decrease of the γ-$^{18}O_4$ species of ATP using ^{31}P NMR. A PIX reaction will be observed if carboxylate group *a* or *c* attacks the γ-P of ATP and the peripheral oxygen atoms of the β-P become torsionally equivalent and are allowed to rotate as shown in **Scheme 20**. The PIX assay contained 1.0 mM [γ-$^{18}O_4$]-ATP, 0.2 μM cobyrinic acid, 50 mM Tris-HCl at pH 7.2, 20 mM KCl, 1.0 mM DTT, 2.0 mM $MgCl_2$, and 1.0 μM cobyrinic acid *a,c*-diamide synthetase at a total volume of 500 μL. The assays were incubated at 30 ºC for 4 hours and then quenched by the addition of 2 drops of CCl_4 with vigorous vortexing.

The precipitated protein was removed by passage through a 0.45 μm Corning syringe filter and then concentrated to near dryness with the aid of a rotary evaporator. The samples were then dissolved in a solution containing 150 mM EDTA, pH 9.0 and D_2O for ^{31}P NMR analysis. Control reactions were run in the absence of cobyrinic acid or enzyme.

PIX Reactions for CbiP. The PIX reactions for cobyric acid synthetase were followed using the same method as that of cobyrinic acid *a,c*-diamide synthetase. If carboxylate groups *b, d, e*, or *g* attacks ^{18}O labeled ATP as outlined in **Scheme 20,** a PIX reaction can be observed. The assay volumes were 1 mL containing 100 mM Tris-HCl pH 7.5, 1.0 mM DTT, 2.0 mM $MgCl_2$, 1.0 mM [γ-$^{18}O_4$]-ATP, 2.0 μM adenosyl-cobyrinic acid *a,c*-diamide, and 2.0 μM cobyric acid synthetase. These assays were incubated for 2 and 4 hours at 30 ºC, and two control assays without adenosyl-cobyrinic acid *a,c*-diamide or cobyric acid synthetase were incubated for 2 hours.

Scheme 20. PIX methodology.

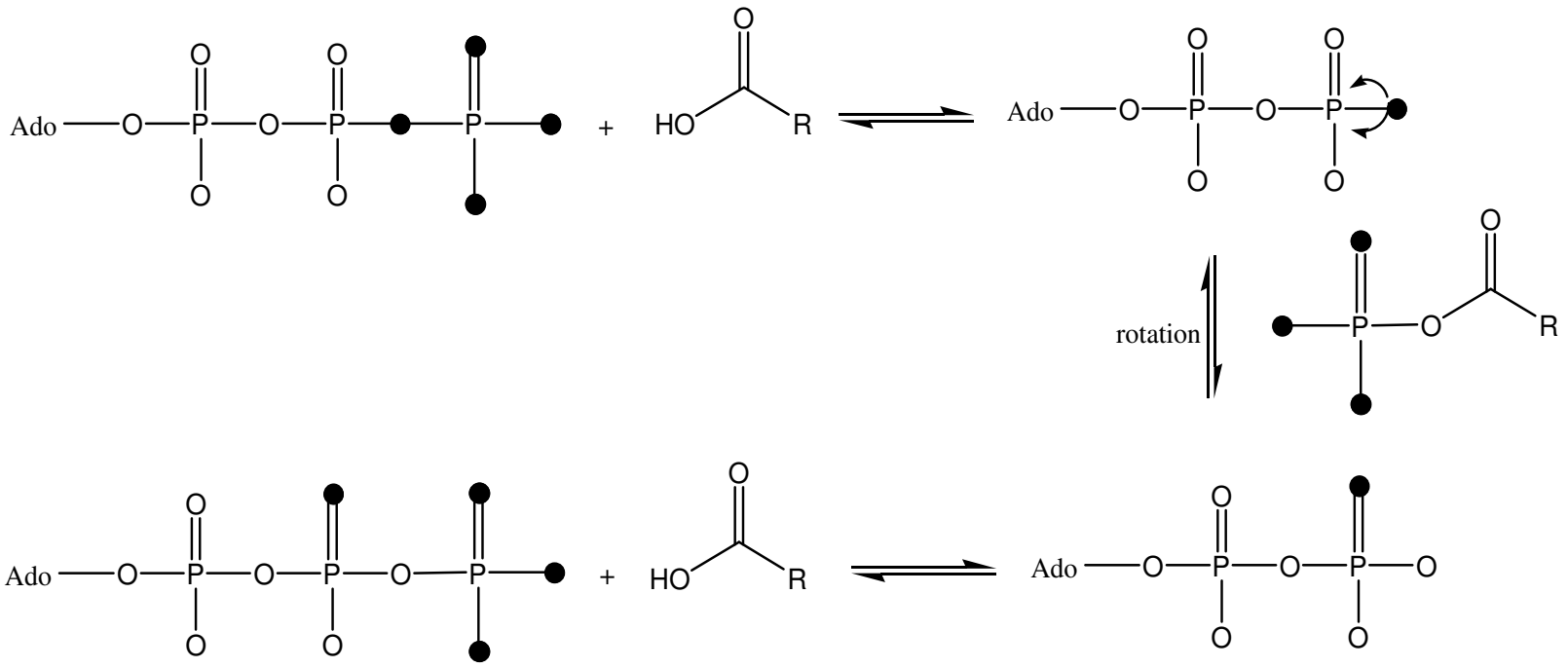

Results

PIX for CbiA. PIX was not observed in the assays which excluded cobyrinic acid or cobyrinic acid *a,c*-diamide synthetase. The fraction of γ-$^{18}O_4$ species decreased from the starting value of 0.75 to 0.61 after 4 hours for assays containing labeled ATP, cobyrinic acid and enzyme. These spectral changes are shown in **Figure 15**. This decrease represents 28% of what would be expected at equilibrium. The equilibrium value for the fraction of γ-$^{18}O_4$ species was calculated based on the fraction of ^{18}O labeling at each oxygen position, 93%, and the probability of [γ-$^{18}O_4$]-ATP reformation once the reaction is initiated. Ninety-three percent ^{18}O incorporation at each oxygen position around the γ-P resonance yields a species which cannot exceed 0.93^4 of the total species. This value, 0.75, is in agreement with the value obtained by NMR analysis. Upon reaction with the substrate, the ^{18}O atom attached to the β-P can rotate and be found in the 2 non-bridging positions or remain in the same position upon reformation of ATP. Since only one of the three reactions results in reformation of [γ-$^{18}O_4$]-ATP, the maximum fraction of the species at equilibrium is $^1/_3 f^4$, where f is 0.93. The value for F in equation 9 is then calculated by dividing the experimental difference by the difference at equilibrium. The experimental difference is the fraction of γ-$^{18}O_4$ species in the starting material, 0.75, minus the fraction of γ-$^{18}O_4$ species after 4 hours, 0.61, which is 0.14. The difference at equilibrium is the maximal value in the starting material, 0.75 (0.93^4), minus the maximal value at equilibrium, 0.25 ($^{0.75}/_3$), which is 0.5. F in equation 9 is thus 0.28 ($^{0.14}/_{0.5}$). Using this value yields a PIX rate for cobyrinic acid *a,c*-diamide synthetase of 0.023 s^{-1}.

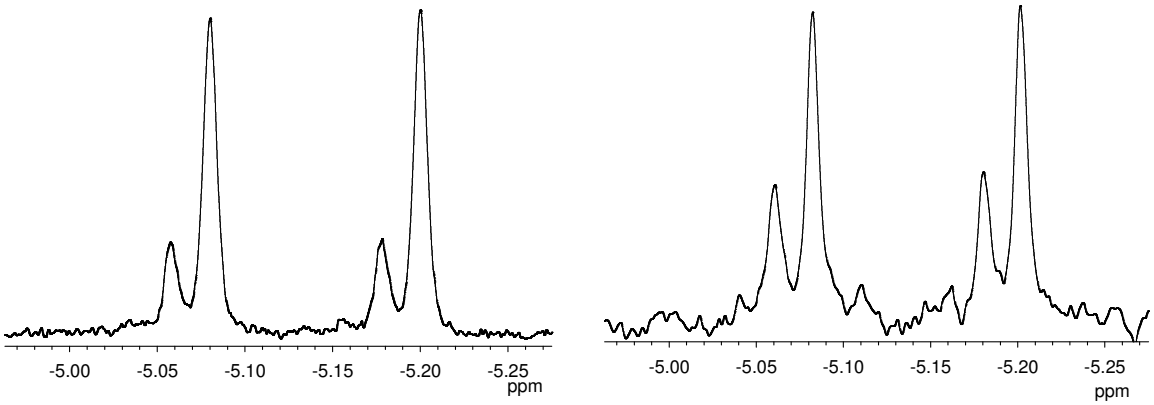

Figure 15. ^{31}P NMR spectra of PIX reaction with CbiA. γ-$^{18}O_4$ resonance of ATP after being incubated with cobyrinic acid, and CbiA for 0 and 4 hours, respectively.

The positional relocation of the β-γ bridge ^{18}O atom to the β non-bridge position only observed when [γ-$^{18}O_4$]-ATP, cobyrinic acid, and CbiA are present is fully consistent with a phosphorylated-cobyrinic acid intermediate. It is very unlikely that a phosphorylated-enzyme intermediate is formed in the course of the PIX reaction since no PIX could be detected upon incubation of [γ-$^{18}O_4$]-ATP with CbiA.

PIX for CbiP. Incubation of labeled ATP with adenosyl-cobyrinic acid *a,c*-diamide or cobyric acid synthetase did not result in PIX activity. The γ-$^{18}O_4$ species decreased from 0.657 to 0.534 and 0.506 in the assays incubated for 2 and 4 hours, respectively, see **Figure 16**. The small difference between 2 and 4 hours indicates either competitive binding of ADP which increases from 6% in the starting material to 17% after 4 hours, or degradation of the enzyme. The decrease of γ-$^{18}O_4$ species after 2 hours is 28% of the equilibrium value. The same methodology used to calculate the equilibrium values for CbiA were employed here with one modification. The fraction of ^{18}O labeling at each oxygen atom in the stock [γ-$^{18}O_4$]-ATP solution used for CbiP is 90%. The data from the 2 hour assay was inserted into equation 9 and the PIX rate calculated to be 0.023 s^{-1}. The PIX rate using the 4 hour assay is 0.015 s^{-1}. The PIX activity is only displayed when [γ-$^{18}O_4$]-ATP, adenosyl-cobyrinic acid *a,c*-diamide, and enzyme are incubated together which supports activation of the carboxylates via phosphorylation. A phosphorylated-enzyme species was not in agreement with these data.

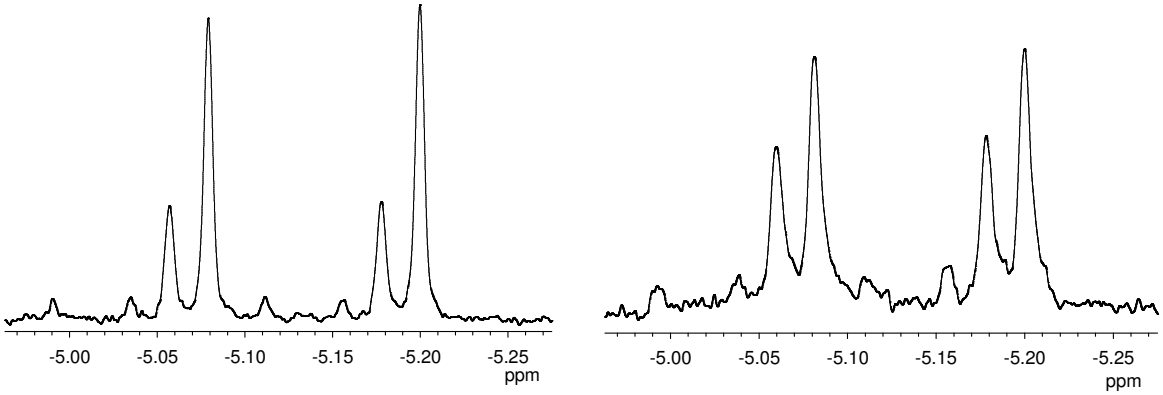

Figure 16. ^{31}P NMR spectra of PIX reaction with CbiP. γ-$^{18}O_4$ resonance of ATP after being incubated with cobyric acid synthetase and adenosyl-cobyrinic acid a,c-diamide for 0 and 2 hours, respectively.

Discussion

Intermediates of enzyme catalyzed reactions are often difficult to capture and characterize. Positional isotope exchange has proved a valuable technique to probe the identity of intermediate species. Carboxylic acid and phosphoric acid functional groups are among the most commonly used for PIX analysis. Both of these functional groups are featured in many synthetase reactions and react to produce activated intermediates. This was found to be true in the reactions catalyzed by CPS, GMP synthetase, glutamine synthetase, pantothenate synthetase, and many others (*49, 50, 54, 57*). Though the functional groups are the same among these reactions, the intermediate species differ. Some are adenylated, like the intermediate species of asparagine synthetase and GMP synthetase (*49, 65*). Others are phosphorylated intermediates like those found in the CPS reaction and glutamine synthetase (*54, 57*). Despite their differences, the PIX technique can be used to confirm the formation of either intermediate and analyze the kinetics of intermediate formation.

The phosphorylated intermediates of CbiA and CbiP have been established by observation of PIX activity. Isotope exchange can be observed if 1) a residue on the enzyme attacks [γ-$^{18}O_4$]-ATP in the absence of the corresponding substrate or 2) a carboxylate group from the substrate attacks [γ-$^{18}O_4$]-ATP. Since no PIX activity was observed with CbiA or CbiP when the corresponding substrate was excluded from the reaction, it is concluded that the phosphorylated intermediate is only formed in the presence of the substrate. Likewise, no PIX activity was observed when the corresponding enzyme was excluded from the assay mixture.

The presence of PIX activity in the CbiA reaction confirms activation of carboxylate groups *c* and *a* by phosphorylation as shown in **Scheme 21**. The calculated PIX rate, 0.023 s^{-1}, is slower than the overall k_{cat} of 1.2 s^{-1} but verifies the formation of the intermediate species. The maximum velocity values for the forward and reverse reactions were not available, therefore, it is not possible to determine the minimum value for the PIX reaction using equation 8. The successive amidations of CbiA were later determined, in the Raushel laboratory, to be sequential and dissociative (*26*). First carboxylate *c* is activated by ATP and the activated intermediate attacked by ammonia to yield cobyrinic acid *c*-monoamide. Then similar events occur for the amidation of carboxylate *a*.

The CbiP reaction catalyzes the ATP dependent amidation of carboxylate groups *b, d, e,* and *g* of the substrate adenosyl-cobyrinic acid *a,c*-diamide. PIX activity was observed once [γ-$^{18}O_4$]-ATP, adenosyl-cobyrinic acid a,c-diamide, and CbiP were incubated together. The calculated PIX rate for this enzyme is 0.023 s^{-1}. These experiments offer strong evidence for a phosphorylated adenosyl-cobyrinic acid *a,c*-diamide intermediate in the reaction catalyzed by CbiP. The processive or dissociative nature of the kinetic mechanism and whether the chemical reaction is ordered or random has not previously been addressed for CbiP.

Scheme 21. Mechanism of carboxylate activation catalyzed by CbiA.

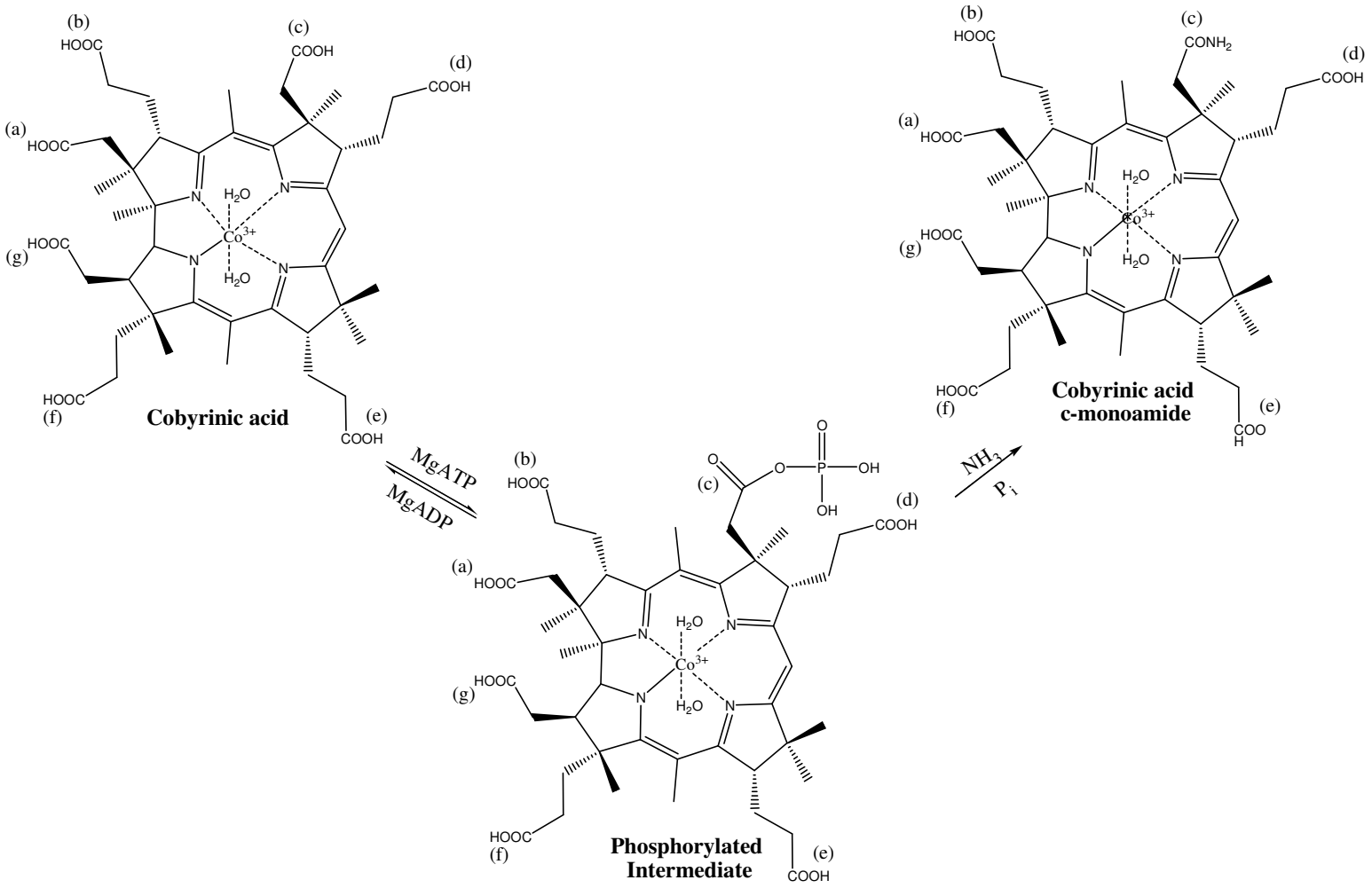

CHAPTER IV

CHARACTERIZATION OF THE SEQUENTIAL AND DISSOCIATIVE MECHANISM OF COBYRIC ACID SYNTHETASE

The mechanisms of successive reactions catalyzed enzymatically are quite fascinating. The overall reaction mechanism can be processive or dissociative and the reactions can occur in a random or sequential fashion. A processive reaction is catalyzed without the substrate ever dissociating from the enzyme active site. DNA polymerase assembles DNA on a template strand by adding nucleotides to the free 3'OH end of previously added bases utilizing a processive mechanism (*66*). Dissociative reactions release the substrate or intermediate from the enzyme after each catalytic cycle. Dissociative successive deaminations are catalyzed by mammalian adenosine deaminase (ADA) to produce a broad-spectrum antiviral drug ribavirin (*67*). Ribavirin is produced after a single irreversible deamination, released from the active site, and another deamination yields an inactive metabolite. This series of reactions is illustrated in **Scheme 22**.

Scheme 22. Successive reactions catalyzed by mammalian ADA to yield an antiviral drug in vivo (*67*).

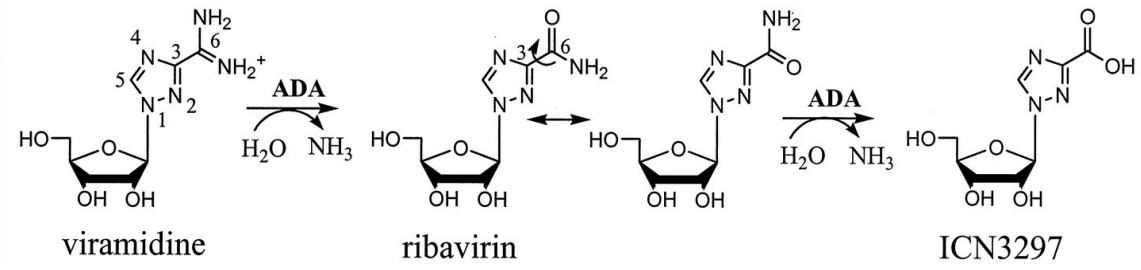

The reaction catalyzed by mammalian ADA with viramidine is successive since the inactive metabolite, ICN3297, can only be produced from ribavirin. Successive reactions utilizing substrates with nearly identical functional groups can be catalyzed randomly or in an ordered manner.

The vitamin B_{12} biosynthetic pathway requires more than 20 enzymes to assemble the complicated cobalt-corrin molecule. The pathway features four genes which encode enzymes catalyzing successive reactions. The cobA gene from *P. denitrificans* encodes an enzyme which catalyzes the methylation of C2 and C7 while cobL encodes the protein catalyzing the methylation of C5 and C15. The corresponding genes in the anaerobic *S. typhimurium* pathway are cysG and cbiE, respectively. The genes and reactions for the anaerobic and aerobic pathway are outlined in **Table 3** (*68*). No experimental evidence has been obtained to support a sequential or random mechanism for these two enzymes. The cobB and cobQ genes in the aerobic *P. denitrificans* pathway encode the two proteins responsible for the amidation of 6 carboxylic acid groups on the periphery of the molecule. The homologous genes in *S. typhimurium* are cbiA and cbiP, respectively.

Table 3. Reactions and genes required for conversion of 5-aminolaevulinic acid (ALA) to adenosylcobalamin (*68*).

Aerobic pathway (*P. denitrificans*)	**Gene**	**Anaerobic pathway (*S. typhimurium*)**	**Gene**
ALA		ALA	
↓condensation of 2 ALA	*hemB*	↓condensation of 2 ALA	*hemB*
Porphobilinogen		Porphobilinogen	
↓tetrapyrrole formation	*hemC*	↓tetrapyrrole formation	*hemC*
Hydroxymethylbilane		Hydroxymethylbilane	
↓cyclization and ring D inversion	*hemD*	↓cyclization and ring D inversion	*hemD*
Uroporphyrinogen III		Uroporphyrinogen III	
↓methylation at C-2 and C-7	*cobA*	↓methylation at C-2 and C-7	*cysG*
Precorrin 2		Precorrin 2	
↓methylation at C-20	*cobI*	↓cobalt insertion	*cbiK*, *cysG*
Precorrin 3		Cobalt–precorrin 2	
↓C-20 hydroxylation	*cobG*	↓methylation at C-20	*cbiL*
↓g-lactone formation			
Precorrin 3 hydroxylactone		Cobalt–precorrin 3	
↓C-17 methylation	*cobJ*	↓C-17 methylation	*cbiH*
↓ring contraction		↓ring contraction	
		↓d-lactone formation	
Precorrin 4		Cobalt–precorrin 4	
↓C-11 methylation	*cobM*	↓C-11 methylation	*cbiF*
Precorrin 5		Cobalt–precorrin 5	
↓C-1 methylation	*cobF*	↓C-1 methylation	Not known
↓acetic acid extrusion		↓acetaldehyde extrusion	
Precorrin 6		Cobalt–precorrin 6	
↓C-18/19 reduction	*cobK*	↓C-18/19 reduction	*cbiJ*
Dihydro-precorrin 6		Cobalt–dihydro-precorrin 6	
↓C-5, C-15 methylation	*cobL*	↓C5, C-15 methylation	*cbiE*
↓decarboxylation	*cobL*	↓decarboxylation	*cbiT*
Precorrin 8		Cobalt–precorrin 8	
↓methyl rearrangement	*cobH*	↓methyl rearrangement	*cbiC*
Hydrogenobyrinic acid		Cobyrinic acid	
↓*a,c* amidation	*cobB*	↓*a,c* amidation	*cbiA*
Hydrogenobyrinic acid *a,c*-diamide		Cobyrinic acid *a,c*-diamide	
↓cobalt insertion	*cobNST*		
Cobyrinic acid *a,c*-diamide			
↓cobalt reduction	Not known	↓cobalt reduction	Not known

Table 3. Continued.

Cob(I)yrinic acid a,c-diamide		Cob(I)byrinic acid a,c-diamide	
↓adenosylation	cobO	↓adenosylation	cobA
Ado-cobyrinic acid a,c-diamide		Ado-cobyrinic acid a,c-diamide	
↓b, d, e, g amidation	cobQ	↓b, d, e, g amidation	cbiP
Ado-cobyric acid		Ado-cobyric acid	
↓aminopropanol attachment	cobC, D	↓aminopropanol attachment	cbiB
Ado-cobinamide		Ado-cobinamide	
↓phosphorylation	cobP	↓phosphorylation	cobU
↓GMP addition	cobP	↓GMP addition	cobU
Ado-GDP-cobinamide		Ado-GDP-cobinamide	
↓a-ribazole addition	cobV	↓a-ribazole addition	cobS
Adenosylcobalamin		Adenosylcobalamin	

Though the substrates for the reactions catalyzed by CobB and CbiA differ, the reactions are identical. These enzymes catalyze the ATP dependent amidation of carboxylate groups *a* and *c* as shown in **Scheme 23**.

Scheme 23. Reaction catalyzed by CbiA.

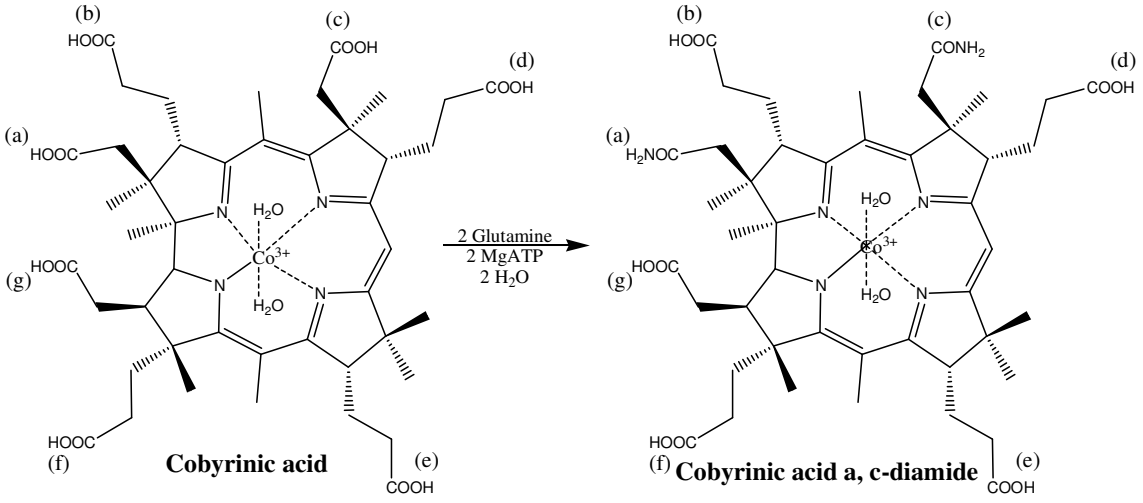

The reverse-phase HPLC for CbiA from *S. typhimurium* showed an accumulation of a single intermediate species with a retention time of ~22 minutes prior to product formation which suggested a dissociative mechanism (*26*). Observed retention times for the cobyrinic acid and cobyrinic acid *a,c*-diamide were 4 and 25 minutes, respectively. Based on HPLC data obtained for cobyrinic acid *a,c*-diamide synthetase (CobB) from *P. denitrificans*, retention times for the cobyrinic acid *a*-monoamide and cobyrinic acid *c*-monoamide are 12 and 22 minutes, respectively (*69*). These data confirmed that the *c*-carboxylate was activated and amidated then released from the enzyme prior to the activation and amidation of carboxylate *a*. Therefore, the mechanism for CbiA and CobB is sequential and dissociative. Kinetic parameters for the substrate and *c*-monoamide intermediate were calculated using the HPLC data and DNRP-RKF program which was obtained from Dr. Ronald Duggleby (*70*). Values for k_{cat} were 0.11 ± 0.01 s^{-1} for cobyrinic acid and 0.2 ± 0.03 s^{-1} for cobyrinic acid *c*-monoamide (*26*). The K_m values were 0.41 ± 0.01 μM and 0.2 ± 0.01 μM for the cobyrinic acid *c*-monoamide and cobyrinic acid, respectively (*26*). A structural explanation for the sequential dissociative mechanism has yet to be elucidated for CobB or CbiA. However, the data for these enzymes could imply similar mechanisms for the cobyric acid synthetase enzymes CobQ and CbiP which also catalyze multiple amidations.

Cobyric acid synthetase (CobQ and CbiP) catalyzes the ATP dependent amidation of carboxylate groups *b, d, e*, and *g* utilizing glutamine or ammonia as a nitrogen donor. Previous experiments with CobQ showed evidence for 3 partially amidated intermediate species by HPLC (*71*). However, the amides were not assigned.

HPLC data was collected by Dr. Vicente Fresquet and revealed that CbiP also shows three distinct intermediate species prior to the formation of cobyric acid. The chromatogram showing all five species and a time course for the reaction catalyzed by CbiP are shown in **Figure 17**. The kinetic parameters for CbiP were calculated using DNRP-RKF and the data points from the HPLC using equations 10-14.

$$S_0 = S + P + Q + \mathrm{R} + \mathrm{T} \quad (10)$$

$$(\mathrm{d}S/\mathrm{dt}) = -k_s E/(1 + K_s/S)(1 + P/K_p + Q/K_q + R/K_r + T/K_t) \quad (11)$$

$$(\mathrm{d}P/\mathrm{dt}) = (\mathrm{d}S/\mathrm{dt}) - (k_p E)/(1 + K_p/P)(1 + S/K_s + Q/K_q + R/K_r + T/K_t) \quad (12)$$

$$(\mathrm{d}Q/\mathrm{dt}) = (\mathrm{d}P/\mathrm{dt}) - (k_q E)/(1 + K_q/Q)(1 + S/K_s + P/K_p + R/K_r + T/K_t) \quad (13)$$

$$(\mathrm{d}R/\mathrm{dt}) = (\mathrm{d}Q/\mathrm{dt}) - (9)/(1 + K_r/R)(1 + S/K_s + P/K_p + Q/K_q + T/K_t) \quad (14)$$

S_0 is the initial concentration of substrate, *S, P*, *Q*, *R* and *T* are the concentrations at any time of ado-Cob and tri-, tetra- and pentamide derivates and cobyric acid, respectively, *E* is the concentration of enzyme, *K* is the Michaelis constant for any of the five corrinoids and t is time. The kinetic parameters are outlined in **Table 4**.

Table 4. Kinetic parameters for reaction catalyzed by CbiP.

Compound	K_m (μM)	k_{cat} (min^{-1})	K_i (μM)
Ado-cobyrinic acid diamide	2.7 ± 0.06	3.6 ± 0.2	
Ado-cobyrinic acid triamide	1.0 ± 0.06	2.4 ± 0.1	
Ado-cobyrinic acid tetraamide	0.8 ± 0.02	3.6 ± 0.2	
Ado-cobyrinic acid pentamide	0.7 ± 0.08	8.4 ± 0.1	
Cobyric acid			5.9 ± 0.2

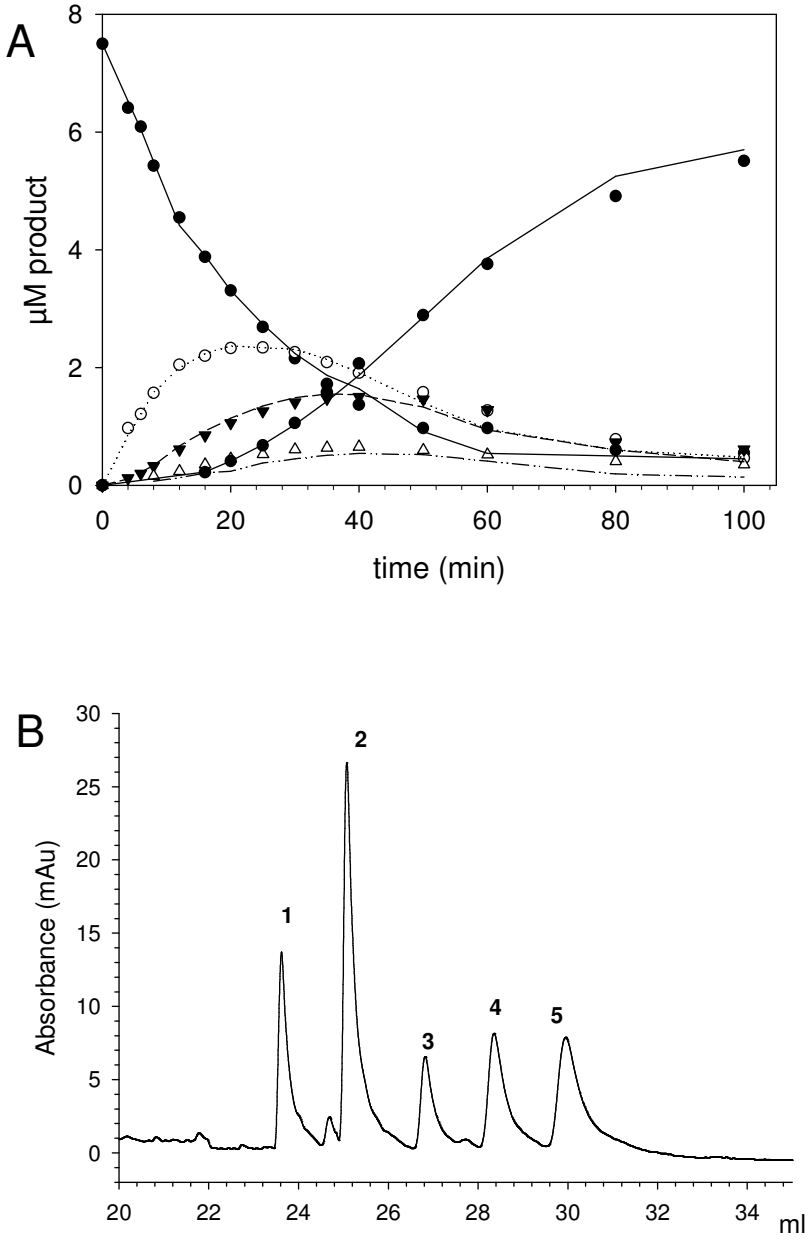

Figure 17. WT-CbiP activity. A) Time course of the reaction catalyzed by CbiP. (●) Ado-cob, (○) tri-, (▼) tetra-, and (Δ) pentamide intermediate, and (♦) cobyric acid. The lines represent fits of the model using DNRP-RKF program. B) HPLC analysis of the activity of wild type CbiP. **1**, Ado-cob; **2**, triamide; **3**, tetraamide; **4**, pentamide intermediates; and **5**, Ado-cobyric acid.

Based on these data, it is proposed that CbiP catalyzes the amidation of carboxylates *b, d, e*, and *g* in a sequential and dissociative manner. There is no crystal structure for cobyric acid synthetase nor has a structural or molecular explanation for the mechanism been proposed. However, a model for the synthetase domain of CobQ has been proposed by Galperin and Grishin based on homology to dethiobiotin synthetase (*14*). The crystal structure of cobyric acid shows that the spatial orientation of the four carboxylates is different (see **Figure 18**). The carboxyl groups *b*, *d*, *e* and *f* are facing to one side of the ring, the side chains *a* and *c* and the adenosyl group are facing to the other side, while the *g* carboxylate is in the plane. This crystal structure also shows that the three carboxylates *b*, *d* and *e* can bind to the same active site by a 90º rotation of the corrinoid. However, the *f* carboxylate can not. This suggests that the asymmetry introduced by the position of the *f* chain could be used by the enzyme to determine the amidation order. In the model of the synthetase domain of CbiP, the carboxylate groups *b*, *d*, *e*, and *f* are facing the binding pocket as illustrated in **Figure 19**. Based on this hypothesis, a residue with a negative charge in the active site or interacting with the substrate could aid or prevent the binding of the molecule in a particular orientation.

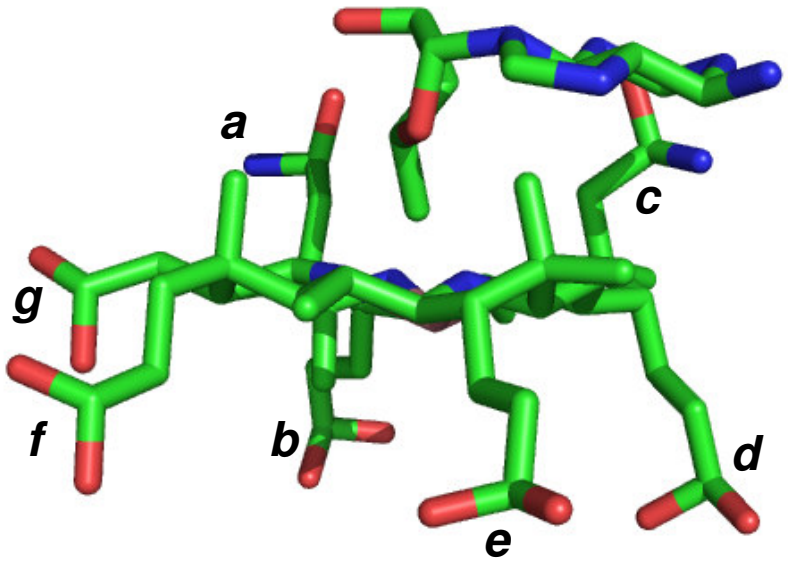

Figure 18. Structure of adenosyl-cobyrinic acid *a,c*-diamide. Coordinates for adenosyl-cobyrinic acid *a,c*-diamide were taken from the crystal structure file for CobA from *Salmonella typhimurium* (PDB id 1G64) (*72*).

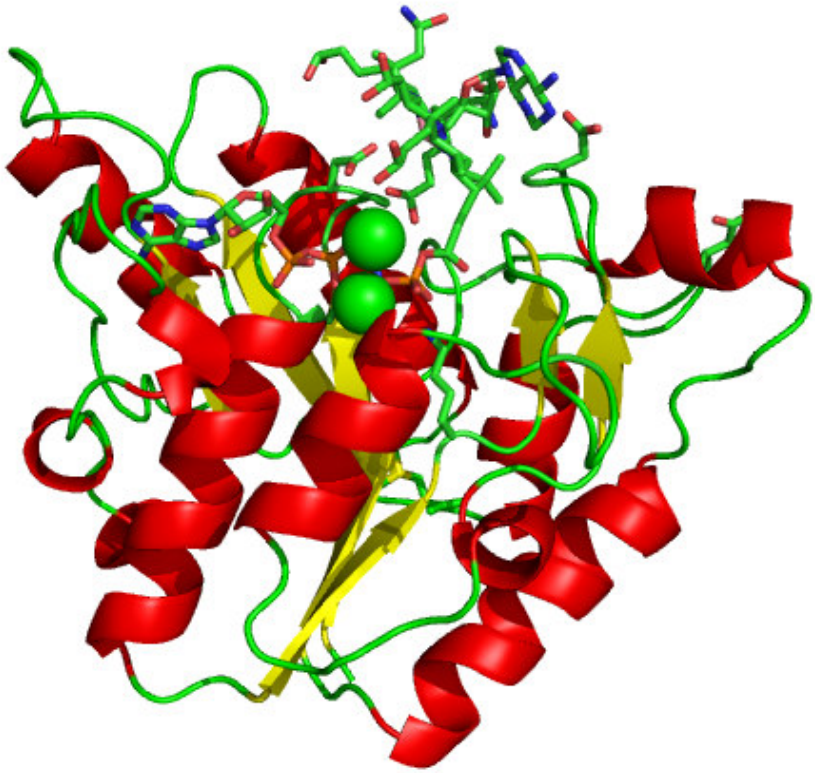

Figure 19. Model of CbiP based on the crystal structure of dethiobiotin synthetase (PDB id 1DAK). Coordinates for adenosyl-cobyrinic acid *a,c*-diamide were taken from the crystal structure file for CobA from *Salmonella typhimurium* (PDB is 1G64) (*14, 72*). The phosphate group on carboxyl group *e* was built using WebLab ViewerPro 4.0. The ADP was in the PDB file for dethiobiotin synthetase.

A comparison of 34 different cobyric acid synthetases shows 5 negatively charged polar amino acids conserved in the synthetase domain. These residues are E54, E132, E139, E234, and D235. Glutamate 54 and E132 are not in the active site nor appear to be in position to interact with ADP, Mg^{2+}, or ado-cob. Glutamate 234 is positioned ~3.6 Å from the ADP amine and D235 is 6 Å from a metal ion and 4 Å from the 3' hydroxyl group of the ADP ribose. Glutamate 139 is located on a loop close to the ado-cob and could serve to stabilize the substrate upon binding. Other negatively charged amino acid residues appeared in many of the synthetases but were not conserved. These residues include D13, D84, D146, D165, and 167.

Aspartate 146 is conserved in 32 of the 34 aligned cobyric acid synthetases and D165 has one exception. Aspartate 167 is conserved in 30 of the aligned sequences and D13 and 84 are conserved in 27. Aspartates 165 and 167 are not in the active site nor do they appear to be in proximity to interact with ADP, Mg^{2+}, or ado-cob. It is evident from the model that D13 could be the negative residue which unfavorably interacts with carboxylate groups *g* and/or *f*. Aspartate 84 is positioned 2.3 Å from the amine on the ado-cob adenine which suggests D84 aides in substrate binding and stabilization. **Figure 20** outlines the interactions of D13 and D84 with the substrate. Aspartate 146 is not located in the binding pocket but is on a loop, with E139, that could move to interact with the substrate upon binding. There are two serine residues in the active site that could serve as cobalt ligands, S12 and S136. These serines are conserved in all the cobyric acid synthetases aligned.

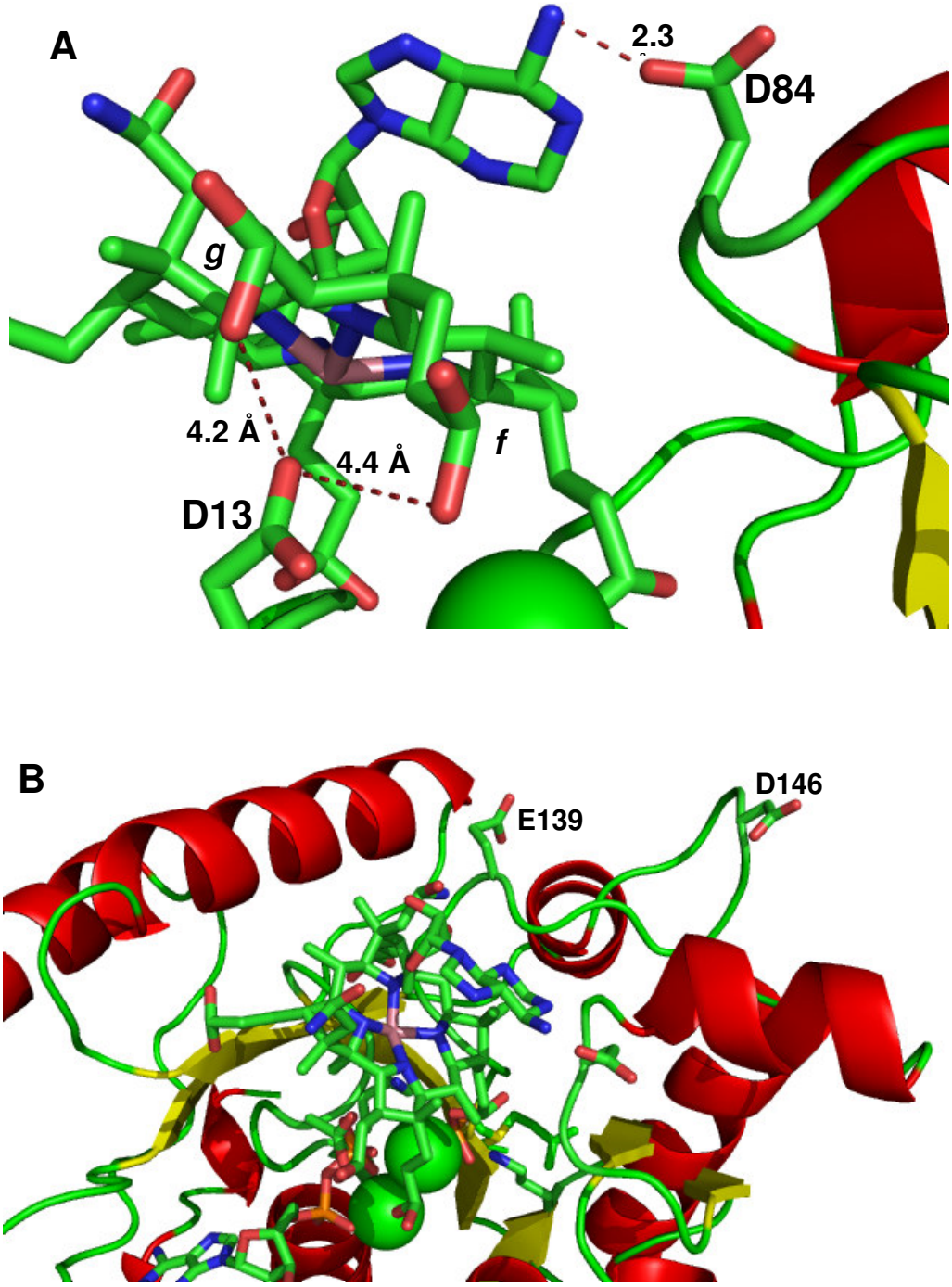

Figure 20. Model of CbiP showing conserved residues D13, D84, E139, and D146. **A**. Interactions of D13 and D84 with ado-cob. **B**. Location of E139 and D146.

These serines are directly under the cobalt and along with D13 are the only polar residues on the two loops under the corrin. Thus it is possible that D13 is a cobalt ligand. The distances between the cobalt and the serines and aspartic acid are shown in **Figure 21**. Though the distances are not optimal for these interactions, conformational changes could occur that could bring the residues in closer proximity of the cobalt.

To investigate if these amino acids are involved in the determination of the amidation order, mutants of residues D146, D165, D167, E234, D235 and D267 were constructed by Dr. Vicente Fresquet. The kinetic parameters for these mutants along with wild-type CbiP are listed in **Table 5**. The substitution by alanine of the E234 and D235 residues has a dramatic effect on the activity. No amidation was detected when glutamine was used and a three order of magnitude decrease in the activity was measured when the reaction was carried out using ammonia. The mutants D146A, D146N, D165A and D167A have a moderate effect on the catalytic activity independent of the nitrogen source. The mutant D267A has only 1% of the wild type activity with ammonia and 0.2-0.6% of the wild type activity with glutamine. No effects on the affinity for ATP, ado-cob or ammonia were detected. However, the substitution of alanine for D267 had a drastic effect on the activity when glutamine was used as nitrogen source. To investigate whether these mutants had an effect on the amidation order, the product distribution was measured via HPLC as a function of time and compared to that of wild-type CbiP.

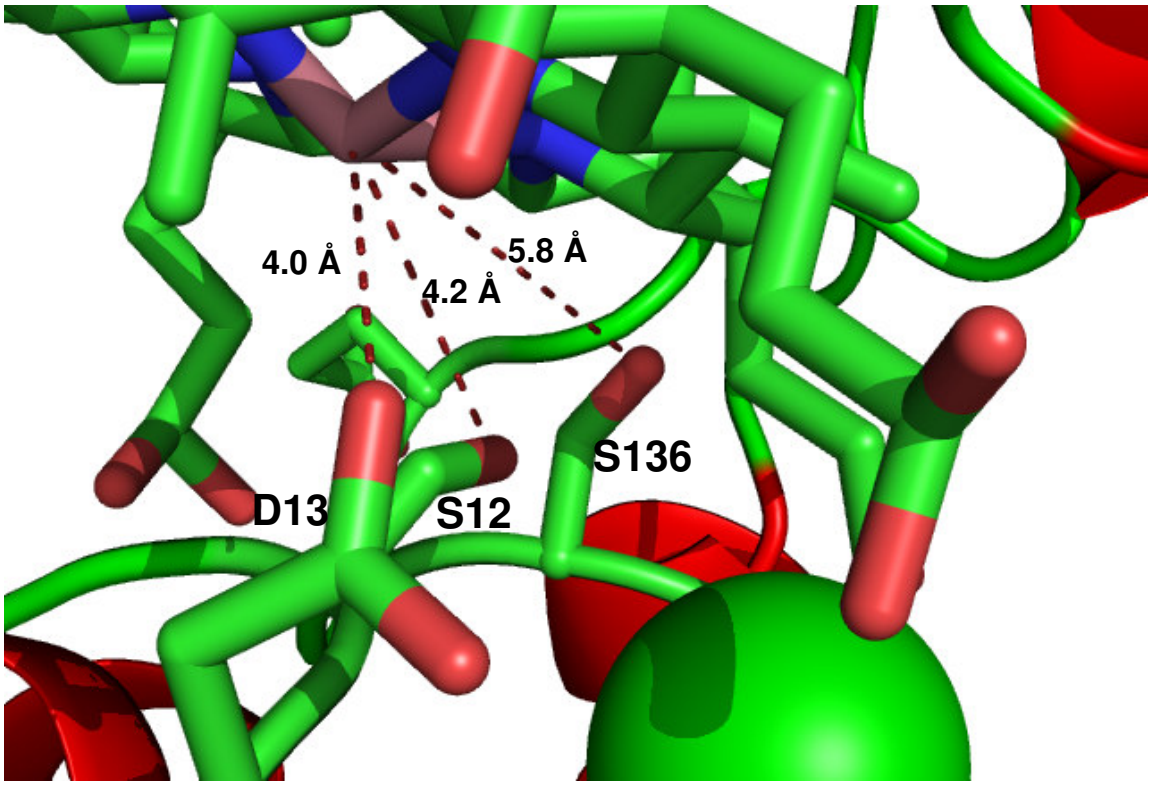

Figure 21. Interactions of S12, D13, and S136 with the corrin cobalt in the active site of CbiP.

Table 5. Kinetic parameters of wild type and mutants of CbiP[a]

Protein	ATP		Ado-cob		Glutamine		Ammonia	
	K_m (μM)	V/K (M^{-1} s^{-1})	K_m (μM)	V/K (M^{-1} s^{-1})	K_m (*23*)	V/K (M^{-1} s^{-1})	K_m (*23*)	V/K (M^{-1} s^{-1})
wt	41 ± 6	3000 ± 400	3.5 ± 0.5	28600 ± 1000	1.2 ± 0.3	108 ± 7	29 ± 5	3.5 ± 0.4
D146A	101 ± 14	104 ± 9	5.2 ± 0.2	2310 ± 150	4 ± 0.6	5 ± 0.8	36 ± 4	0.3 ± 0.02
D146N	83 ± 2	330 ± 30	3.9 ± 0.5	5130 ± 800	1.4 ± 0.2	14 ± 2	33 ± 5	0.9 ± 0.1
D165A	30 ± 5	1670 ± 200	3.5 ± 0.6	11400 ± 1000	3.5 ± 3	35 ± 3	33 ± 2	1.8 ± 3
D167A	30 ± 5	3300 ± 500	5.8 ± 0.8	7070 ± 900	1.8 ± 0.4	50 ± 10	26 ± 4	3.1 ± 0.4
E234A	-	<0.05	-	<0.05	-	<0.05	-	<0.05
D235A	-	<0.05	-	<0.05	-	<0.05	-	<0.05
D267A[b]	48 ± 6	246 ± 29	7.7 ± 0.8	727 ± 80	-	<0.05	30 ± 4	0.3 ± 0.02

[a]Activity was determined by quantification of the rate of ADP formation.
[b]The ATP and Ado-cob parameters were obtained using ammonia as nitrogen source.

As previously discussed, the HPLC chromatograms for wild-type CbiP show three intermediate species that accumulate prior to formation of the product, cobyric acid. The peak distribution pattern agrees with previous studies with CobQ, and is indicative of a sequential and dissociative mechanism. This suggests that the enzyme catalyzes one amidation reaction during each catalytic cycle. The product of the first reaction is released into solution and binds to the enzyme in a different orientation for the next catalytic cycle. For the mutant enzymes, only small differences in the kinetic parameters were observed with the exception of E234A and D235A. The HPLC data for the mutants D165A, D167A, and D267A display similar distributions as obtained for wild-type CbiP. However, the HPLC traces for the D146 mutants display very peculiar patterns not characteristic of the wild-type enzyme. At early incubation times, a new peak is observed with D146A and D146N. This peak has a retention time between the substrate and the triamide species. For the D146A mutant, a small peak is observed with a retention time slightly longer than the original triamide species. A comparison of the HPLC assays are shown in **Figure 22**. The exact mass of the corrinoids contained in these peaks was measured with a PE Sciex APJ Qstar Pulsar mass spectrometer by the Laboratory for Biological Mass Spectrometry at Texas A&M University. A mass of 935.5 amu was obtained for the first peak (**a** in **Figure 22**) generated by both mutants.

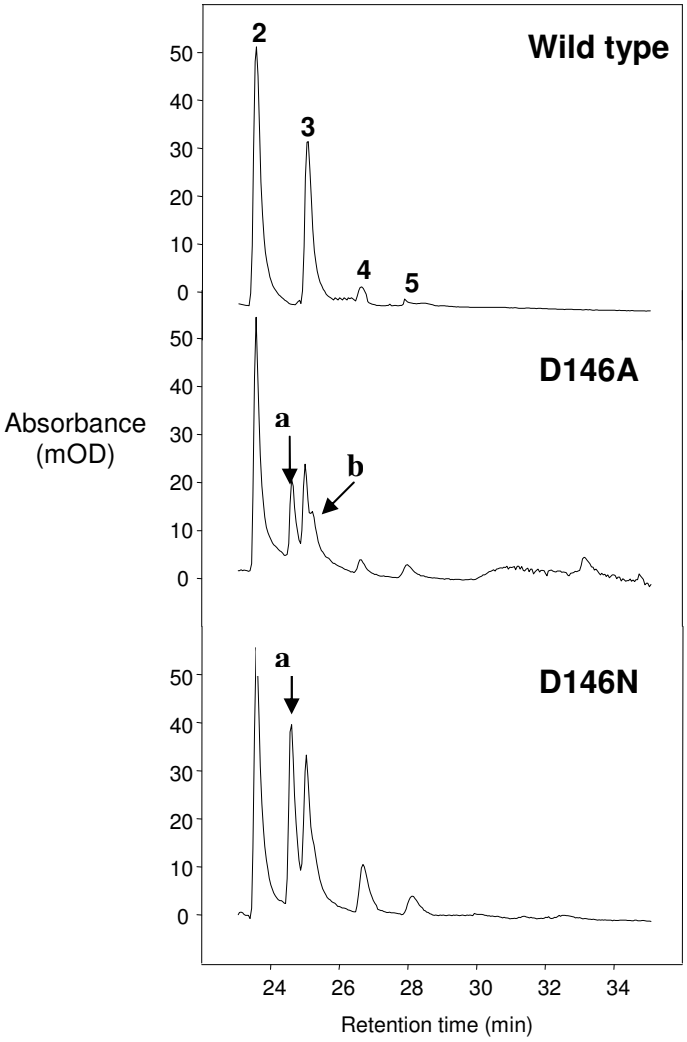

Figure 22. HPLC chromatograms for WT-CbiP, D146A, and D146N. **2**, triamide; **3**, tetraamide; **4**, pentamide intermediates; and **5**, Ado-cobyric acid. **a** and **b**, new triamide intermediate species.

This mass is consistent with the loss of a hydroxyl group and formation of an amide. This indicates the synthesis of a different triamide intermediate by both mutants. An identical mass was found for the second peak (**b** in **Figure 22**) in the chromatogram for the D146A mutant. These results demonstrate that all the peaks, **a**, **2**, and **b** observed in the time courses of the mutant enzymes are triamide intermediates. This would suggest that mutating D146 perturbs the strict order of amidation and causes some randomization.

Assignment of the amidation order for wild-type CbiP has been achieved by utilizing ^{15}N labeled ammonia and ^{1}H-^{15}N HSQC NMR spectroscopy. Quenching the reactions at varied times and the use of isotope edited spectroscopy allowed the identification of amides labeled with ^{15}N as the reaction progressed. Investigations of the random amidations catalyzed by the D146 mutant of CbiP were carried out with ^{15}N labeled glutamine.

Materials and Methods

Cobyrinic acid was a gift from the laboratory of Dr. Ian Scott. Cobyrinic acid *a,c*-diamide synthetase (CbiA), cobyric acid synthetase (CbiP), mutant cobyric acid synthetase (D146N), and cob(I)yrinic acid *a,c*-diamide adenosyltransferase (CobA) were cloned and purified by Dr. Vicente Fresquet in the Raushel laboratory. Stab agar cultures of hexahistidine-tagged ferredoxin (flavodoxin), $NADP^+$ reductase (Fpr) and flavodoxin (FldA) from *E. coli* K-12 were obtained from the NARA Institute of Science and Technology in Japan. Nitrogen-15 labeled ammonium chloride was purchased from Cambridge Isotope Laboratories and ^{15}N-glutamine was purchased from Aldrich. The 4.6 x 150 mm Microsorb 100 C18 5-μm reverse-phase chromatography column was purchased from Varian, Inc. All other chromatography columns and resins were purchased from Amersham Biosciences. All other materials were purchased from Sigma.

Synthesis of Cobyrinic Acid a,c-Diamide. Cobyrinic acid *a,c*-diamide was synthesized enzymatically from cobyrinic acid. Cobyrinic acid (100 μM), 20 mM KCl, 2 mM DTT, 4 mM L-glutamine, 1.0 mM ATP, 2.0 mM $MgCl_2$, and 50 mM Tris-HCl, pH 7.7 were incubated at 30 ºC for 15 minutes. The total volume varied between 35-40 mL per preparation. The reaction was initiated by adding CbiA to a final concentration of 3.6 μM and the mixture was incubated for 12 hours. The reaction progress was monitored by reverse-phase HPLC at 360 nm (*69*). If the reaction was not complete, additional ATP, $MgCl_2$, DTT, L-glutamine, and CbiA were added and incubated for an additional 8 hours. The reaction was quenched with KCN (10 mM final concentration) and heated in an 80 ºC water bath for 10 minutes. The solution was applied to a HiLoad™ 16/10 Q

Sepharose anion exchange column and eluted with buffer A, 25 mM TEA-HCO_3, pH 8 and buffer B, 500 mM TEA-HCO_3, pH 8 using a five segment gradient. The elution gradient was started at 0% buffer B and increased to 50% buffer B over 3 column volumes followed by isocratic elution at 50% buffer B for 4 column volumes. The concentration of buffer B was then increased to 100% over 10 column volumes and isocratic elution at 100% buffer for an additional 10 column volumes. The fractions which absorbed at 360 nm were analyzed by HPLC and the fractions containing cobyrinic acid *a,c*-diamide were pooled and concentrated. The compound was washed four times with water to remove excess salt, redissolved in water and the pH adjusted to 7.5.

Synthesis of Adenosyl-cobyrinic Acid a,c-Diamide. The substrate for the CbiP reaction was synthesized enzymatically with Fpr, FldA, and CobA. A solution containing 300 nmol cobyrinic acid *a,c*-diamide, 10 μmol NADPH, 80 μmol DTT, 160 μmol ATP, 320 μmol $MgCl_2$, 190 nmol Fpr, 252 nmol FldA, and 50 mM Tris-HCl pH 8, was degassed with argon for 90 minutes. CobA, 0.2 mg mL^{-1}, was used to initiate the reaction and the solution was incubated overnight in the dark at 30 ºC. The reaction was monitored by the decrease in the absorbance at 360 nm which is characteristic of the cobyrinic acid *a,c*-diamide (*69*). Adenosyl-cobyrinic acid *a,c*-diamide was detected at 303 nm ($\varepsilon = 21\ mM^{-1}\ cm^{-1}$) and 456 nm ($\varepsilon = 9\ mM^{-1}\ cm^{-1}$) (*71*). Once the absorbance at 360 nm ceased to decrease, the sample was applied to an anion exchange column and eluted with 1 M TEA-HCO_3, pH 7.5 with a linear gradient. All fractions absorbing at

both 303 and 456 nm were pooled and concentrated to dryness. The residue was washed 5 times with water to remove excess salt and the pH adjusted to 7.5.

Purification of $(His)_6$-Fpr and $(His)_6$-FldA. Cells from the stab agar cultures were streaked on LB agar with 25 μg mL^{-1} chloramphenicol. The selected cells were used to inoculate 5 mL overnight cultures which were used to inoculate 500 mL cultures. Protein expression was induced by adding 0.1 mM IPTG to a mid-log phase cell culture. The cells were incubated at 37 ºC for 24 hours then collected by centrifugation. The cell paste was resuspended in a solution containing 20 mM Tris-HCl, pH 7.5, 500 mM NaCl, and 5.0 mM imidazole. Cells were lysed by sonication and the lysate clarified by centrifugation. The cell lysate was applied to a Chelating Sepharose Fast Flow resin (25 mL) previously charged with 50 mM $NiSO_4$ and washed with a buffer containing 20 mM Tris-HCl, pH 7.6, 500 mM NaCl, and 5.0 mM imidazole. The column was treated with an additional 100 mL of buffer to remove any unbound protein. A 50/50 mixture of binding buffer/elution buffer (150 mL) was applied to the column followed by 80 mL of 100% elution buffer. The elution buffer contained 20 mM Tris-HCl, pH 7.6, 500 mM NaCl, and 1.0 M imidazole. An absorption maximum at 456 nm for Fpr is characteristic of the bound FAD with an extinction coefficient (ε) of 8 mM^{-1} cm^{-1} (Fujii, 1977 #83). Fractions absorbing at both 280 and 456 nm were analyzed by SDS-PAGE for Fpr and fractions containing the protein pooled and dialyzed against 50 mM Tris-HCl, pH 7.6. Activity of Fpr was confirmed by using a cytochrome c reduction assay outlined by Fujii and Huennekens (*73*). FldA contains bound FMN which absorbs at 464 nm with an extinction coefficient (ε) 8.4 mM^{-1} cm^{-1} (*74*). Fractions absorbing at 280 and 456 nm

were analyzed by SDS-PAGE for FldA and fractions containing the protein pooled and dialyzed against 50 mM Tris-HCl, pH 7.6. FldA activity was assessed in the adenosyl-cobyrinic acid *a,c*-diamide synthesis reaction.

Adenosyl-cobyric Acid Synthesis. The production of adenosyl-cobyric acid and intermediate species was monitored by HPLC (*69, 75*). A 1.0 mL sample was loaded onto the C18 column equilibrated in 0.1 M potassium phosphate, pH 6.5, 10 mM KCN (buffer A). The products were eluted at a flow rate of 1 mL/min at room temperature in a mobile phase using buffer A and 0.1 M potassium phosphate, pH 8.0, 10 mM KCN and 50% acetonitrile (buffer B). The linear gradient system used was: 0 to 2% buffer B in 5 min, 2 to 5% buffer B in 5 min, 5 to 20% buffer B in 10 min, followed by 10 min of isocratic elution at 20% buffer B, 20 to 50% buffer B in 5 min, 50 to 100% in 5 min and 100 to 0% buffer B in 5 min. The elution of the adenosyl-cobyric acid and derivates was monitored by the absorption at 303 nm (*71*).

Synthesis of Adenosyl-cobyric Acid and Intermediates. Adenosyl-cobyrinic acid *a,c*-diamide (100 μM) was incubated with 25 mM Tris-HCl, pH 7.5, 25 mM ^{15}N-$NH_4^+Cl^-$, 4.0 mM $MgCl_2$, 2.0 mM ATP, 1.0 mM DTT, and 200 μg mL^{-1} wild-type CbiP at 30 ºC in the dark for various times. The total volume of each assay was 1.0 mL. The reactions were quenched by lowering the pH to 5. Wild-type CbiP samples were prepared for NMR analysis by adding 50 μL of D_2O and transferring the solution to a 5 mm NMR tube wrapped in aluminum foil. Analysis of mutant D146N CbiP was achieved by incubating 37.5 μM adenosyl-cobyrinic acid *a,c*-diamide, 20 mM Tris-HCl, pH 7.5, 1.0 mM ^{15}N-glutamine, 1.0 mM DTT, 4.0 mM ATP, 8.0 mM $MgCl_2$, and 50 or

200 μg mL^{-1} D146N CbiP. The total volume of the mutant assays was 1.5 mL. The reactions were quenched by reducing the pH to 5. The glutamine was hydrolyzed by adding 10 units of glutaminase and incubating for an hour at 30 ºC in the dark. The sample was then concentrated and brought up to 650 μL with 600 μL H_2O containing 5 units of glutaminase and 50 μL of D_2O. The sample was transferred to a 5 mm NMR tube wrapped in foil. All samples were manipulated in the dark and stored in eppendorfs covered in foil to prevent hydrolysis of the cobalt-carbon bond.

NMR Acquisition Parameters. ^{1}H-^{15}N heteronuclear single quantum correlation (HSQC) spectra were obtained according to the pulse sequence outlined by Kay et. al. (*76*). The acquisition time was 80 ms with a relaxation delay of 1.1 seconds. The sweep width in the proton dimension was set at 7000 Hz and 1000 Hz in the nitrogen dimension. All chemical shift values are reported from $^{15}NH_3$.

Results

Synthesis of Cobyrinic Acid a,c-Diamide. Cobyrinic acid *a,c*-diamide was synthesized from cobyrinic acid, L-glutamine, ATP, $MgCl_2$, and CbiA. The final solution of cobyrinic acid *a,c*-diamide displayed a maximum absorbance at 360 nm which is characteristic of cobalt corrinoid compounds (*69*). The exact mass of the corrinoid compound was measured by the Laboratory for Biological Mass Spectrometry at Texas A&M University and a mass of 936.4 amu was obtained. This is in agreement with the mass for the cobyrinic acid *a,c*-diamide. The compound was obtained in 87% yield.

Purification of $(His)_6$-Fpr and $(His)_6$-FldA. Fpr was pooled and the activity checked using the cytochrome *c* reductase assay (*77*). Using the extinction coefficient for cytochrome *c*, the specific activity was calculated to be 425 units mg^{-1}. The enzyme was divided into 1 mL aliquots containing 2.4 mg of Fpr. FldA was pooled and stored in 1 mL aliquots containing 2.5 mg of protein. The activity of FldA was assessed in the synthesis of ado-cob.

Synthesis of Adenosyl-cobyrinic Acid a,c-Diamide. Adeonsyl-cobyrinic acid *a,c*-diamide (Ado-cob) was synthesized using Fpr, FldA, CobA, NADPH, ATP, $MgCl_2$, and cobyrinic acid, *a,c*-diamide. The final product is a pale yellow solution with absorbance maxima at 303 and 456 nm which is consistent with literature values (*71*). The ado-cob was determined by HPLC to be pure. The corresponding HPLC is shown in **Figure 23A**. The compound was obtained in 44-47% yield.

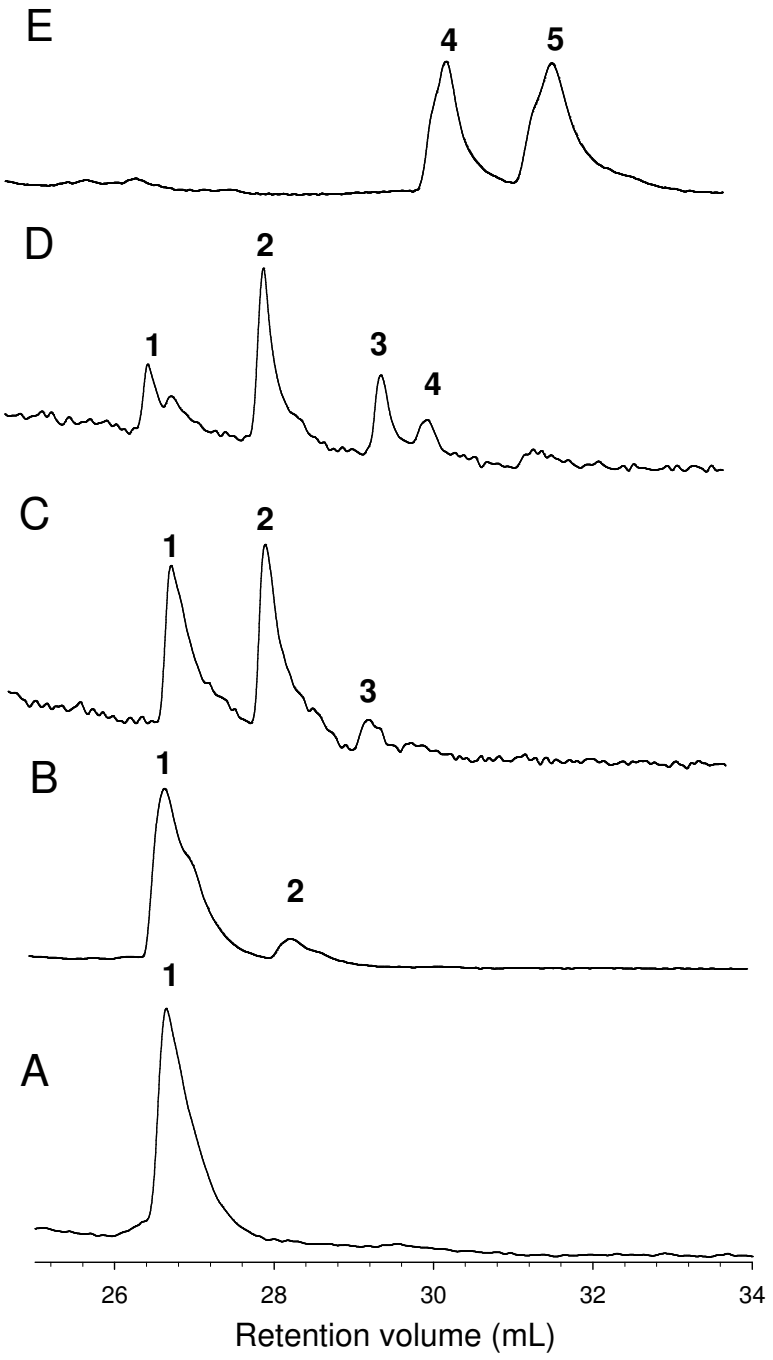

Figure 23. HPLC chromatograms for WT-CbiP. **A**, Ado-cob starting material; **B**, CbiP reaction quenched after 15 minutes in 1:0:0:0 ratio (triamide:tetraamide:pentamide:cobyric acid); **C**, CbiP reaction quenched after 30 minutes in 6:1:0:0 ratio; **D**, CbiP reaction quenched after 60 minutes in 13:7:4:0 ratio; **E**, CbiP reaction incubated overnight in 0:0:1;1 ratio. **1**, Ado-cob; **2**, triamide; **3**, tetraamide; **4**, pentamide; and **5**, cobyric acid.

Synthesis of Adenosyl-cobyric Acid and Intermediates. Ado-cob was incubated with CbiP and saturating concentrations of ATP, $MgCl_2$, and ^{15}N labeled ammonium chloride. The reaction progress was monitored by HPLC and samples prepared based on the distribution of species at various time intervals. Incubating the reaction for 15 minutes yields a chromatogram that is primarily the starting material and the triamide species as shown in **Figure 23B**. The reaction was allowed to incubate for 30 and 60 minutes which yielded the chromatograms shown in **Figure 23C** and **D**, respectively. The distribution of the partially amidated species in the 30 and 60 minute sample are 6:1:0:0 and 13:7:4:0 (triamide:tetraamide:pentamide:cobyric acid), respectively. An overnight incubation of the reaction produces the chromatogram shown in **Figure 23E** which shows the pentamide species and the final product, cobyric acid, in a 1:1 ratio. These samples were analyzed by ^{1}H-^{15}N HSQC NMR to establish the amidation order. The chemical shift values have been reported in literature for a series of cobinamide and cobalamin species (*78*). Cobalamins feature axial nucleotides connected at carboxylate *f* which chelate the cobalt ion. Cobinamides lack this axial nucleotide ligand and have groups covalently attached to the cobalt ion on the same side of the molecule as groups *a* and *c* similar to ado-cob. The ^{15}N NMR chemical shift assignments for two cobinamide species in H_2O are shown in **Table 6**.

Table 6. ^{15}N chemical shift assignments (ppm) (*78*).

	Amide *d*	Amide *b*	Amide *e*	Amide *g*
CH_3-Cbi	108.7	110.2	109.2	111.9
Ado-Cbi	108.2	110.2	109.0	111.5

Based on these data it is possible to establish the amidation order according to the ^{15}N chemical shift trend.

The 2D NMR spectrum of the pentamide:cobyric acid sample, HPLC **E** in **Figure 23**, is shown in **Figure 24**. The spectrum displays four carboxamides with the *syn* and *anti* protons separated very well. The ^{15}N chemical shifts are in agreement with the trend reported in the literature. Carboxamides *d, e, b*, and *g* resonate at 108.2, 109.1, 110.1, and 111.3 ppm, respectively. All chemical shifts are reported relative to a $^{15}NH_3$ standard. When the reaction was quenched after 15 minutes, the predominant species according to the HPLC chromatogram, see **Figure 23B**, is the triamide intermediate. The NMR spectrum of this sample showed one amide resonance which corresponds to carboxamide *e*. The chemical shift of this amide is 109.2 ppm as shown in **Figure 25**. The NMR spectrum of the sample corresponding to the HPLC in **Figure 23C** was quenched after 30 minutes. The NMR shows two species, the triamide and tetraamide intermediates in a 6:1 ratio, see **Figure 26**. The new resonance at 108.2 ppm agrees with the chemical shift values reported for carboxamide *d*. The first intermediate, triamide *e*, is still the predominant species and the chemical shift of the new peak is within the range of chemical shifts for carboxamide *e*. Therefore, it is concluded that the chemical shift of carboxamide *e* changes slightly once the adjacent carboxylic acid becomes amidated and the chemical shift of the *e* carboxamide in the tetraamide species is 109.1 ppm. This spectrum establishes carboxylic acid *d* as the second group to be amidated by CbiP.

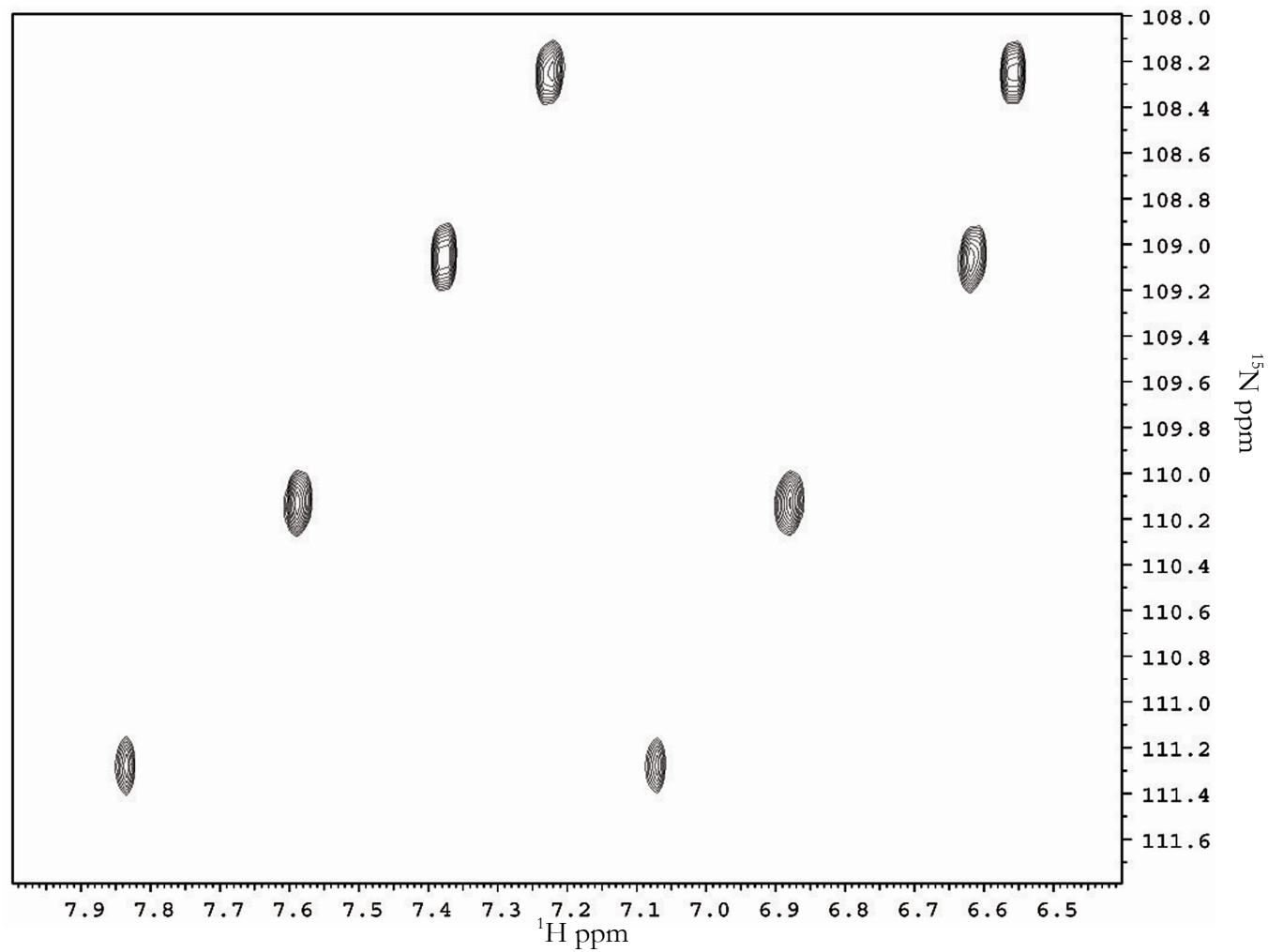

Figure 24. 2D NMR spectrum of sample incubated overnight with CbiP. The ratio of species is 0:0:1:1 (triamide:tetraamide:pentamide:cobyric acid).

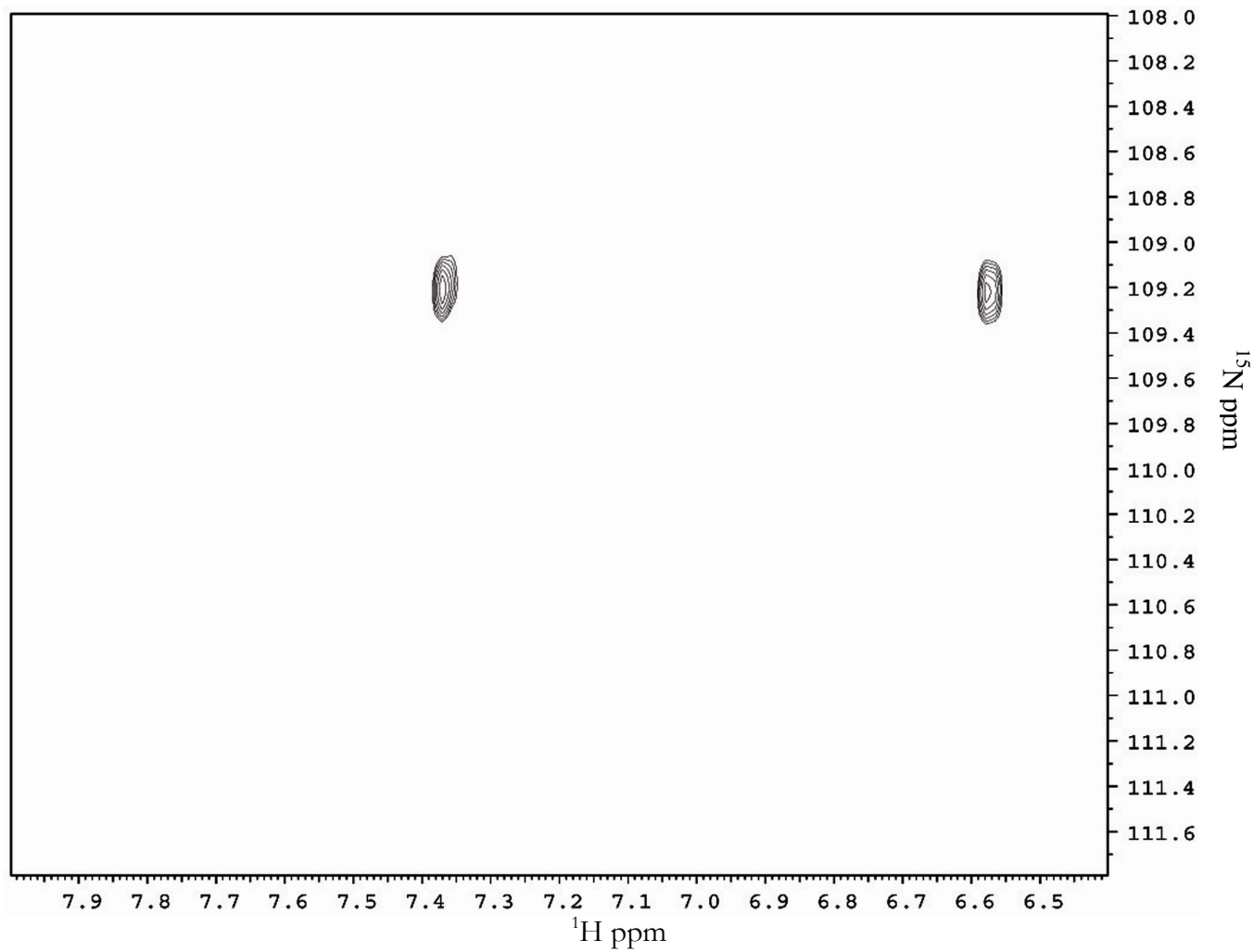

Figure 25. 2D NMR spectrum of the CbiP reaction quenched after 15 minutes. Ratio of species is 1:0:0:0 (triamide:tetraamide:pentamide:cobyric acid).

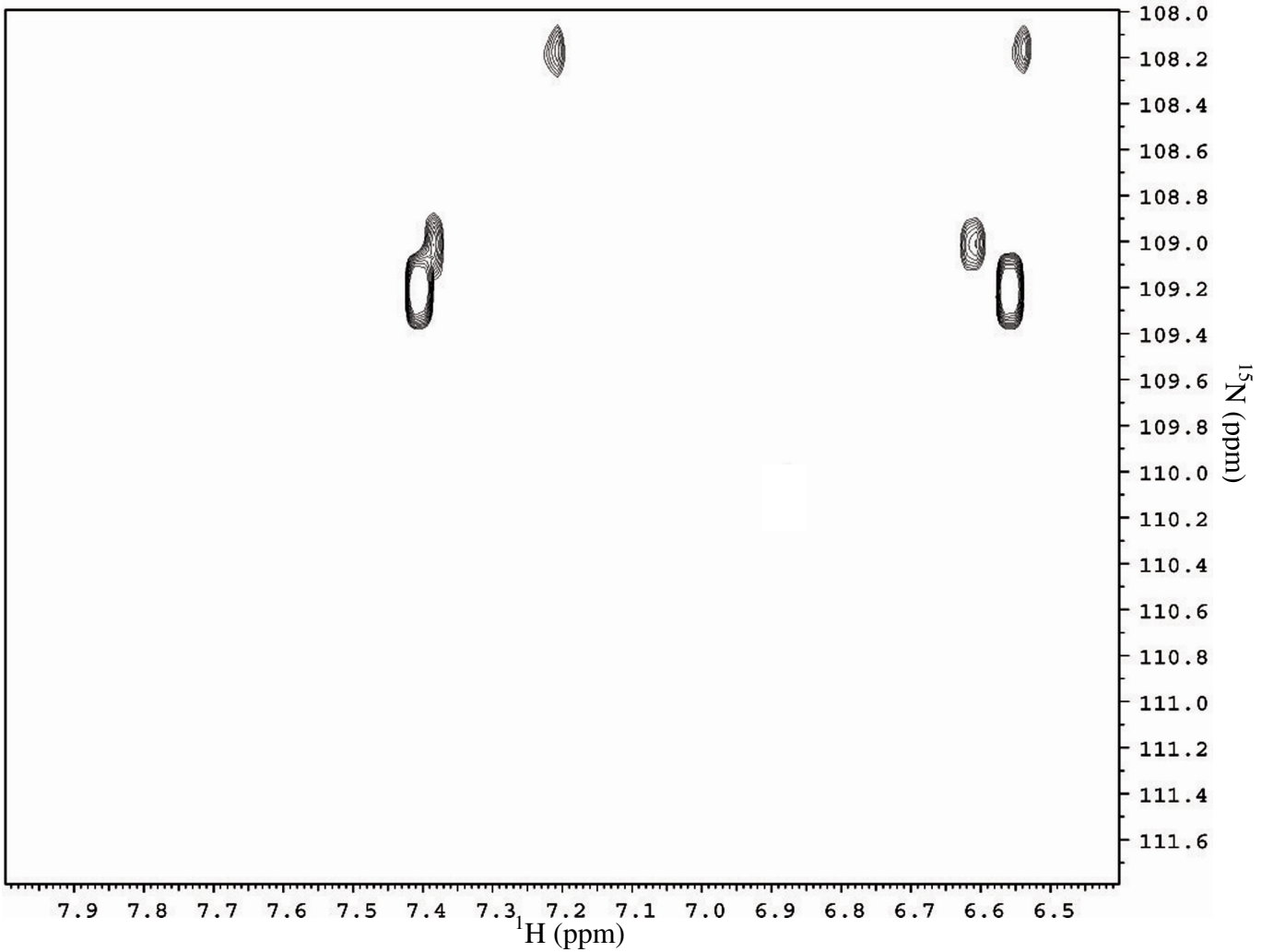

Figure 26. 2D NMR spectrum of sample incubated with CbiP for 30 minutes. Ratio of species is 6:1:0:0 (triamide:tetraamide:pentamide:cobyric acid).

The chemical shift differences can be explained by the vastly different spatial orientation of carboxylate *g* relative to carboxylates *b, d,* or *e*. Carboxylates *b, d*, *e,* and *f* extend below the plane of the corrin molecule while carboxylate *g* is in the plane of the corrin ring. As the negative charge at carboxylate *e* is eliminated the adjacent carboxylic acids, *d* and *f*, could form ion-dipole interactions with the resulting amide. Once carboxylic acid *d* is amidated, one of the ion-dipole interactions changes into a dipole-dipole interaction thus slightly changing the resonating frequency of carboxamide *e*. Since carboxylic acid *g* is not in the same orientation as carboxylate *b*, these interactions may not be present or are too weak to produce significant chemical shift changes in the sample containing the pentamide:cobyric acid in equal amounts. The differences in chemical shift per sample could be due to slight variations in pH.

The next sample prepared for NMR analysis was allowed to react for 60 minutes. The HPLC is shown in **Figure 23D** and the corresponding NMR spectrum, shown in **Figure 27**, reveals three intermediate species. There are new peaks at 110.2 ppm corresponding to carboxamide *b* and no evidence of an amide at carboxylate *g*. This confirms that the next amide to be formed is carboxamide *b*. It is also clear that the amidation of carboxylate *b* has an effect on the chemical shift of carboxamide *d*, primarily in the proton dimension. These spectra identify the order of amidation catalyzed by CbiP as *e, d, b*, then *g*.

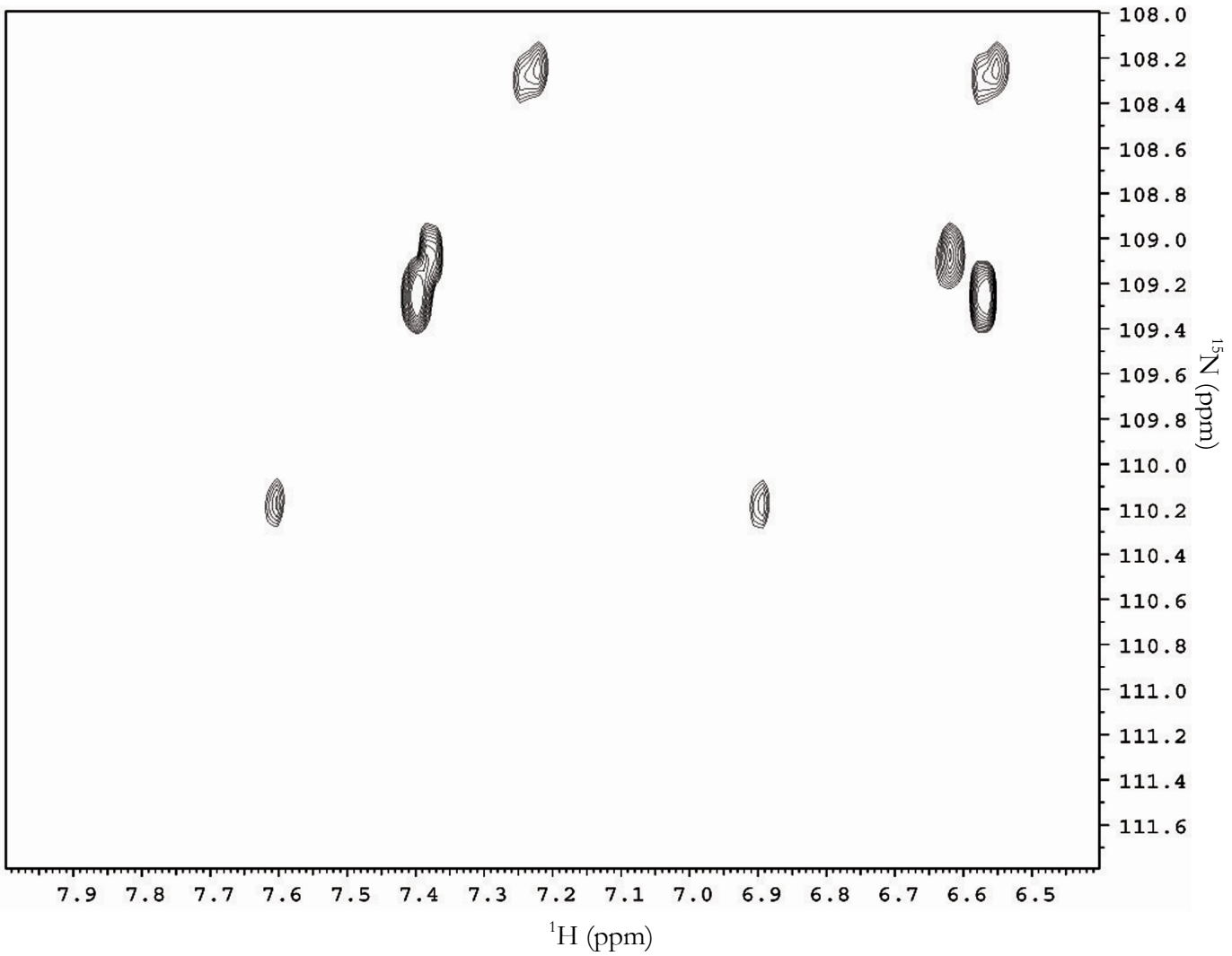

Figure 27. 2D NMR spectrum of sample incubated for 1 hr with CbiP. The ratio of species is 13:7:4:0 (triamide:tetraamide:pentamide:cobyric acid).

The formation of different triamide species is evident in the HPLC of the mutant D146A and D146N CbiP. The identification of the different species was investigated by utilizing ^{15}N glutamine instead of ^{15}N ammonium chloride since multiple triamide species were not present in the HPLC where ammonia was used. The first reaction, incubated with 50 μg mL^{-1} of D146N, was quenched after 60 minutes and treated with glutaminase. The HPLC, see **Figure 28A**, shows two triamide species present in a 1:1 ratio. The NMR spectrum confirms the presence of two distinct triamide species as illustrated in **Figure 29**. The ^{15}N chemical shift values are 108.6 and 109.3 ppm for the upfield and downfield peaks respectively. The experiments with wild-type CbiP have previously established the chemical shift of 109.2 ppm for the carboxamide *e* triamide. The peak at 108.6 ppm is in the range reported for species amidated at carboxylate *d* thus must represent a triamide intermediate with an amide in the *d* position only. This spectrum confirms the formation of multiple triamide species. The lack of multiple peaks in the HPLC for the tetraamide and pentamide species suggests that the triamide species converge to a common tetraamide species or the retention time for the multiple tetraamide species are nearly identical. Unfortunately the tetraamide species never accumulates to a significant extent before the pentamide species is formed. However, the relative concentrations of various species can be elucidated by integrating the HPLC and calculating NMR peak volumes in a sample void of cobyric acid. The HPLC of a sample incubated 30 minutes with 200 μg mL^{-1} D146N is shown in **Figure 28B**.

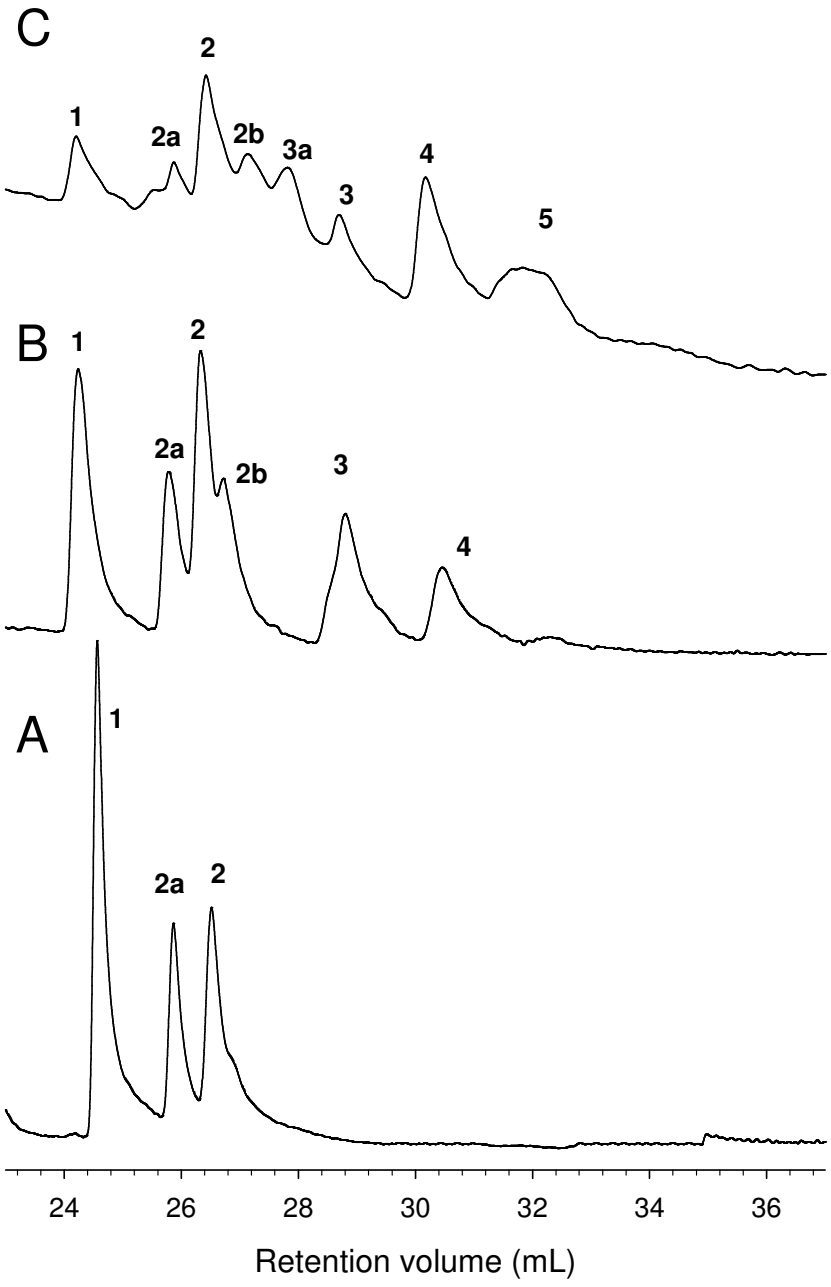

Figure 28. HPLC traces for D146N NMR samples. A) Sample incubated with 50 μg mL^{-1} D146N for 60 minutes showing two triamide species in a 1:1 ratio. B) Sample incubated with 200 μg mL^{-1} D146N for 30 minutes showing triamide, tetraamide, and pentamide species in an 8:1:2 ratio. C) Sample incubated with 200 μg mL^{-1} D146N for 60 minutes showing all species in a 5:2:2:1 ratio. Species assignments are as follows: **1**, Ado-cob; **2**, normal triamide species; **2a** and **2b**, new triamide species; **3**, tetraamide species; **3a**, possible new tetraamide species; **4**, pentamide species; **5**, cobyric acid.

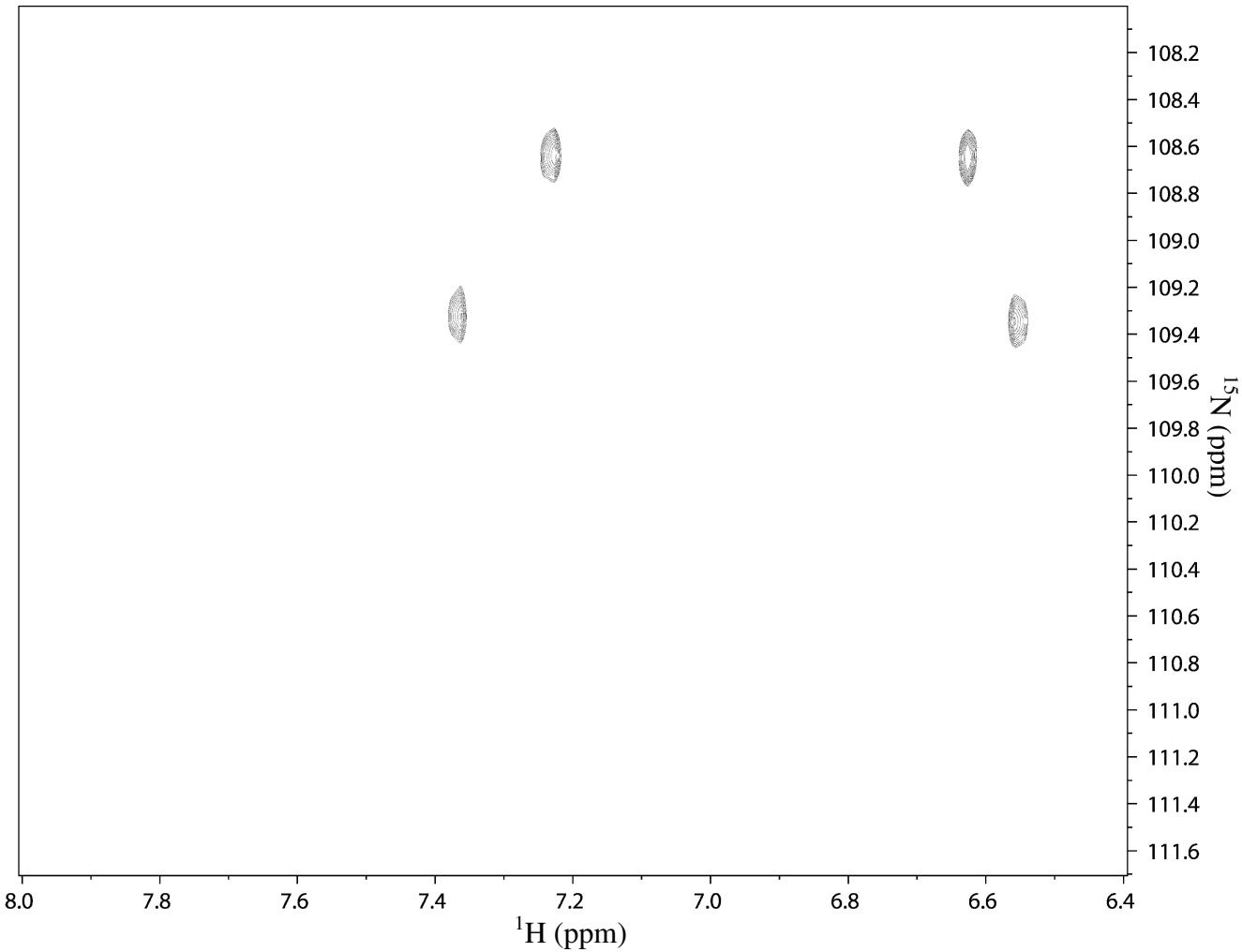

Figure 29. 2D NMR spectrum of D146N sample incubated with 50 μg mL^{-1} enzyme for 60 minutes. The ratio of triamide species is 1:1.

The distribution of triamide:tetraamide:pentamide:cobyric acid species in this sample is 8:1:2:0. The NMR spectrum, shown in **Figure 30**, shows ~5 sets of peaks in the regions of carboxamides *d*, *e*, and *g*. For clarity, each region in **Figure 30** will first be addressed separately.

The chemical shift region for *d* carboxamides is between 108-109 ppm. This region contains two sets of peaks. The set of peaks at 108.6 ppm have been assigned as the *d* triamide species from the previous NMR spectrum in **Figure 29**.

The peaks at 108.3 ppm are identical to the peaks observed for the *d* amide in the wild-type CbiP shown in **Figure 26**. Therefore, the peaks in this region appear to represent carboxamide *d* species from the triamide species at 108.6 ppm and tetraamide species at 108.3 ppm. The chemical shift range of 109-110 ppm is the region where the *e* carboxamides resonate. The two most upfield peaks in the proton dimension are coupled to protons both resonating at 7.36 ppm, thus, the downfield peak represents two protons which overlap. Therefore, all further references to the two resonances in the *e* carboxamide region refer to the well separated upfield peaks at 6.55 and 6.59 ppm. The peaks in the ^{15}N dimension at 109.3 ppm were observed in the previous NMR spectrum and have been assigned to the *e* triamide species. The peaks at 109.2 ppm can be identified as the *e* amide of the tetraamide and pentamide intermediate species from comparisons with the NMR spectra of wild-type CbiP, **Figure 26**. The region of the *g* amides is between 111-112 ppm. The peaks at 111.3 ppm represent the species amidated at position *g* which is in agreement with the chemical shift of carboxamide *g* in the wild-type CbiP NMR spectrum shown in **Figure 24**.

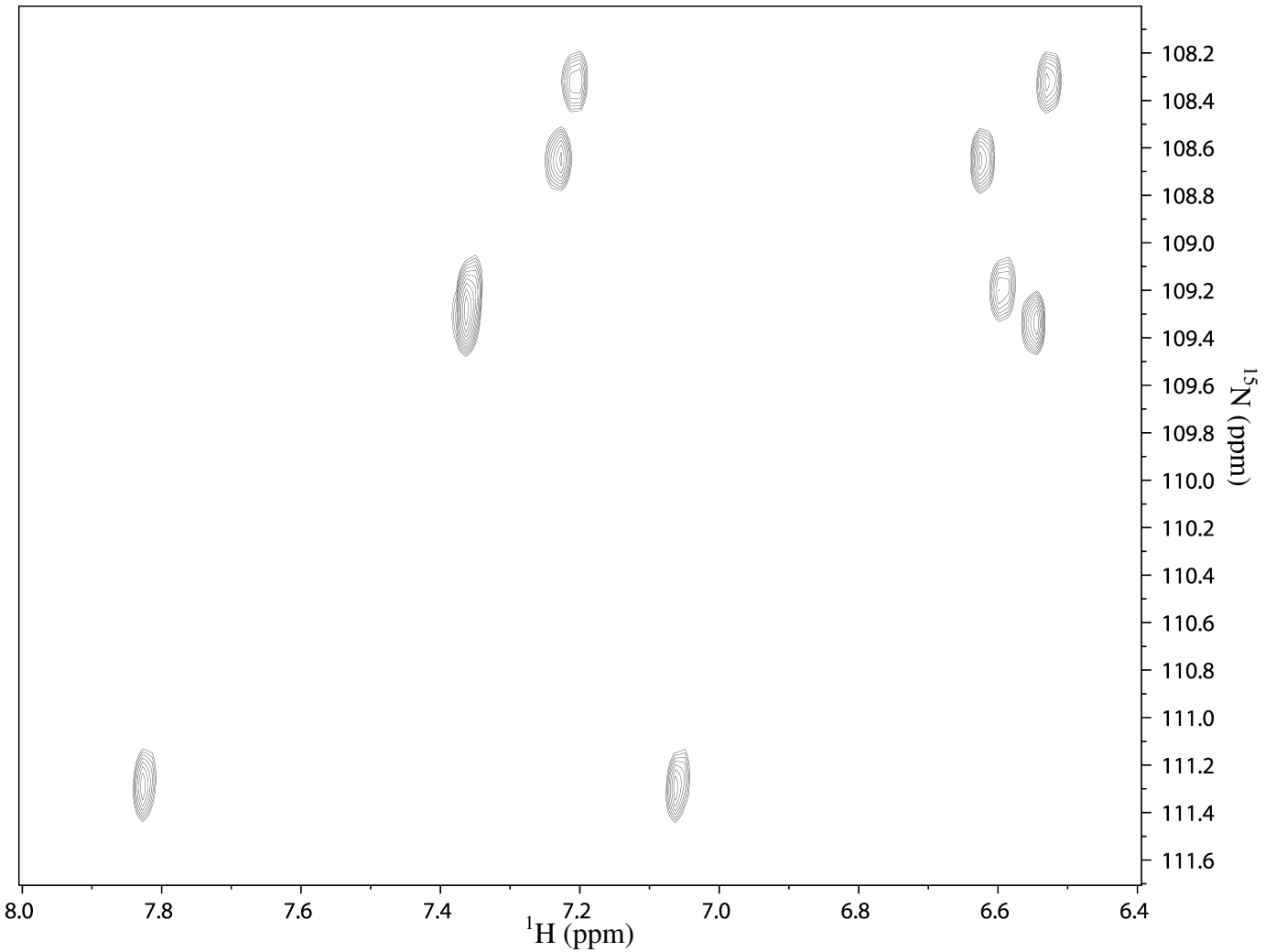

Figure 30. NMR spectrum of D146N sample incubated with 200 μg mL^{-1} enzyme for 30 minutes. The species are in an 8:1:2 ratio (triamide:tetraamide:pentamide:cobyric acid).

There are no peaks observed in the *b* carboxamide region, 110-111 ppm, which establishes carboxylate *b* as the last group to be amidated. Though the NMR spectrum in **Figure 30** appears to conclusively identify the species present, there are species present in the HPLC (**2b** in **Figure 28B**) that are not visually identifiable. Species containing *dg* or *eg* tetraamides and *g* triamides would not show an effect in the NMR spectrum. For example, consider the chemical shift changes that were observed for carboxamides *e* and *d* once carboxylates *d* and *b* became amidated, respectively, for the wild-type CbiP as demonstrated in **Figures 26** and **28**. The chemical shifts for carboxamides *e* and *d* were not affected by the formation of carboxylate *g* as indicated by **Figure 24**. Therefore, the presence or lack of the *g* triamide, *eg*, and *dg* tetraamide species must be deduced from the HPLC integration and NMR peak volume calculations.

There are 24 different pathways possible for the amidation of carboxylate groups *e, d, b*, and *g*. These pathways are outlined in **Scheme 24**.

Scheme 24. The 24 different pathways possible for the amidation of carboxylate groups *b, d, e*, and *g*.

1. e=> b=> d=> g	13. d=> e=> b=> g
2. e=> b=> g=> d	14. d=> e=> g=> b
3. e=> d=> b=> g	15. d=> b=> e=> g
4. e=> d=> g=> b	16. d=> b=> g=> e
5. e=> g=> b=> d	17. d=> g=> b=> e
6. e=> g=> d=> b	18. d=> g=> e=> b
7. b=> d=> e=> g	19. g=> d=> e=> b
8. b=> d=> g=> e	20. g=> d=> b=> e
9. b=> e=> d=> g	21. g=> e=> d=> b
10. b=> e=> g=> d	22. g=> e=> b=> d
11. b=> g=> d=> e	23. g=> b=> d=> e
12. b=> g=> e=> d	24. g=> b=> e=> d

Since the NMR spectrum verifies that carboxylate *b* is amidated last, this eliminates 18 of the 24 possible pathways. The remaining pathways are shown in **Scheme 25**.

Scheme 25. Remaining possible pathways for amidation of carboxylate groups *e, d, g*, and *b*.

```
 4. e=> d=> g=> b
 6. e=> g=> d=> b
14. d=> e=> g=> b
18. d=> g=> e=> b
19. g=> d=> e=> b
21. g=> e=> d=> b
```

The HPLC integration of the triamide, tetraamide, and pentamide intermediates in **Figure 28B** shows the percentages of the species as 74, 9, and 17% respectively. Nitrogen-15 labeled amides are considered here since only those amides contribute to the NMR signal. Hence 74% of the total pool contains one amide, 9% of the pool contains 2 amides, and 17% contains 3 amides. To calculate the fractions for each NMR signal, the number of amides in each pool must be considered. If 74 of the 100 species contain one amide they contribute 74 to the NMR signal. Likewise, 9 of the 100 species contain two amides thereby contributing 18 to the total NMR signal and 17 contain three amides thus contributing 51. So out of 143 total signals, the 74 triamides should make up ~52% of the total NMR signal, the 9 tetraamides give rise to ~13% , and the 17 pentamides contribute ~36% of the NMR signal. The *g* carboxamide resonance contains the signal for the *g* triamide, *dg* and *eg* tetraamide species, and *deg* pentamide species. However, since the amidation of carboxylate *g* has no affect on the chemical shift of the *de* tetraamide species, the *deg* pentamide species contributes equally to the *de* tetraamide

signal at 108.3 ppm, the *de* tetraamide signal at 109.2 ppm, and the *deg* pentamide signal at 111.3 ppm. Therefore, the pentamide species which contribute 36% of the total NMR signal is divided by 3 and will be 12% of the signals at 108.3, 109.2, and 111.3 ppm. The peak volumes for the five NMR signals show that each signal contributes almost ~20% of the total, see **Table 7**.

Table 7. Percentages for NMR signals and species which comprise the signal.

^{15}N Chemical shift (ppm)	Species at signal	% of the total NMR signal
108.3	de + deg	20
108.6	d + dg	21
109.2	de + deg	20
109.3	e + eg	19
111.3	g + dg + eg + deg	20

Since the *deg* pentamide species contributes 12% to the signals at 108.3, 109.2, and 111.3 ppm, the two *de* species at 108.3 and 109.2 contribute 8% each. Therefore the total percentage that tetraamide *de* contributes to the NMR signal is 16%. Recalling the percentages calculated for the total tetraamide NMR signal, 13%, it is clear that there are no *eg* and *dg* tetraamide species in this sample. This does not rule out the possibility of these species being formed later in the reaction. Pentamide species *deg* contributes 12% to the species at 111.3 thus leaving 8% of the remaining signal for the *g* triamide species which must be the identity of **2b** in **Figure 28B**. Therefore, *dg* and *eg* tetraamide species will be formed but are not represented in the NMR spectrum shown in **Figure 30**.

A sample confirming the last amidation at position *b* was obtained by incubating 200 μg mL^{-1} D146N with the substrates for 60 minutes, see the HPLC in **Figure 28C**. The NMR spectrum is shown in **Figure 31**. This spectrum confirms the amidation of carboxylate *b* as the last step in the reaction catalyzed by D146N CbiP. The carboxamide *d* resonance is now shifting because of the amidation of its adjacent carboxylic acid. This further supports the idea that amidations at carboxylate *g* have no affect on the chemical shifts of carboxamides *d* and *e*. The appearance of another new peak in the HPLC, **3a** in **Figure 28C**, could be for the *dg* and/or *eg* tetraamide species. However, the overlapping resonances at 108.3 ppm prevent accurate peak volume calculations of the corresponding species.

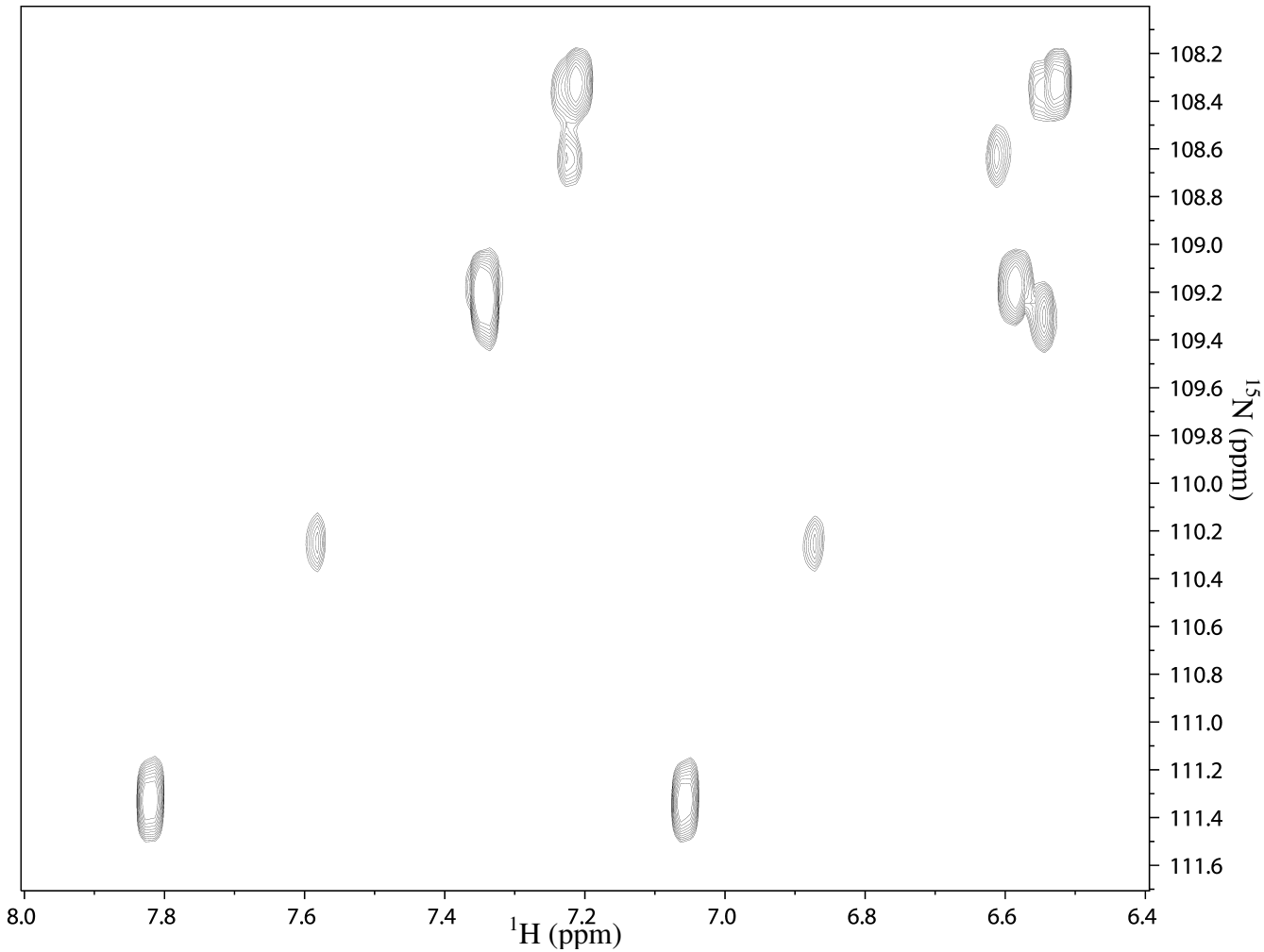

Figure 31. 2D NMR spectrum of sample incubated for 60 minutes with 200 μg mL^{-1} D146N. The ratio of species is 5:2:2:1 (triamide:tetraamide:pentamide:cobyric acid).

Discussion

Cobyric acid synthetase (CbiP) from *Salmonella typhimurium* catalyzes the ATP dependent amidation of carboxylate groups *b, d, e*, and *g* in a sequential and dissociative manner. The strict order of the amidations catalyzed by the wild-type enzyme has been probed using ^{1}H-^{15}N HSQC NMR spectroscopy. During the course of the reaction, three partially amidated species can be observed by reverse-phase HPLC. The first intermediate has been identified as the *e* triamide. The amidation of the next carboxylic acid was established by preparing a sample quenched later in the reaction. The sample contained two species, the triamide and tetraamide intermediates in a 6:1 ratio, identified as the *e* and *d* amide species. This establishes *d* as the second carboxylate group to be amidated by CbiP. Later samples confirmed carboxamide *b* as the third amidation product and the formation of carboxamide g follows.

A structural or molecular explanation for this strict ordered reaction has not yet been outlined. In the sequence, 11 aspartates and glutamates are conserved in more than 80% of the cobyric acid synthetases aligned. Some of these residues could interact with the substrate to assist or prevent the binding of the substrate in a particular orientation. To probe this idea, some of these conserved residues were mutated and the HPLC patterns of the mutants compared to the patterns observed for wild-type CbiP. Among all the mutants tested, the two D146 mutants displayed HPLC unlike the chromatogram obtained for the wild-type enzyme.

Multiple species were observed in the HPLC for the first intermediate formed and multiple species for the tetraamide intermediate were determined by HPLC

integration and in-depth NMR analysis. The multiple triamide species have been identified as *e*, *d*, and *g* triamides. Although multiple triamide and tetraamide species have been identified, no evidence for multiple pentamide species has been observed. The data clearly established carboxylate *b* as the last group to be amidated by D146N CbiP. Thus the multiple triamide and tetraamide species converge to a common *deg* pentamide species. These data support a partially randomized amidation order catalyzed by D146N mutant CbiP. Aspartate 146 is located on a loop with E139 above the ATP and ado-cob binding pocket. These residues, along with D84 on another loop above the binding pocket, may be key residues in stabilizing and binding the substrate in the correct orientation for the ordered amidations. In the model of CbiP, D84 is within hydrogen bonding distance to the adenine amide on ado-cob. Conformational changes involving the D146 and E139 loop could bring these two residues within hydrogen bonding distance of amides *c* and *a* to facilitate proper binding of the substrate for catalysis. Once the amidation at carboxylate *e* is completed in the reaction catalyzed by wild-type CbiP, the substrate is released from the active site.

Therefore, the interactions of D146, E139, and D84 with the substrate/intermediate must be different after the first, second, and third catalytic cycles thus allowing a different binding orientation of the substrate. Mutation of D146 perturbs the strict order of amidation catalyzed by CbiP perhaps by allowing multiple interactions of equal magnitude between E139 and D84 with the substrate/intermediate. For example, in wild-type CbiP D146, E139, and D84 could interact with carboxamide *a*, carboxamide *c*, and the amine group on the adenine covalently bound to the cobalt ion. Mutation of

D146 eliminates one ion-dipole interactions which leaves E139 and D84 to interact with two of the three groups. Thus there are three different sets of interactions possible for the binding of ado-cob. These interactions include carboxamides *a* and *c*, carboxamide *a* and the amine on the adenine, and carboxamide *c* and the amine on the adenine. This would support the presence of three different triamide intermediate species for the D146N mutant. Nevertheless, wild-type CbiP follows the strict amidation of *e, d, b*, then *g*, whereas D146N CbiP catalyzes random amidation for the triamide and tetraamide species, followed by convergence of the species to the *deg* pentamide, and finally the amidation of carboxylate *b*.

CHAPTER V

CONCLUSIONS

Divergent evolution within the amidohydrolase superfamily has been studied for years. The superfamily contains seven structurally characterized enzymes with binuclear metal centers, four members with mononuclear metal centers, and one with no metal ion (*5*). Uronate isomerase has been established as the only characterized member of this superfamily that does not require metal ions for catalytic activity (*46*). Another distinguishing feature of uronate isomerase is the reaction catalyzed by the enzyme. Uronate isomerase catalyzes the isomerization of D-glucuronate and D-galacturonate to D-fructuronate and D-tagaturonate, respectively. Among the structurally characterized amidohydrolase superfamily members, uronate isomerase is the only member which catalyzes a nonhydrolytic reaction (*5*). The data presented in this dissertation clearly establishes the isomerization mechanism of uronate isomerase as a proton transfer. These differences suggest that uronate isomerase represents one of the most highly evolved members of the amidohydrolase superfamily.

Adenosine-5'-triphosphate (ATP) has many roles in enzyme catalyzed reactions. The hydrolysis of ATP generates energy which could be used by the enzyme or cell, ATP could be a substrate, and/or ATP could be used to activate a substrate. In the ATP dependent amidations catalyzed by cobyrinic acid *a,c*-diamide synthetase and cobyric acid synthetase from *S. typhimurium*, ATP has been established as a substrate activator by positional isotope exchange. The corresponding substrate is phosphorylated by ATP

at a carboxylate group prior to nucleophilic attack by ammonia affording the amine products or intermediates. These experiments confirm the lack of a phosphorylated enzyme species for both cobyrinic acid *a,c*-diamide synthetase and cobyric acid synthetase from *S. typhimurium*.

Successive enzymatic reactions are very interesting, but random or ordered mechanisms have not been established for many of these enzyme systems. Identifying preferential binding orientation or explaining the structural basis for the regiochemistry is very difficult without a crystal structure. The biosynthetic pathway of vitamin B12 continues to be of great interest to many researchers. The complex corrin compound is synthesized with more than 20 enzymes. Two of the enzymes in the pathway catalyze successive methylation reactions and two catalyze successive amidations. Cobyrinic acid *a,c*-diamide synthetase catalyzes the amidation of carboxylate groups *a* and *c*. Cobyric acid synthetase catalyzes the amidation of carboxylate groups *b, d, e* and *g*. The ordered dissociative mechanism of cobyrinic acid *a,c*-diamide synthetase from *P. denitrificans* and *S. typhimurium* was previously established by HPLC characterization of the intermediates (*26, 69*). The ordered dissociative mechanism of cobyric acid synthetase from *S. typhimurium* has been established by ^{1}H-^{15}N HSQC NMR. The wild-type enzyme catalyzes the formation of carboxamide *e, d, b*, then *g*. A thorough understanding of the structural basis for this specificity is unknown. However, mutation of aspartate 146 to alanine causes partial randomization of the first three amidations. The final amidation always occurs at carboxylate *b*. These data support the idea of substrate-

enzyme interactions which dictate binding orientation but a thorough understanding for the specificity is still lacking.

REFERENCES

1. Holm, L., and Sander, C. (1997) An evolutionary treasure: Unification of a broad set of amidohydrolases related to urease, *Proteins: Struct., Funct., Genet. 28*, 72-82.
2. Banner, D. W., Bloomer, A. C., Petsko, G. A., Phillips, D. C., Pogson, C. I., Wilson, I. A., Corran, P. H., Furth, A. J., Milman, J. D., Offord, R. E., Priddle, J. D., and Waley, S. G. (1975) Structure of chicken muscle triose phosphate isomerase determined crystallographically at 2.5 Å resolution: Using amino acid sequence data, *Nature 255*, 609-614.
3. Reardon, D., and Farber, G. (1995) The structure and evolution of alpha/beta barrel proteins, *FASEB J. 9*, 497-503.
4. Voet, D., and Voet, J. G. (1995) *Biochemistry*, 2nd ed., John Wiley & Sons, Inc., New York.
5. Seibert, C. M., and Raushel, F. M. (2005) Structural and catalytic diversity within the amidohydrolase superfamily, *Biochemistry 44*, 6383-6391.
6. Benning, M. M., Shim, H., Raushel, F. M., and Holden, H. M. (2001) High resolution x-ray structures of different metal-substituted forms of phosphotriesterase from *Pseudomonas diminuta*, *Biochemistry 40*, 2712-2722.
7. Wang, Z., and Quiocho, F. A. (1998) Complexes of adenosine deaminase with two potent inhibitors: X-ray structures in four independent molecules at pH of maximum sctivity, *Biochemistry 37*, 8314-8324.

8. Liaw, S. H., Chen, S. J., Ko, T. P., Hsu, C. S., Chen, C. J., Wang, A. H. J., and Tsai, Y. C. (2003) Crystal structure of D-aminoacylase from *Alcaligenes faecalis* DA1. A novel subset of amidohydrolases and insights into the enzyme mechanism, *J. Biol. Chem. 278*, 4957-4962.

9. Schwarzenbacher, R., Canaves, J. M., Brinen, L. S., Dai, X., Deacon, A. M., Elsliger, M. A., Eshaghi, S., Floyd, R., Godzik, A., Grittini, C., Grzechnik, S. K., Guda, C., Jaroszewski, L., Karlak, C., Klock, H. E., Koesema, E., Kovarik, J. S., Kreusch, A., Kuhn, P., Lesley, S. A., McMullan, D., McPhillips, T. M., Miller, M. A., Miller, M. D., Morse, A., Moy, K., Ouyang, J., Robb, A., Rodrigues, K., Selby, T. L., Spraggon, G., Stevens, R. C., van den Bedem, H., Velasquez, J., Vincent, J., Wang, X., West, B., Wolf, G., Hodgson, K. O., Wooley, J., and Wilson, I. A. (2003) Crystal structure of uronate isomerase (TM0064) from *Thermotoga maritima* at 2.85 Å resolution, *Proteins: Struct. Funct. and Genet. 53*, 142-145.

10. Peekhaus, N., and Conway, T. (1998) What's for dinner?: Entner-doudoroff metabolism in Escherichia coli, *J. Bacteriol. 180*, 3495-3502.

11. Dutton, G. J. (1966) *Glururonic Acid: Free and Combined*, Academic Press, New York.

12. Raux, E., Lanois, A., Levillayer, F., Warren, M., Brody, E., Rambach, A., and Thermes, C. (1996) *Salmonella typhimurium* cobalamin (vitamin B_{12}) biosynthetic genes: Functional studies in *S. typhimurium* and *Escherichia coli*, *J. Bacteriol. 178*, 753-767.

13. Kirke, P. N., Molloy, A. M., Daly, L. E., Burke, H., Weir, D. C., Scott, J. M. (1993) Maternal plasma folate and vitamin B_{12} are independent risk factors for neural tube defects, *QJM 86*, 703-708.

14. Galperin, M. Y., and Grishin, N. V. (2000) The synthetase domains of cobalamin biosynthesis amidotransferases cobB and cobQ belong to a new family of ATP-dependent amidoligases, related to dethiobiotin synthetase, *Proteins 41*, 238-247.

15. Thoden, J. B., Holden, H. M., Wesenberg, G., Raushel, F. M., and Rayment, I. (1997) Structure of carbamoyl phosphate synthetase: A journey of 96 angstroms from substrate to product, *Biochemistry 36*, 6305-6316.

16. Tesmer, J. J. G., Klem, T. J., Deras, M. L., Davisson, V. J., and Smith, J. L. (1996) The crystal structure of GMP synthetase reveals a novel catalytic triad and is a structural paradigm for two enzyme families, *Nature 3*, 74-86.

17. Huang, X., and Raushel, F. M. (1999) Deconstruction of the catalytic array within the amidotransferase subunit of carbamoyl phosphate synthetase, *Biochemistry 38*, 15909-15914.

18. Zalkin, H., and Smith, J. L. (1998) Enzymes utilizing glutamine as an amide donor, *Adv. Enzymol. Relat. Areas Mol. Biol. 72*, 87-144.

19. Smith, J. L. (1998) Glutamine PRPP amidotransferase: Snapshots of an enzyme in action, *Curr. Opin. Struct. Biol. 8*, 686-694.

20. Raushel, F. M., Thoden, J. B., Reinhart, G. D., and Holden, H. M. (1998) Carbamoyl phosphate synthetase: A crooked path from substrates to products, *Curr. Opin. Chem. Biol. 2*, 624-632.

21. Raushel, F. M., Thoden, J. B., and Holden, H. M. (1999) The amidotransferase family of enzymes: Molecular machines for the production and delivery of ammonia, *Biochemistry 38*, 7891-7899.

22. Galperin, M. Y., and Koonin, E. V. (1997) A diverse superfamily of enzymes with ATP-dependent carboxylate-amine/thiol ligase activity, *Protein Sci 6*, 2639-2643.

23. Wimmer, M. J., Rose, I. A., Powers, S. G., and Meister, A. (1979) Evidence that carboxyphosphate is a kinetically competent intermediate in the carbamyl phosphate synthetase reaction, *J. Biol. Chem. 254*, 1854-1859.

24. Takahashi, S., Zhao, Y., O'Maille, P. E., Greenhagen, B. T., Noel, J. P., Coates, R. M., and Chappell, J. (2005) Kinetic and molecular analysis of 5-epiaristolochene 1,3-dihydroxylase, a cytochrome P450 enzyme catalyzing successive hydroxylations of sesquiterpenes, *J. Biol. Chem. 280*, 3686-3696.

25. de Verneuil, H., Sassa, S., and Kappas, A. (1983) Purification and properties of uroporphyrinogen decarboxylase from human erythrocytes. A single enzyme catalyzing the four sequential decarboxylations of uroporphyrinogens I and III, *J. Biol. Chem. 258*, 2454-2460.

26. Fresquet, V., Williams, L., and Raushel, F. M. (2004) Mechanism of cobyrinic Acid *a,c*-diamide synthetase from *Salmonella typhimurium* LT2, *Biochemistry 43*, 10619-10627.

27. Topper, Y. J. (1957) On the mechanism of action of phoshpglucose isomerase and phosphomannose isomerase, *J. Biol. Chem. 225*, 419-426.

28. Harris, T. K., Cole, R. N., Comer, F. I., and Mildvan, A. S. (1998) Proton transfer in the mechanism of triosephosphate isomerase, *Biochemistry 37*, 16828-16838.

29. Hausler, H., and Stutz, A. E. (2001) D-Xylose (D-glucose) isomerase and related enzymes in carbohydrate synthesis, *Top. Current Chem. 215*, 77-114.

30. Allen, K. N., Lavie, A., Farber, G. K., Glasfeld, A., Petsko, G. A., and Ringe, D. (1994) Isotopic exchange plus substrate and inhibition kinetics of D-xylose isomerase do not support a proton-transfer mechanism, *Biochemistry 33*, 1481-1487.

31. Seeholzer, S. (1993) Phosphoglucose isomerase: A ketol isomerase with aldol C2-epimerase activity, *PNAS 90*, 1237-1241.

32. Rose, I. A., O'Connell, E. L., and Mortlock, R. P. (1969) Stereochemical evidence for a cis-enediol intermediate in Mn-dependent aldose isomerases, *Biochm. Biophys. Acta 178*, 376-379.

33. Fenn, T. D., Ringe, D., and Petsko, G. A. (2004) Xylose isomerase in substrate and inhibitor michaelis states: Atomic resolution studies of a metal-mediated hydride shift, *Biochemistry 43*, 6464-6474.

34. Balaban, R. S., and Ferretti, J. A. (1983) Rates of enzyme-catalyzed exchange determined by two-dimensional NMR: A study of glucose 6-phosphate anomerization and isomerization, *PNAS 80*, 1241-1245.

35. Willem, R., Biesemans, M., Hallenga, K., Lippens, G., Malaisse-Lagae, F., and Malaisse, W. (1992) Dual anomeric specificity and dual anomerase activity of

phosphoglucoisomerase quantified by two-dimensional phase-sensitive ^{13}C EXSY NMR, *J. Biol. Chem. 267*, 210-217.

36. Cleland, W. W. (1990) Steady-State Kinetics, in *The Enzymes* (Sigman, D. S., and Boyer, P. D., Eds.) Third edition ed., pp 143-155, Academic Press, New York.

37. Fersht, A. (1985) *Enzyme Structure and Mechanism*, 2nd ed., W. H. Freeman New York.

38. Podlasek, C. A., Wu, J., Stripe, W. A., Bondo, P. B., and Serianni, A. S. (1995) [^{13}C]-Enriched methyl aldopyranosides: structural interpretations of ^{13}C-^{1}H spin-coupling constants and ^{1}H chemical shifts, *J. Am. Chem. Soc. 117*, 8635-8644.

39. Karplus, M. (1963) Vicinal proton coupling in nuclear magnetic resonance, *J. Am. Chem. Soc. 85*, 2870-2871.

40. Karplus, M. (1959) Contact electron-spin coupling of nuclear magnetic moments, *J. Chem. Phys. 30*, 11-15.

41. Serianni, A. S., Pierce, J., Huang, S., and Barker, R. (1982) Anomerization of furanose sugars: Kinetics of ring-opening reactions by ^{1}H and ^{13}C saturation-transfer NMR spectroscopy, *J. Am. Chem. Soc. 104*, 4037-4044.

42. Snyder, J. R., Johnston, E. R., and Serianni, A. S. (1989) D-Talose anomerization: NMR methods to evaluate the reaction kinetics, *J. Am. Chem. Soc. 111*, 2681-2687.

43. Perrin, C. L., and Dwyer, T. J. (1990) Application of two-dimensional NMR to kinetics of chemical exchange, *Chem. Rev. 90*, 935-967.

44. Rose, I. A., and O'Connell, E. L. (1961) Intramolecular hydrogen transfer in the phosphoglucose isomerase reaction, *J. Biol. Chem. 236*, 3086-3092.

45. Kozarich, J. W., Chari, R. V. J., Wu, J. C., and Lawrence, T. L. (1981) Fluoromethylglyoxal: Synthesis and glyoxalase I catalyzed product partitioning via a presumed enediol intermediate, *J. Am. Chem. Soc. 103*, 4593-4595.

46. Williams, L., Nguyen, T., Li, Y., Porter, T. N., and Raushel, F. M. (2006) Uronate isomerase: A nonhydrolytic member of the amidohydrolase Superfamily with an ambivalent requirement for a divalent metal ion, *Biochemistry 45*, 7453-7462.

47. Maier, G. D., Kusiak, J. W., and Bailey, J. M. (1977) The study of the mutarotation of -glucose, -fructose, and -ribose by use of their circular dichroism, *Carbohydr. Res. 53*, 1-11.

48. Wertz, P. W., Garver, J. C., and Anderson, L. (1981) Anatomy of a complex mutarotation. Kinetics of tautomerization of α-D-galactopyranose and ß-D-galactopyranose in water, *J. Am. Chem. Soc. 103*, 3916-3922.

49. Von der Saal, W., Crysler, C. S., and Villafranca, J. J. (1985) Positional isotope exchange and kinetic experiments with *Escherichia coli* guanosine 5'-monophosphate synthetase, *Biochemistry 24*, 5343-5350.

50. Williams, L., Zheng, R., Blanchard, J. S., and Raushel, F. M. (2003) Positional isotope exchange analysis of the pantothenate synthetase reaction, *Biochemistry 42*, 5108-5113.

51. Lowe, G., Sproat, B. S., and Tansley, G. (1983) A stereochemical and positional isotope exchange study of the mechaism of activation of methionine by methionyl-tRNA synthetase from *Eschericia coli*, *Eur. J. Biochem. 130*, 341-345.

52. Lowe, G., Sproat, B. S., Tansley, G., and Cullis, P. M. (1983) A stereochemical and positional isotope exchange study of the mechanism of activation of isoleucine by isoleucyl-tRNA synthetase from *Escherichia coli*, *Biochemistry 22*, 1229-1236.

53. Lowe, G., and Tansley, G. (1984) A stereochemical and positional isotope exchange study of the mechanism of activation of tyrosine by tyrosyl-tRNA synthetase from *Bacillus stearothermophilus*, *Tetrahedron 40*, 113-117.

54. Midelfort, C. F., and Rose, I. A. (1976) A stereochemical method for detection of ATP terminal phosphate transfer in enzymatic reactions. Glutamine synthetase, *J. Biol. Chem. 251*, 5881-5887.

55. Wang, H. C., Ciskanik, L., Dunaway-Mariano, D., Von der Saal, W., and Villafranca, J. J. (1988) Investigations of the partial reactions catalyzed by pyruvate phosphate dikinase, *Biochemistry 27*, 625-633.

56. Hilscher, L. W., Hanson, C. D., Russell, D. H. and Raushel, F. M. (1985) Measurement of positional isotope exchange rates in enzyme-catalyzed reactions by fast atom bombardment mass spectrometry: Application to argininosuccinate synthetase, *Biochemistry 24*, 5888-5893.

57. Raushel, F. M., and Villafranca, J. J. (1980) Phosphorus-31 nuclear magnetic resonance application to positional isotope exchange reactions catalyzed by

Escherichia coli carbamoyl-phosphate synthetase: Analysis of forward and reverse enzymatic reactions, *Biochemistry 19*, 3170-3174.

58. Raushel, F. M., and Garrard, L. J. (1984) A positional isotope exchange study of the argininosuccinate lyase reaction, *Biochemistry 23*, 1791-1795.

59. Mullins, L. S., and Raushel, F. M. (1995) Positional isotope exchange as probe of enzyme action, *Methods Enzymol. 249*, 398-425.

60. Cohn, M., and A., H. (1980) Isotopic oxygen-18 shifts in phosphorus-31 NMR of adenine nucleotides synthesized with oxygen-18 in various positions, *J. Am. Chem. Soc. 102*, 913-916.

61. Cleland, W. W. (1990) Kinetic competence of enzymic intermediates: fact or fiction?, *Biochemistry 29*, 3194-3197.

62. Rose, I. A. (1979) Positional isotope exchange studies of enzyme mechanisms, *Adv. Enzymol. Relat. Areas Mol. Biol. 50*, 361-395.

63. Risley, J. M., and Van Etten, R. L. (1978) A convenient synthesis of crystalline potassium phosphate-$^{18}O_4$ (monobasic) of high isotopic purity, *J. Labelled Compd. Radiopharm. 15*, 533-538.

64. Werhli, W. E., Verheyden, D. L. M., and Moffatt, J. G. (1965) Dismutation reactions of nucleoside polyphosphates. II. Specific chemical syntheses of a-, ß-, and γ-^{32}P-nucleoside 5'-triphosphates, *J. Am. Chem. Soc. 87*, 2265-2277.

65. Fresquet, V., Thoden, J. B., Holden, H. M., and Raushel, F. M. (2004) Kinetic mechanism of asparagine synthetase from *Vibrio cholerae*, *Bioorg. Chem. 32*, 63-75.

66. Tsai, Y. C., and Johnson, K. A. (2006) A new paradigm for DNA polymerase specificity, *Biochemistry 45*, 9675-9687.

67. Wu, J. Z., Walker, H., Lau, J. Y. N., and Hong, Z. (2003) Activation and deactivation of a broad-spectrum antiviral drug by a single enzyme: Adenosine deaminase catalyzes two consecutive deamination reactions, *Antimicrob. Agents Chemother. 47*, 426-431.

68. Scott, A. I., and Roessner, C. A. (2002) Biosynthesis of cobalamin (vitamin B_{12}), *Biochem. Soc. Trans. 30*, 613-620.

69. Debussche, L., Thibaut, D., Cameron, B., Crouzet, J., and Blanche, F. (1990) Purification and characterization of cobyrinic acid *a,c*-diamide synthase from *Pseudomonas denitrificans*, *J. Bacteriol.*, 6239-6244.

70. Duggleby, R. (1994) Analysis of progress curves for enzyme-catalyzed reacitons: Application to unstable enzymes, coupled reactions, and transient-state kinetics, *Biochim. Biophys. Acta. 1205*, 268-274.

71. Blanche, F., Couder, M., Debussche, L., Thibaut, D., Cameron, B., and Crouzet, J. (1991) Biosynthesis of vitamin B_{12}: stepwise amidaiton of carboxyl groups *b, d, e*, and *g* of cobyrinic acid *a,c*-diamide is catalyzed by one enzyme in Pseudomonas denitrificans, *J. Bacteriol. 173*, 6046-6051.

72. Bauer, C. B., Fonseca, M. V., Holden, H. M., Thoden, J. B., Thompson, T. B., Escalante-Semerena, J. C., and Rayment, I. (2001) Three-dimensional structure of ATP:corrinoid adenosyltransferase from Salmonella typhimurium in its free

state, complexed with MgATP, or complexed with hydroxycobalamin and MgATP, *Biochemistry 40*, 361-374.

73. Fujii, K., Galivan, J. H., and Huennekens, F. M. (1977) Activation of methionine synthase: Further characterization of the flavoprotein system, *Arch. Biochem. Biophys. 178*, 662-670.

74. Osborne, C., Chen, L. M., and Matthews, R. G. (1991) Isolation, cloning, mapping, and nucleotide sequencing of the gene encoding flavodoxin in *Escherichia coli*, *J. Bacteriol. 173*, 1729-1737.

75. Blanche, F., Thibaut, D., Couder, M., and Muller, J. C. (1990) Identification and quantitation of corrinoid precursors of cobalamin from Pseudomonas denitrificans by high-performance liquid chromatography, *Anal. Biochem. 189*, 24-29.

76. Kay, L., Keifer, P., and Saarinen, T. (1992) Pure absorption gradient enhanced heteronuclear single quantum correlation spectroscopy with improved sensitivity, *J. Am. Chem. Soc. 114*, 10663-10665.

77. Van Gelder, B. F., and Slater, E. C. (1962) Extinction coefficient of cytochrome c, *Biochim. Biophys. Acta. 58*, 593-595.

78. Brown, K. L., and Zou, X. (1997) Heteronuclear NMR studies of cobalt corrinoids part-19: Amide ^{1}H and ^{15}N NMR studies of cobalamins and cobinamides in water, *Magn. Res. Chem. 35*, 889-895.

VITA

The author, LaKenya Williams, enrolled at Prairie View A&M University in August 1995 and received a B.S. in Chemistry in May 2000. In August 2000, she enrolled at Texas A&M University where she began her graduate studies under the supervision of Dr. Frank Raushel. LaKenya received her M.S. in Chemistry in May 2003 and continued her graduate studies in Dr. Raushel's laboratory. LaKenya may be reached by mail at TAMU-Department of Chemistry, PO Box 30012, College Station, TX 77843 or via e-mail at cenbnherd@hotmail.com.